CHALMERS
UNIVERSITY OF TECHNOLOGY

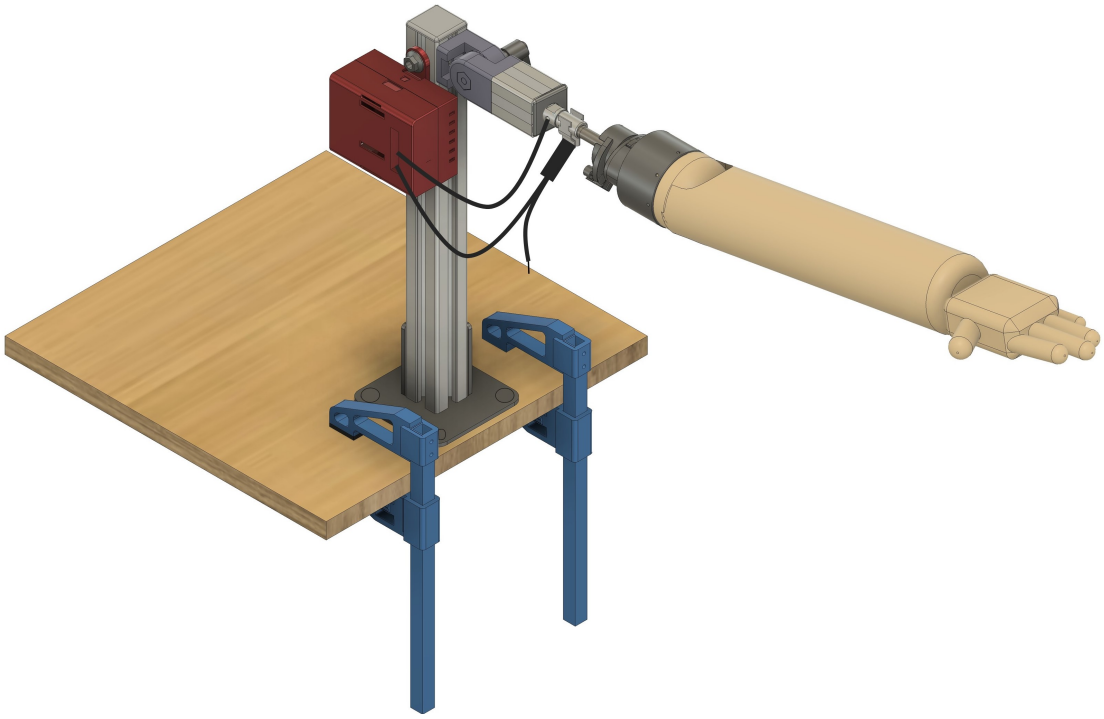

Design and Development of a Test System for an Artificial Limb Controller

Master's thesis in Biomedical Engineering

SUSANNA AURORA KATAJA
LELÍTA RÓS YCOT

DEPARTMENT OF ELECTRICAL ENGINEERING

CHALMERS UNIVERSITY OF TECHNOLOGY
Gothenburg, Sweden 2023
www.chalmers.se

MASTER'S THESIS 2023:EENX30

Design and Development of a Test System for an Artificial Limb Controller

SUSANNA AURORA KATAJA
LELÍTA RÓS YCOT

CHALMERS
UNIVERSITY OF TECHNOLOGY

Department of Electrical Engineering
CHALMERS UNIVERSITY OF TECHNOLOGY
Gothenburg, Sweden 2023

Design and Development of a Test System for an Artificial Limb Controller
SUSANNA AURORA KATAJA
LELÍTA RÓS YCOT

Supervisor: Björn Davidsson, Integrum AB
Examiner: Silvia Muceli, Department of Electrical Engineering

Master's thesis 2023
Department of Electrical Engineering
Division of Biomedical Engineering
Chalmers University of Technology
SE-412 96 Gothenburg
Sweden
Telephone +46 31 772 1000

Cover: CAD-model of the ALC Test System designed with Fusion 360.

Typeset in LaTeX
Gothenburg, Sweden 2023

Design and Development of a Test System for an Artificial Limb Controller
SUSANNA AURORA KATAJA
LELÍTA RÓS YCOT
Department of Electrical Engineering
Chalmers University of Technology

Abstract

Implanted muscular electrodes offer a promising method for controlling Artificial Limbs (ALs) and, when combined with an Osseointegrated Implant System (OIS), can significantly enhance the lives of amputees. However, the control of ALs with electromyography (EMG) data is complex and requires an advanced control system. Testing of such a system is an iterative process and is difficult to perform without utilizing a human test subject with implanted muscular electrodes in their Residual Limb (RL). Consequently, this creates problems and delays in the testing phase of the control systems, inconveniencing all parties involved.

The aim of this thesis is to develop a test system for an Artificial Limb Controller (ALC) designed by a Swedish medical device company called Integrum AB. Specifically targeting their model for transhumeral (TH) amputations (above the elbow) called ALC-TH. The ALC Test System is a combination of a Test Rig, a Test Device, and Test Software. It facilitates realistic testing of the ALC without relying on human test subjects by utilizing recorded EMG data from amputees. Moreover, it allows for testing of the ALC with an artificial arm attached in various positions by incorporating a lockable joint with a range of motion of 125° within the Test Rig. The Test System exhibits modularity, enabling convenient replacement of components in the event of issues or for future implementation and expansion purposes.

Initial assumptions were made to acquire conservative minimum tolerances for the component selections of the Test Rig. Thorough investigations led to the component selections for each part of the Test System. Simulations were performed for assessing the maximum stress and safety factor of the final Test Rig design. The functionality of each Test Device component was individually tested using electrical equipment.Comprehensive integration testing was conducted to assess the performance of the Test System. Evaluation of the Test Rig's mechanical strength was carried out by applying a conservative load, and a demonstration of the functionality of the Test System with the ALC and an AL was performed. These testing procedures confirmed that all components of the Test System operated as intended and met the desired functionality criteria to enable realistic testing of the ALC.

Keywords: osseointegrated implant, artificial limb, control, EMG simulator, test system, joint, test rig, digital-to-analog converter

Acknowledgements

We extend our heartfelt appreciation to our supervisor, Björn Davidsson, for the valuable guidance, consistent support, and constructive feedback provided throughout the project. We also want to thank our examiner Silvia Muceli for the guidance. In addition, we want to thank Alexander Thesleff and Robin Long, mechanical engineers at Integrum AB, for providing us with their knowledge and help during the project. Finally, we want to thank our spouses (Óðinn Páll Tjörvason and Philip Wild) for their patience and support, and our pets (Gvendur the cat and Gaia the snake) for the emotional support they have provided us during the thesis process. We are also immensely grateful to energy drinks and 24/7 shops, as we couldn't have done this without them.

Lelíta Rós Ycot and Susanna Aurora Kataja, Gothenburg, June 2023

List of Acronyms

AL	Artficial Limb
ALC	Artificial Limb Controller
ALC-TH	Artificial Limb Controller for Transhumeral amputations
DLL	Dynamic Link Library
DoF	Degree of Freedom
EMG	Electromyography
e-OPRA	enhanced OPRA
GUI	Graphical User Interface
I^2C	Inter-Integrated Circuit
OIS	Osseointegrated Implant System
OPRA	Osseoanchored Prostheses for the Rehabilitation of Amputees
PCB	Printed Circuit Board
RL	Residual Limb
SPI	Serial Peripheral Interface
UART	Universal Asynchronous Receiver-Transmitter
USB	Universal Serial Bus

Contents

List of Figures

List of Tables

1

Introduction

This report describes a master thesis project conducted at the Swedish medical device company Integrum AB. The project involved creating a test system for their Artificial Limb Controller (ALC) developed for transhumeral (above the elbow) amputations called ALC-TH.

The ALC Test System created in this thesis project can be seen in Figure 1.1. Its design and development process will be outlined in this report.

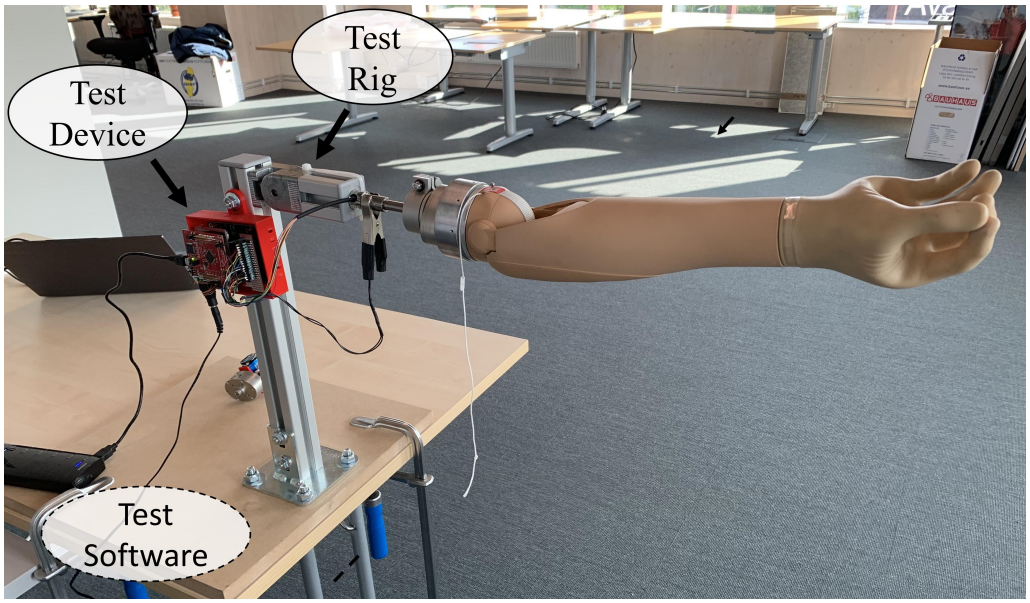

Figure 1.1: The final product.

Realistic testing of the ALC is needed to fulfill Integrum's Quality Management System (QMS) and verification on design, system integration, system verification, and service and manufacturing. This will in turn improve user experience [1].

Generally, in order to evaluate the control algorithms of an Artificial Limb (AL), it is necessary for amputees to take part in the testing process in person. As frequent testing and repetition are necessary for reliable results, it is not convenient or efficient to need to

utilize human subjects in this process.

Therefore, by reducing the reliance on participants with transhumeral amputations in the testing of the ALC-TH, the aim is to enhance the efficiency of the testing process, which aligns with the purpose of the ALC Test System.

This chapter introduces the project's aim and limitations.

1.1 Aim

This thesis aims to initialize the design and development process of automatic verification, validation, and development testing for the ALC-TH. The objective is to create a modular and portable test system for the ALC-TH. It should provide fast, efficient, and realistic testing without the need for a human test subject.

The Test System designed in this thesis is a combination of software and hardware. The hardware includes the Test Rig, which will be used to mount the ALC and an artificial arm, as well as the Test Device which will handle all electronic communications between a computer and the ALC. The Test Software communicates between the Test Device and a computer.

The Test System is essentially created for verification and integration testing of the ALC-TH system components in operation with a robotic artificial arm.

1.2 Scope and limitations

The development of the Test System is an integral part of a larger project aimed at creating a comprehensive test system for the ALC that comprises multiple functions. The primary objective of this thesis project is to initiate the design process of the comprehensive test system for the ALC. The finalized test system for the ALC, to be developed by the company, will comprise five essential parts: an electromyography (EMG) simulator, an AL control verification system, a simulation of pressure sensor data of an AL, a neurostimulation verification system, and a test rig that will offer easier testing by mounting the ALC along with an AL.

An illustration of how the finalized test system for the ALC can replace a human test subject can be seen in Figure 1.2.

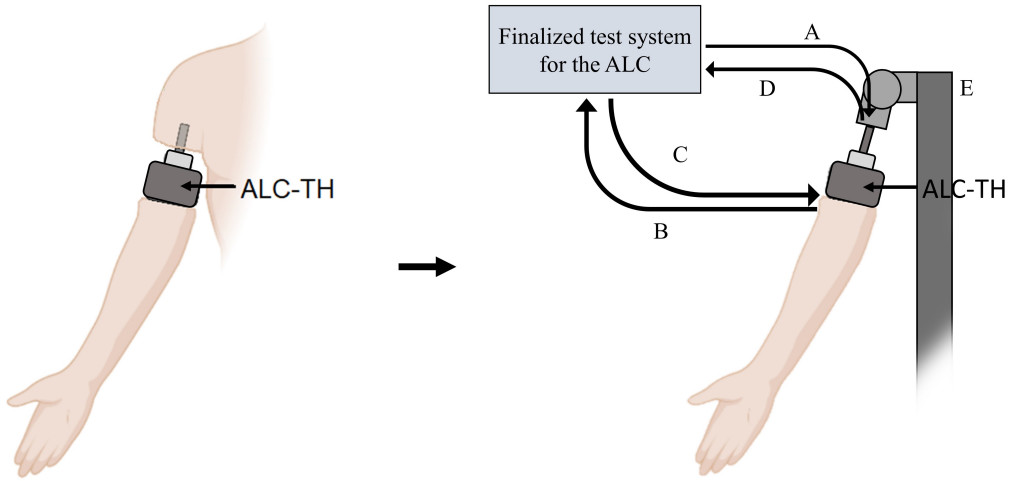

Figure 1.2: Flow of information between the ALC-TH and the finalized test system for the ALC. A: EMG simulation, B: AL control, C: Pressure sensor input simulation, D: Neurostimulation. Then E: A test rig for mounting the ALC and AL.

This thesis will specifically focus on two key parts of the larger ALC test system, namely the EMG simulator and test rig. While designing these parts, careful consideration will be given to the integration and compatibility with the AL control verification system, simulation of data from pressure sensors of an AL, and neurostimulation verification system, which are integral parts of the overall ALC test system.

This includes creating a robust Test Rig, a realistic simulation of the EMG signals of human subjects (both software and electronics) as well as a Graphical User Interface (GUI) for the software for controlling the Test System from a computer.

The biggest limitation to the work of this project is time due to the fact that it as a whole is rather extensive. Therefore, the scope of this thesis project will be limited to the EMG simulation and the Test Rig. For simplification, in section 4.2 the AL control validation and artificial sensory feedback (including the simulation of pressure sensor data of an AL and neurostimulation validation) will be called parts three and four, respectively.

Another main limitation to the project work is the company Integrum AB's budget for it, which was set at 25 000 SEK. This is mainly a limiting factor to the hardware since, for example, the Test Device might need components such as complex input/output devices. These components might cost close to the amount of the whole budget but are necessary for communication between the test system software and the ALC-TH. In addition, manufacturing the final design of the Test Rig could be costly as well, depending on the chosen materials.

2

Background

Limb amputation impairs a person's mobility and ability to function physically, and a study made in 2016 estimated that there were around 3 million amputees only in the European Union [2].

After an amputation, the amputee will need an AL to perform activities of daily living [2]. An Osseointegrated Implant System (OIS) is one solution to attach an AL to the Residual Limb (RL) of an amputee. Osseointegration refers to the integration of a titanium implant into a bone [3].

Figure 2.1 shows one type of OIS. It is three-parted; the fixture is the part implanted into a bone, the abutment penetrates the skin and is connected to the fixture for connection to an AL, and the abutment screw is then attached to connect the abutment and the fixture together [4]. An OIS is made out of biocompatible metal, typically medical-grade titanium alloy, Ti6Al4V [5], [6]. This method is intended to establish a stable long-term anchor for an AL as well as avoid problems related to having a traditional socket. The sockets use negative pressure, or suction to attach an AL as seen in Figure 2.2 [7], [8]. They have commonly been reported by users to cause infections, restrictive movement, and sweating [7], [8]. Therefore, an OIS offers improved quality of life, including increasing the range of motion and avoiding socket-related skin irritations and infections [9]. They also offer the possibility of sensing surfaces such as sand and grass [10].

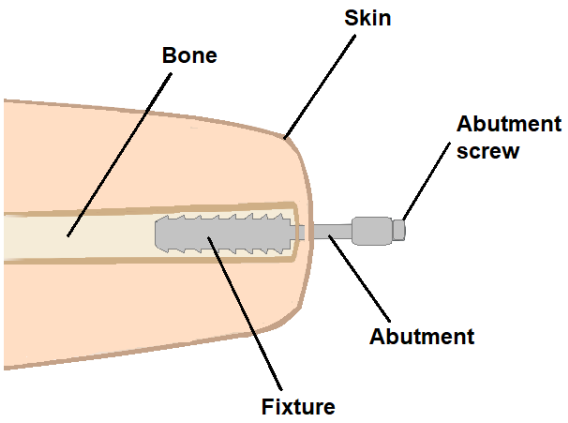

Figure 2.1: An example of an OIS.

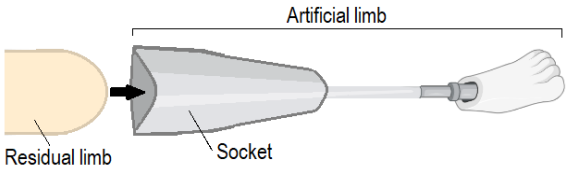

Figure 2.2: Display of a traditional socket for prosthesis attachment.

While OISs have a lot of benefits, there is room for improvement regarding the control of the AL. The control is traditionally done through EMG signals acquired by surface electrodes that are applied on the surface of the skin of the user [11]. These surface electrodes tend to pick up a lot of motion artifacts and background noise [12], [13]. Therefore, there is still a need for a more reliable control of robotic ALs which could be achieved with both implanted EMG electrodes and neurostimulation. Neurostimulation provides sensory feedback that offers an improved feeling of body ownership [14].

2.1 The OPRA and the e-OPRA

The Swedish medical device company Integrum AB developed the Osseoanchored Prosthesis for the Rehabilitation of Amputees (OPRA), which is one of the state-of-the-art OISs of the type seen in Figure 2.1. Additional to the abutment, abutment screw, and fixture, a central screw was incorporated into the OPRA design. Which is located on the proximal end of the abutment screw. While the central screw currently serves no function in the OPRA, it was included to allow for potential electrode installation in the future [1].

Integrum AB is currently developing the enhanced OPRA (e-OPRA) (seen in Figure 2.3) to satisfy the need for better AL control. The main difference between the OPRA and e-OPRA is that the central screw is being utilized for electrode installation in the e-OPRA.

The benefits of the OPRA will be enhanced by the e-OPRA, including improved control of an AL, as the e-OPRA uses EMG signals acquired from the muscles of the user's residual limb [16] to control an AL [17]. These signals are obtained with 16 implanted muscular electrodes, either epimysial or intramuscular [15], [18]. Epimysial electrodes are implanted and sutured to the surface of muscles while the intramuscular electrodes are implanted into the muscle tissue [19]. The communication between the nerves and muscles of the amputee and the AL is handled by the advanced ALC from Integrum [15], [20].

Furthermore, the e-OPRA will offer neural sensory feedback by sending electrical pulses to the nerves of the amputee through neural cuff electrodes. This is also known as neurostimulation [17], and the sensations created by it are intuitive and give the amputee a better sense of body ownership over the AL [14], [21]. These electrical pulses are based on information acquired by pressure sensors in an AL, and they elicit the perception of touch and its intensity [22].

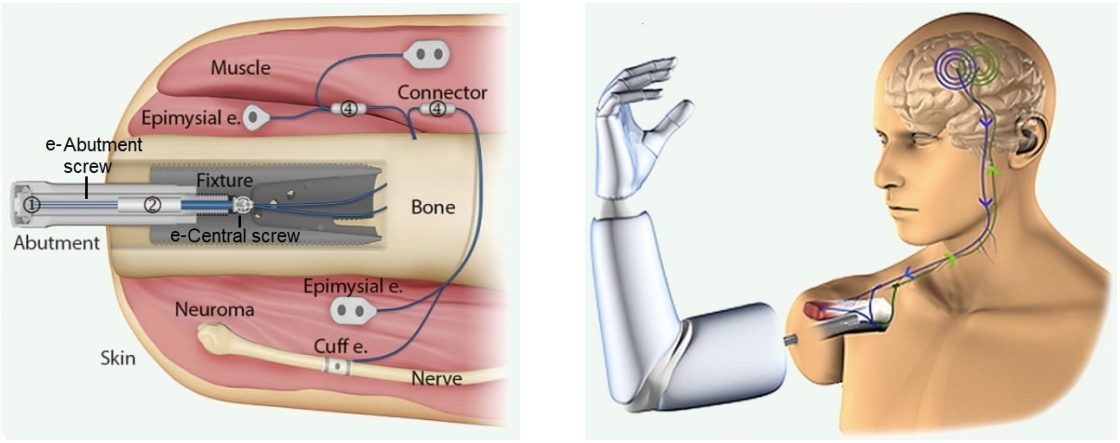

(a) **(b)**

Figure 2.3: Explanation of the e-OPRA [15] (Images courtesy of Integrum AB). (a) The abutment, e-abutment screw, and fixture are as described for OISs. On the proximal end of the e-abutment screw, there is an e-central screw (seen in Figure 2.5) to enable the use of implanted electrodes. (b) The e-OPRA together with an AL. The blue arrows represent the flow of information to control the AL movements, and the green arrows the flow of information for the artificial sensory feedback.

Research has shown that controlled stimulation of peripheral nerves could also help relieve phantom limb pain by simulating sensations coming from the missing limb [23], [24]. Phantom limb pain is a term for pain in the missing limb (phantom limb) of an amputee, and it affects up to 80% of all amputees [25], [26].

The OPRA implanted into an amputee can easily be upgraded into the e-OPRA since the standard OPRA central screw and abutment screw are interchangeable with the e-central screw and e-abutment screw of the e-OPRA. This means that they can be installed without removing or altering the fixture and abutment of the OPRA [18].

2.2 The ALC

To enable the movement of an AL using the EMG signals acquired from the user's RL, the application of a control method is necessary [27]. For this purpose, Integrum is currently developing the ALC for use in conjunction with the e-OPRA. It is a combination of hardware and software that act as a link between a human RL and an AL [17].

The ALC has an electrode connector (female part) that mates with the e-abutment screw distal connector (male part, seen as E in Figure 2.5a) from Omnetics Connector Corporation. They both have 16 contacts/pins for the 16 channels [18]. The ALC electrode connector, also known as the Omnetics connector, establishes a secure and steady electrical linkage between the ALC and the implanted electrodes of the e-OPRA, ensuring reliability and stability [20]. The ALC communicates in two directions: it reads EMG

signal input from either epimysial or intramuscular electrodes inside the RL and converts them to control signals for the AL, and reads data from the AL's pressure sensors and converts it into stimulating signals for the neural cuff electrodes in the RL [22].

Physically, the ALC is mounted between the e-OPRA and an AL with an attachment device, as can be seen in Figure 2.4. It will be available for transhumeral amputees and later for transradial (below the elbow) amputees [20]. In this project, the focus will be on the ALC-TH.

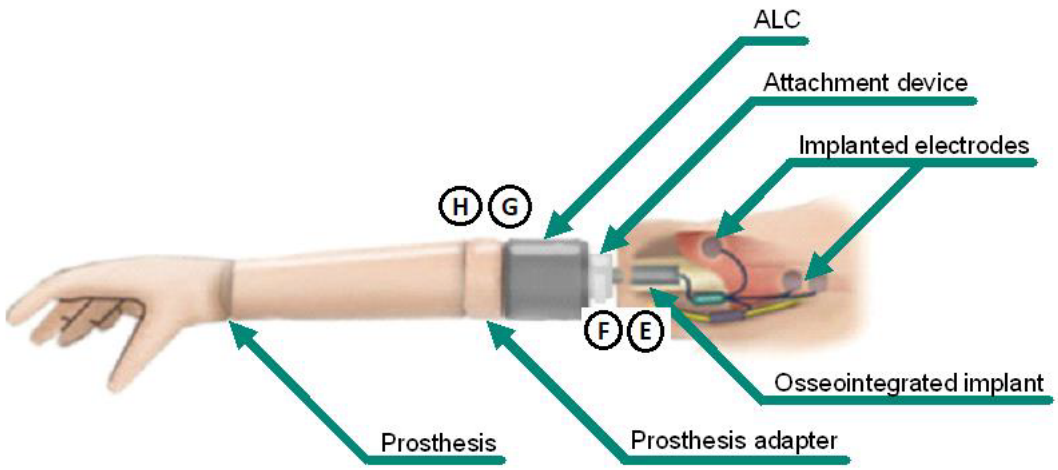

Figure 2.4: The ALC is mounted between the AL and the RL of amputees. (Image courtesy of Integrum AB).

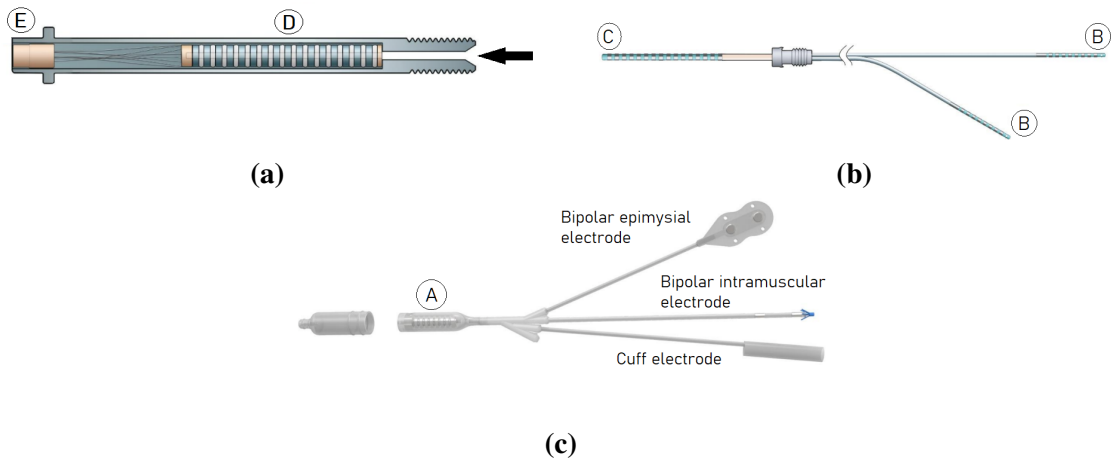

Figure 2.5: The components of the e-OPRA [18]. (Images courtesy of Integrum AB). (a) The e-abutment screw has a distal connector (E) for connection with the ALC-TH, and a proximal connector (D) for connection to the e-central screw. (b) The e-central screw is inserted into the e-abutment screw. It has a distal connector (C) for connection with the (D) connector and a proximal connector (B) for connection with the electrode set. (c) The electrode set. Omnetics connector (A) and a combination of various types of electrodes to the left. The Omnetics connector mates with the proximal connector (B).

2.3 State of the art

At present, testing of the ALC-TH is done by using real time EMG signals from human subjects, or a generic signal generator such as a function generator that creates a simple sine wave, which is not ideal to create a realistic EMG signal [1]. In addition, the company has been working on a prototype to enable testing without a human subject, but that system can only enable testing using a single EMG or neurostimulation channel at a time, whereas, in a real-world scenario involving a human subject using the ALC, all 16 EMG or neurostimulation channels would be operating simultaneously [1].

There are a few examples of state of the art simple EMG simulation devices [28]–[34] that have been created for multiple different purposes, including testing of prosthetic control algorithms [31]. The identified EMG simulators, upon evaluation, have a maximum capacity of only three EMG signals [29], with most of them only simulating one channel while the ALC requires the simulation of 16 channels. However, the EMG signal parameters such as frequency (10-2 500 Hz) and voltage amplitude (0.001-850 mV), with slight variance between the devices, encompass the requirements of the ALC which records the EMG signals in 500 - 1 000 Hz and $\pm$5 mVpp to control an AL.

When it comes to physical testing rigs and AL mounting, similar systems have been created before [35]–[38] but mainly for lower ALs and mechanical testing [35], [37], [38]. These test rigs are mostly made of metal, heavy and big [35], [37], [38], and thus not portable as the ALC Test System rig needs to be in order to be used in multiple locations and easily transported between them.

There are some verification systems existent in the field of biomedical engineering. One method was implemented in a Chinese registry study [39], where they used an automated data verification approach for improving data quality in a clinical registry. The method uses optical character recognition (OCR) and retrieval of information to identify data errors in a registry. For validation and verification of prosthetic control algorithms, data sets consisting of EMG recordings have been used [40]–[42].

3

Theory

This chapter provides theoretical aspects relevant to some main features of the thesis, providing a comprehensive overview. All main features of the project can be seen in Table 3.1.

Table 3.1: The parts of the Test System

Test System part	Test Rig	Test Device	Test Software
Feature:	Skeleton	Digital-to-Analog converter	.mat-file conversion
	Lockable joint	Power Unit	Interface conversion
	Table attachment	Voltage attenuators	Graphical user interface
	Abutment attachment	Interface adapter	Output handling

3.1 Electronic communication precision

If an electronic component, such as a digital-to-analog converter, is to output data with high precision, it needs to have a high resolution. The resolution of an electronic component is measured in bits, and a component with x bits can output 2^x different voltage levels within its voltage output range [43]. This means that, for example, a component with an 8-bit resolution and an output voltage of 0-5 V, can output $2^8 = 256$ different voltage levels within the range of 0-5 V. Therefore, the voltage difference between adjacent voltage levels is

$$\frac{5\ \mathrm{V}}{256} = 0.00195\ \mathrm{V} = 1.95\ \mathrm{mV}$$

This voltage difference is referred to as the least significant bit voltage [43].

If the data the electronic component is supposed to output is much lower in voltage range than the total output voltage range of the component, the resolution and the least significant bit voltage can play an important role in how precisely the data is preserved. As an example, with the least significant bit voltage of 1.95 mV, a signal with a voltage range of

6 mV would only be outputted with four different voltage levels; 0 mV, 1.95 mV, 3.9 mV and 5.85 mV. If the original signal was of high precision, most of it would be lost during the transmission through the electronic component.

To utilize the resolution of the electronic component to its full extent, the data could be, for example, upscaled (amplified) to match the output voltage range of the component, and later downscaled (deamplified) back to its original voltage range.

This is important to keep in mind when designing a device for simulating realistic EMG signals as is done in this thesis project.

3.2 Voltage attenuators

Voltage attenuation is a term that can be used to describe the process of lowering an amplitude of a voltage with an external device. This can be done, for example, with two-resistor voltage dividers or with inverting amplifiers in combination with two resistors [44]. The schematics of the two options can be seen in Figure 3.1.

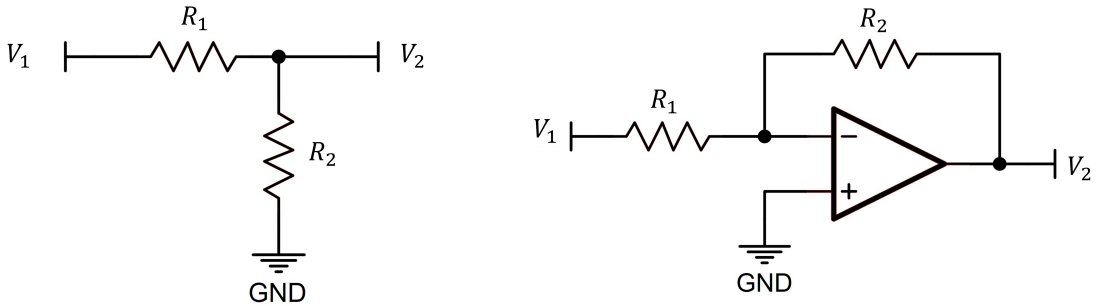

(a) **(b)**

Figure 3.1: Two attenuator options. (a) The voltage divider circuit. (b) The inverting amplifier circuit.

The voltage divider circuit seen in Figure 3.1a is the simpler of the two options since it only utilizes two resistors. Its gain can, according to [45], be calculated as

$$V_2 = \left(\frac{R_2}{R_1 + R_2}\right) V_1. \tag{3.1}$$

The attenuator in Figure 3.1b is slightly more complex in that it uses an inverting amplifier together with two resistors to attenuate the voltage. Its gain can, as described in [46], be calculated as

$$V_2 = -\left(\frac{R_2}{R_1}\right)V_1. \tag{3.2}$$

Voltage attenuators can be very useful when designing a device that needs to output a low-voltage signal such as an EMG signal, as will be done in this thesis project.

3.3 Communication interfaces

The electronic device to be designed in this thesis project should be able to communicate with a computer of a user to simplify the testing process. Many standard communication protocols or interfaces exist for the purpose of communication between a computer and peripheral devices [47]. Some of the most commonly used protocols will be introduced in this section.

3.3.1 Universal Asynchronous Receiver-Transmitter (UART)

UART is a simple, two-wire serial communication protocol that does not use a shared clock to synchronize its two wires, transmitter (TX) and receiver (RX), and their communication [47]. Connecting two devices with a UART interface is very simple, as the TX pin of one device has to be connected to the RX pin of the other one, and vice versa [48].

3.3.2 Serial Peripheral Interface (SPI)

SPI is a commonly used communication interface that utilizes four wires - clock, device select, master input/slave output (MISO), and master output/slave input (MOSI) [48]. The communication on each of the wires works in one direction, and the clock is used to synchronize them [47]. The master, such as a computer or a microcontroller, can be connected to multiple slaves or peripheral devices at once [47].

3.3.3 Inter-Integrated Circuit (I^2C)

I^2C is more complex than SPI and UART in that it utilizes only two wires, a serial clock, and serial data, and the communication in these wires is bidirectional [47], [48]. It also allows multiple controllers as well as multiple peripheral devices to be connected on the same I^2C bus [47].

3.3.4 Universal Serial Bus (USB)

USB is an interface commonly used by computers to communicate with peripheral devices [47]–[49]. It works in a host-device mode, meaning that the host is able to use services provided by the device [47]. A USB interface communicates with four wires - D+ and D- for data transfer in both directions, ground and a 5 V power supply [48].

3.4 Bending moment and stress of structural members

The Test Rig designed in this thesis project will be used to mount and hold an artificial arm as demonstrated in Figure 3.2. In the design of a structural member, such as the skeleton of a test rig, it is crucial to consider the bending moment and stress. This consideration is necessary to ensure the structural member has the strength needed to support the applied loading, especially when the loading has the potential to cause bending.

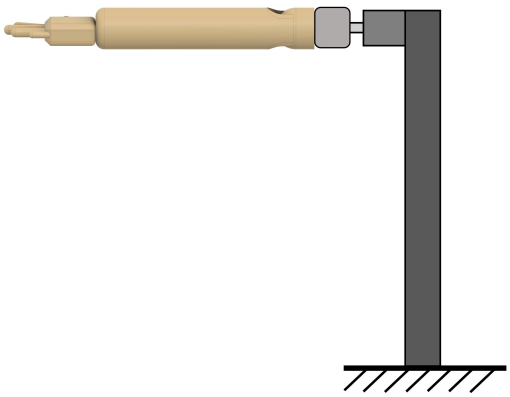

Figure 3.2: The Test Rig should be able to hold an artificial arm.

A bending moment causes the material within a certain portion of the structural member to experience tensile stress and the material within the other portion to experience compressive stress [50]. As a result, the cross-section of the structural member contains a neutral axis that separates the portions where the fibers experience zero stress and strain [50].

Therefore, it is necessary to locate the neutral axis of the cross-section of the structural member for calculating the maximum bending stress. For symmetrical cross-sections, their neutral axis is located along the centroid (C) at mid-height of the cross-section [51] as seen in Figure 3.3. The centroid of a cross-section refers to the point (C) that represents the geometric center of the area [52].

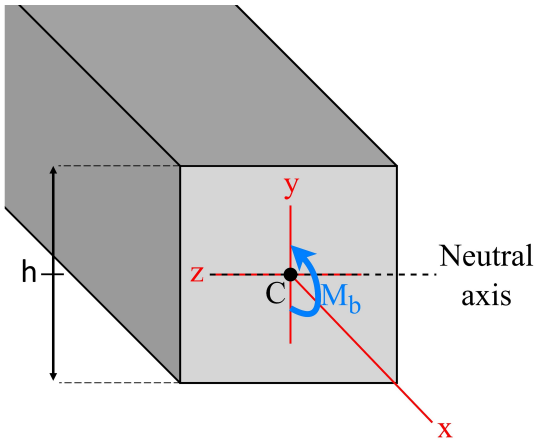

Figure 3.3: Neutral axis location in a symmetrical cross-section.

If a structural member is made out of several components with different masses, the center of mass has to be calculated in order to locate the gravitational force.

This center of mass ($r_{CM,x}$) can be calculated as

$$r_{CM,x} = \frac{1}{M} \sum_{i=1}^{N} m_i x_i \tag{3.3}$$

where M is the sum of all masses, N number of masses, and m_i is the mass and x_i is the length of the corresponding parts [53].

3.4.1 Analysis for cantilever beams

The arm of the test rig seen in Figure 3.2 can be considered a cantilever beam. A cantilever beam is a type of structural member that is horizontal and supported at one end only, with the other end extending freely beyond the support [54] as seen in Figure 3.4. The free end of the beam is called the cantilever [54].

When a load (F) is applied at a location a on a cantilever, the bending moment in any location x (before location a) of the cantilever beam can be calculated as

$$M_b = F(x - a) \tag{3.4}$$

where M_b is the internal bending moment (bending moment) about the neutral axis of the cross-section and F is the load as demonstrated by [54], [55].

If the load is caused by masses of several objects, the center of mass $(r_{CM,x})$ has to be calculated to find the location a which will therefore be equal to $r_{CM,x}$. The load of the combined masses, F_g, will then be located at this point, as seen in Figure 3.4.

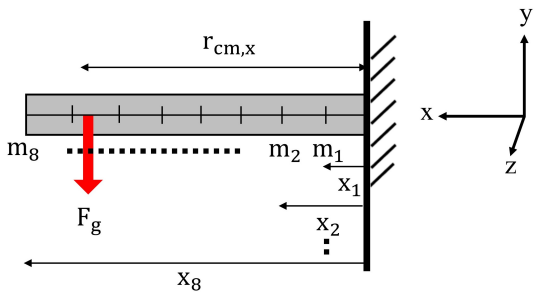

Figure 3.4: Gravitational force (F_g) caused by multiple masses.

The maximum bending stress can be calculated as

$$\sigma_{max} = \frac{M_b \cdot c}{I} \tag{3.5}$$

where M_b is the internal bending moment (bending moment) about the neutral axis of the cross-section, c is the perpendicular distance from the neutral axis to the farthest point on the section, I is the moment of inertia of the cross-sectional area about the neutral axis [54], [56].

3.4.2 Analysis for columns

The vertical structural member of the test rig seen in Figure 3.2 can be considered a column. In designing a column that is responsible for sustaining a load acting on a cantilever beam attached to its side, it is important to consider the bending moment M_b that results from the eccentric loading [57]. This is necessary to ensure that the column can effectively support the load.

The bending moment can be calculated as

$$M_b = F \cdot e \tag{3.6}$$

where F is the eccentric load, and the eccentricity (e) refers to the distance between the center of a column's cross-section and the point where an eccentric load is applied [57].

If the load is caused by masses of several objects, the center of mass $(r_{CM,x})$ has to be calculated and then the equation for the eccentricity can be expressed as

$$e = r_{CM,x} + \frac{h}{2} \tag{3.7}$$

where h is the height of the beam's cross-section, as demonstrated in Figure 3.3.

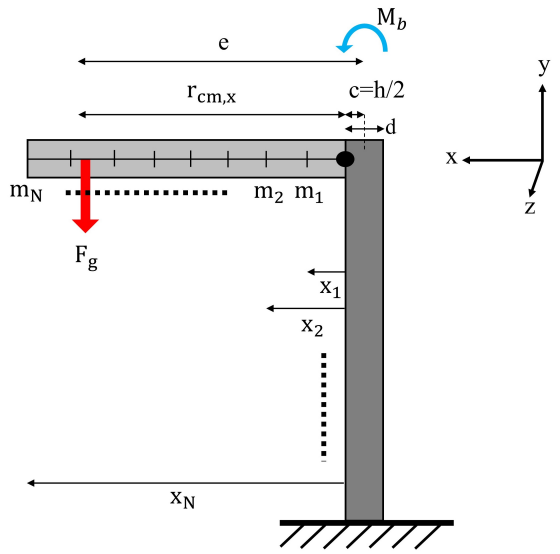

Figure 3.5: Bending moment diagram.

The maximum bending stress that a column needs to withstand in order to provide sufficient resistance to a bending moment can be calculated as

$$\sigma_{max} = \frac{F}{A} + \frac{M_b \cdot c}{I} \tag{3.8}$$

as provided by [56], [57].

$\frac{F}{A}$ represents the stress due to compressive load [58] and $\frac{M_b \cdot c}{I}$ the stress due to bending [54], [56] [57].

A is the cross-sectional area of the profile, c the perpendicular distance from the neutral axis to the farthest point on the section, I is the moment of inertia of the cross-sectional area about the neutral axis, and M_b is the internal bending moment (bending moment) about the neutral axis of the cross-section [57].

The moments of inertia ($\bar{I}$) of common cross-sections can be found in textbooks [57], [59], [60].

3.5 Torque tolerance

When designing a test rig that should replace the body of a human test subject, as is done in this thesis project, it is important to consider its torque tolerance. The torque tolerance of joints that have one end fixed and the other free, with loading on the free end, can be calculated as

$$\tau = F_g \cdot r_{CM,x} \tag{3.9}$$

where F_g is the load and $r_{CM,x}$ the center of mass as demonstrated in equation 3.3 [61].

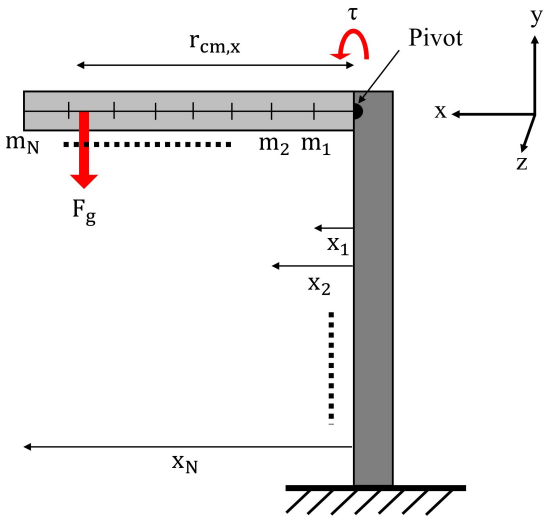

Figure 3.6: Torque calculations.

4

Methods

This chapter serves as an extensive examination of the methodologies employed in the thesis. It comprehensively outlines the entire process undertaken, such as the establishment of initial assumptions that formed the basis for selecting components for the Test System.

4.1 Investigation of the state of the art

The work on this thesis started with an initial phase including a literature review. The review focused on three aspects; state of the art testing systems for AL control, state-of-the-art EMG simulation systems, and state-of-the-art physical mounting rigs for ALs. The investigation of the state of the art was based on a literature search in the databases of IEEExplore [62], PubMed [63], Web of Science [64], Chalmers Library [65] and Google Scholar [66]. The main keywords that were used include; *bone anchor, osseointegrated, AL control, test systems, electromyography, EMG simulator, EMG simulation, test rig, validation, verification*. The results of the investigation can be seen in section 2.3.

4.2 Design requirements

Design requirements in Table 4.1, including technical requirements in Table 4.2, were obtained through consultation with the project supervisor who is an employee of the company the thesis was conducted at. Requirements were different depending on each of the four parts of the larger ALC test system project, parts one and two are the scope of this thesis project (EMG simulation and a test rig) but parts three and four (AL control validation and artificial sensory feedback) were kept in mind during the whole design process.

In the investigation for components of the Test System, these requirements were kept in mind along with the implementation time needed. Therefore, the shipping time of components also influenced the component selections.

Firstly, the company the thesis is conducted at expressed the need for the Test System to be transportable and adaptable for various locations, emphasizing the importance of portability. This feature can prove beneficial in optimizing office space utilization and storage, as well as allow the Test System to be used in, for example, conferences and expos for demonstration purposes. This includes ease of attachment and detachment from the table the Test System is mounted on as well as the Test System being lightweight.

The e-OPRA's abutment and abutment screw need to be easily removable and attachable from the Test System. This is to allow for easy replacement in case of a broken component.

The electronics of the Test Device need to be easily accessible to the user of the Test System. This is required for the user to be able to use an oscilloscope or do minor changes on the Test Device when necessary without having to disassemble the Test System.

Table 4.1: Test System design requirements.

Requirement	**Description**	**Part**
Portable	Movable table attachment and not too heavyweight, for ease of use	2
Replaceable abutment	In case the abutment breaks, it can be replaced to extend the Test System's service life	2
Electronic accessibility	To be able to access the electronics on the rig to use an oscilloscope for testing	1, 2
Budget of 25 000 SEK	A budget set by the company the thesis is conducted at	All parts

Part 1: Test Device (EMG simulation), part 2: Test Rig

4.2.1 Technical requirements

All of the technical requirements that are needed to fulfill each part of the project can be seen in Table 4.2.

The 16 analog output channels of the Test Device are needed in order to send out the recorded EMG data of each of the 16 EMG electrodes of the e-OPRA simultaneously. Similarly, the six analog input channels are needed for part two to be able to read the six channels of AL control data that the ALC sends to the AL.

The ALC samples data with a resolution of 16 bits. Therefore, to be able to transmit a recorded signal to the ALC without distortion and without having to scale the signal, a requirement was made for the Test System to approximately match this resolution.

The pre-recorded EMG signals that are to be sent to the ALC through the Test System have been sampled with the frequency of 500 - 1 000 Hz by the ALC. Therefore, the sampling frequency requirement of the Test System is set at 1 kHz or more per channel (16 kHz in total) to match that.

Regarding the input voltages, the Test Device needs to tolerate and be able to read signals of 0-3.3 V and ± 8 V for the AL control data and the neurostimulation data from the ALC, respectively.

The EMG signal recordings are to be sent to the Test Device from a computer and they communicate via a USB interface [49]. This is to allow the user to easily use new recordings simply by having them in a folder on their computer. In part two, the ALC outputs the AL control data via a serial UART interface. Therefore, the Test Device is required to be able to communicate both with a USB and a UART interface. To accomplish this, protocol conversion between USB and interfaces such as SPI or I^2C might be needed, since these are some of the most common interfaces that peripheral devices use [67], [68].

The Test Software should have a user-friendly interface that is compatible with Windows 10 or 11 since these are the operating systems used in the company the thesis is conducted at. It needs to be written in the programming language C/C# on a .NET developer platform. This will simplify the Test System usage and ensure compatibility with the ALC software, which is also written in C# on the .NET platform.

The Test Software should be able to read in files of the type .mat. This is due to the fact that the EMG and the neurostimulation data recordings are saved in this format, and for ease of use, requiring manual file type conversion from the user should be avoided.

For the physical Test Rig, the main requirement is for it to be able to bear the ALC and an artificial arm. Robotic artificial arms weigh on average 1.2 kg [69], therefore an assumption was made that the ALC and artificial arm weighed approximately 2 kg and there is a 3 kg test object in the hand of the artificial arm. This weight distribution assumption is done to ensure that the Test Rig can effectively accommodate a wide range of artificial arms, irrespective of their weight distributions.

The lockable joint of the Test Rig is required to have at least one Degree of Freedom (DoF) and a movement range of 45° up and 80° down from the horizontal plane. This is to allow for testing of the ALC with an artificial arm in different positions.

Table 4.2: Test Device and Test Rig technical requirements.

Requirement	Value	Part	Reason
Channels	16 analog output, 6 analog input	1, 3	For EMG signals, for AL control data
Resolution	12 bits or more	1	Accommodates for realistic epimysial EMG signal to noise ratio [70] and produces a low least significant bit voltage for clear $\pm$5 mVpp EMG signal output [71]
Sampling rate	1 kHz or more per channel	1	To match the sampling rate of the ALC
Input voltage	0-3.3 Vdc, $\pm$8 Vpp	3, 4	Output voltage from the ALC for the AL control and neurostimulation, respectively
Interfaces	USB, Serial UART	1, 3	To communicate with the computer and the ALC, respectively
Software	User interface: Compatible with Windows 10/11, C/C#, .NET	1	To enable control of testing via a computer for the user, for compatibility with ALC
Playback support	File type .mat	1	To send EMG signal and neurostimulation recordings to the ALC
Grounding the abutment	—-	1	Emulate grounding by the bone of an amputee
Weight-bearing capacity	min. 5 kg	2	To carry seven components - a 3 kg test object, an artificial arm, wrist and elbow, the ALC, and the e-OPRA.
Lockable joint	1 DoF and 125° range	2	Facilitates testing of the ALC with an artificial arm in different positions

1: part 1 - Test Device (EMG simulation), 2: part 2 - Test Rig

4.3 Workflow

After the initial phase (the literature review), the workflow of this project (seen in Figure 4.1) is structured into three sections; the Test Software, the Test Rig, and the Test Device. The work on the Test Device will be done first since the decisions connected to it and the electronic design will affect the Test Software and the Test Rig. The other two parts were worked on simultaneously at the end of the Test Device part.

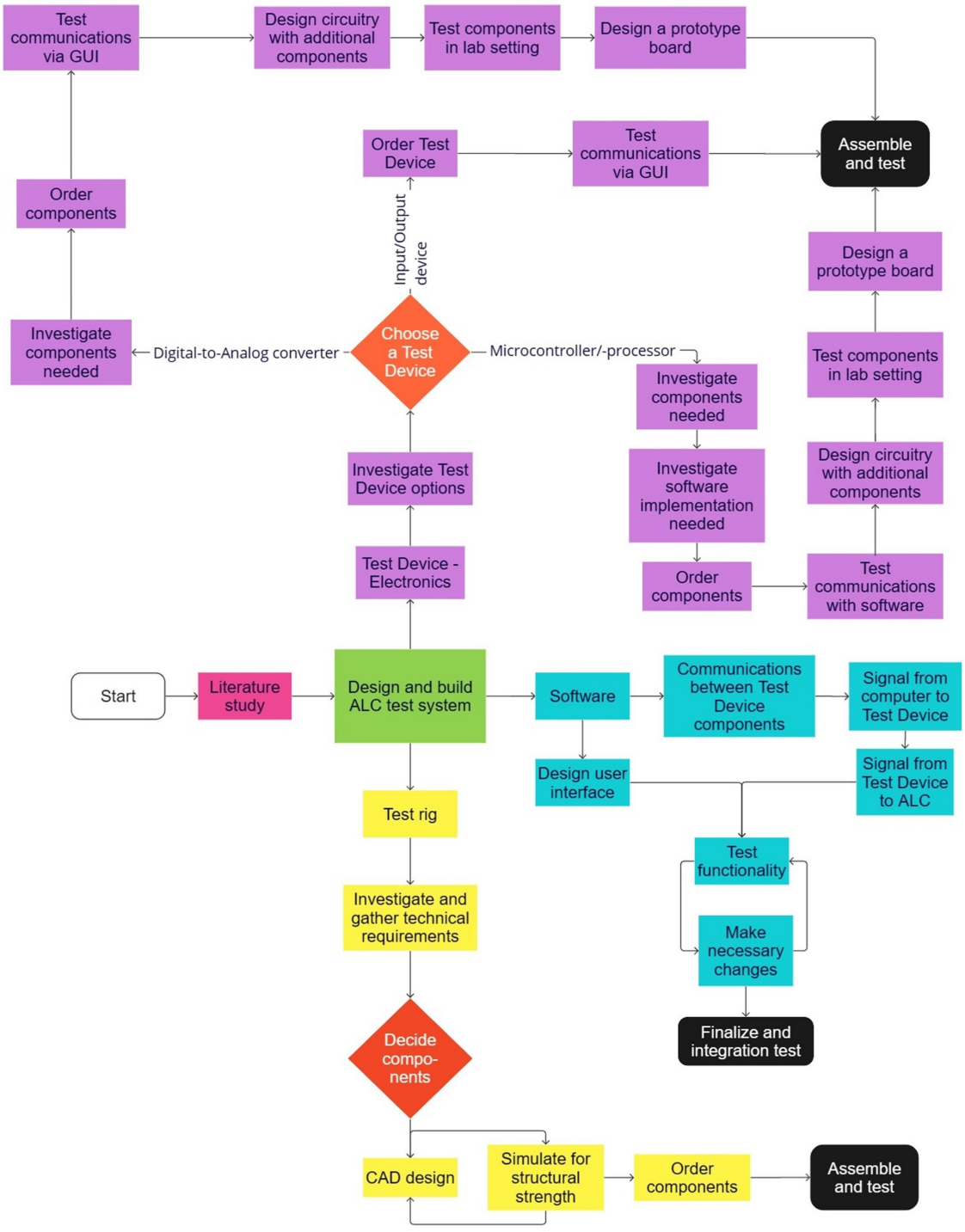

Figure 4.1: The workflow of the project. Blue: Test Software, purple: Test Device, yellow: Test Rig.

4.4 Test Device

A thorough investigation went into finding a device that fulfilled all of the technical requirements in Table 4.2. The investigation involved researching online retailers and manufacturers of electrical components and communicating with companies such as DigiKey, Texas Instruments, AD Instruments, RS Components, and National Instruments.

The primary factors considered in the investigation for the components of the Test Device were the technical requirements in Table 4.2, the budget of 25 000 SEK, and an estimated implementation time.

4.4.1 Main Test Device component investigation

The options were to create a Test Device using a microcontroller or -processor like an Arduino or Raspberry Pi, use an off-the-shelf I/O device, or create a custom signal generator and acquisition system. [72].

Three devices from Texas Instruments were deemed the most promising as the main component of the Test Device and therefore investigated more thoroughly. These are the AMC7836EVM [73], the DAC81416EVM [74] and the Tiva EK-TM4C123GXL [75], and their comparison with the technical requirements of the Test Device in mind can be seen in Table 4.3.

As visible in the table, the DAC81416EVM was the only component that fulfilled all technical requirements set for part one of the final test system, and thus, based on this comparison, it was chosen as the main component.

Table 4.3: Comparison of three options for the Test Device main component [73]–[75]. The grey color represents the aspects where the requirements for part one of the final test system have been met.

Requirement	**Required value**	**AMC7836**	**DAC81416**	**EK-TM4C123G**
Analog channels	16 output (part 3: 6 input)	21 input and 16 output	16 output	12 input
Resolution	12 bits or more	12 bits	16 bits	12 bits
Output voltage	±5 mV or more	0-5 V	±2.5 V	no outputs
Sampling frequency	16 kHz or more	87 kHz	83 kHz	125-1 000 kHz
Input voltage	(part 3: 0-3.3 V, part 4: 0-8 V)	±12.5 V	No inputs	-0.3 Vdd to 5.5 Vdd
Sofware compatibility	Windows 10/11	Windows XP and 7	Windows XP and newer OS	Windows XP and newer OS
Communication interfaces	USB, SPI (part 3: UART)	USB (provided by SM-USB-DIG), SPI	USB (provided by USB2ANY), SPI	UART, USB, SPI (firmware support needed)
Cost	Under 25 000 SEK	2 139.42	1 045.76	179.36

4.4.2 Digital-to-analog converter option

During the investigation of the Test Device components, it became clear that the Test Device, when using the DAC81416EVM [74] as its main component, needs to be an assembly of multiple devices - the DAC81416EVM, an interface adapter, attenuators, and a power unit. The interface adapter is needed since the Test Device should be controlled from a computer that communicates via the USB interface [49], and the DAC only communicates via the SPI bus [74]. Both of these interfaces are explained in more detail in section 3.3.

4.4.2.1 Assessing interface adapter options

The investigation of interface adapters that could facilitate communication between a USB and an SPI interface resulted in two different devices being ordered and tested for this purpose - the USB2ANY interface adapter from Texas Instruments [76] and the Tiva

series EK-TM4C123GXL board also from Texas Instruments [75].

Both of these devices were tested together with the DAC as well as the Test System software to validate their functionality and speed. The testing involved sending a sine wave through one channel, then through all channels, and finally sending an EMG recording through all channels. The sampling times of the interface adapters were observed on an oscilloscope and recorded.

4.4.2.2 Attenuators

The DAC's lowest voltage output is $\pm$2.5V and the ALC's maximum input voltage is $\pm$5mV, therefore, attenuators are needed to reduce the output voltage of each of the DAC analog output channels to a level that can be safely inputted to the ALC.

Both voltage divider circuits and inverting amplifiers, as described in section 3.2 were tested in a laboratory setting on a breadboard with a power supply, multimeter, suitable resistors, and an operational amplifier that functions with the input voltage of 2.5 V. The resistors to be used were determined by choosing the resistance of R_2 and calculating R_1 with equations 3.1 and 3.2 for the voltage divider and the inverting amplifier, respectively.

4.4.2.3 Power unit and connecting to Tiva

The Test System needed to be portable, so a simple and lightweight power unit was needed to deliver power to it.

The DAC needs four DC voltage levels as well as the ground as an input [74]. The four input voltages and their tolerances are V_{CC} at 9-41.5 V, V_{SS} at -21.5-0 V, V_{AA}/V_{DD} at 4.5-5.5 V, and V_{IO} at 1.7-5.5 V [74]. Therefore, the power unit had to be able to regulate the voltage amplitude to all these levels.

One option was to use a simple AC/DC adapter as a power source of the positive voltage V_{CC} at 12 V. The exact amplitude of 12 V was chosen since adapters providing this amplitude were on hand within the company. AC/DC adapters are commonly used for peripheral devices, and they can take in AC voltage from a wall plug and supply a DC voltage of a determined amplitude between zero and twice the input AC voltage [77]. There are also AC/DC adapters for sale that can provide both positive and negative DC voltage outputs simultaneously, but mostly at a very high price compared to single output adapters [78].

With the 12 V provided by the 12 V adapter option, a linear voltage regulator such as the L7805 from STmicroelectronics could be used to achieve the amplitude of 5 V [79]. Linear voltage regulators can provide a regulated DC voltage of a specific positive amplitude that is lower than the amplitude of their input voltage [80].

When using the DAC to give a bipolar voltage level, such as $\pm 2.5V$, as an output, the voltage input of V_{SS} needs to be negative and cannot be connected to ground (0 V) [74]. Thus, if a single positive-output voltage adapter was to be used, a switching voltage reg-

ulator, or a DC/DC converter including one, such as the TMR 1-1222 from Traco power [81] was needed to achieve the negative amplitude of -12 V. Switching voltage regulators are able to supply an output voltage that has a greater amplitude and, in some cases, opposite polarity in comparison to their input voltage [82]. In addition to providing the -12 V output, this specific DC/DC converter could also regulate the positive output of 12 V [81].

Another option for the power source was using simple DC voltage batteries. Two 12 V batteries could be connected in series and the middle terminals, connected together, used as a ground. This circuit would then provide the voltage outputs of 12 V and -12 V. The L7805 linear voltage regulator could then be used to achieve the 5 V output.

Once the components of the power unit were chosen they were soldered on a prototype board and the components for connecting the DAC to the Tiva were soldered onto the same board.

4.4.3 The test Omnetics connector setup

A test Omnetics connector was used to enable access to the ALC. This test Omnetics connector reads the outputs of the 16 channels from that DAC81416EVM and sends them to the ALC. The mating part for the Omnetics connector was acquired from a third party. Wires were then connected accordingly.

4.4.4 Grounding of the abutment and ALC

The abutment and ALC need to be grounded to ensure a realistic emulation of an OIS in an amputee. The bone grounds the abutment when implanted into the amputee [83], but in the Test System, this needs to be done manually. This grounding needs to be a common ground with the Test Device to prevent any signal distortion [83]. Available components at the lab were used to assemble a ground wire for this purpose.

4.4.5 Test Device casing

A housing enclosure, casing, was required for the Test Device to safeguard the vulnerable internal components and facilitate a secure attachment to the Test Rig. In addition to its functional benefits, the Test Device casing also serves to enhance the visual appearance of the Test Device, projecting a more polished and sophisticated image.

To ensure ease of use and accessibility, two key requirements were identified: the ability to disconnect and connect the test Omnetics connector and the capability to read signals

with an oscilloscope without opening the Test Device casing.

The Test Device casing was made in Fusion 360 [84]. Measurements were made of the assembled Test Device and the Test Device casing was sized after those. The gaps were then added accordingly.

4.5 Test Rig

To begin the designing process of the Test Rig, some assumptions were made to estimate conservative tolerance requirements to aid with component selection. This chapter will go into how each of the components of the Test Rig was chosen.

The choice depended on the Test Rig's design requirement as described in section 4.2. The components of the Test Rig are the skeleton, the lockable joint, the table attachment, and the attachment for the abutment. The ALC then connects to the abutment.

Once the components were chosen, a 3D design of the assembled Test Rig was sketched in Fusion 360 [84] and stress simulations were performed to ensure that the design met the technical requirements before proceeding with the order placement.

4.5.1 Skeleton: Estimating maximum bending stress and assessing component strength

Mechanical engineers within the company the thesis was conducted at were consulted for component decisions of the skeleton.

Initial assumptions were made to acquire a conservative value for the maximum bending stress ($\sigma_{max,e}$) the horizontal and vertical part of the skeleton would need to tolerate using equations 3.5 and 3.8. This value then served as the minimum bending stress tolerance for the components that were to be used for this application.

For simplification, an artificial arm along with the ALC, the lockable joint, and all other components forming an arm were regarded as a cantilever beam (described in section 3.4.1) and the vertical part of the skeleton as a column. Additionally, to further simplify the analysis, it was assumed that the cross-sections of the components were symmetrical.

The cantilever beam under consideration in this project is composed of several components therefore the center of mass had to be estimated using equation 3.3 with the origin being by the column. To ensure a safe estimate and simplify calculations the center of mass of each component of the cantilever beam was estimated to be at its furthest end from the column. The first step was to estimate the total length of the cantilever beam by using dimensions of body segments in relation to the height of the human body as demon-

strated in [85]. A conservative estimate was made by assuming a relatively high human body height resulting in a cantilever beam length of L_e. Some of the components of the cantilever beam have their lengths and weights available in their respective data sheets [86]–[88], while others needed to be determined through further design. Therefore, the next step was to estimate the lengths of the unknown components by subtracting the summarized lengths of the known components from the exact estimated total length of the cantilever beam (L_e). Then the height of the cross-section of the column was estimated as h_e to get an estimated value for the eccentricity e_e.

The final step for acquiring a conservative estimate for the center of mass was to estimate the weight of the unknown components to acquire an estimated m_{ie}. The weights of the unknown components were estimated using the weight-bearing capacity requirement of the Test Rig seen in 4.2.

The estimated conservative value for the bending moment was then found using these assumptions and equations 3.4 and 3.6.

With the assumption that the cross-section of the column is square, A_e and I_e in equations 3.5 and 3.8 could easily be estimated and therefore an estimated maximum bending stress for both the column and the cantilever beam could be acquired.

To obtain the allowable bending stress of the components under investigation, data from a catalog [89] and planning software for assembly systems known as MTPro [90], provided by the manufacturer, were employed.

For the components to work for this application the conservative estimated value for the maximum bending stresses had to be within the allowable bending stress limit of the component selected [89] which can be observed in [89].

The structural strength of the components chosen was verified with simulations in Fusion 360 [84] and physical testing.

4.5.2 Lockable joint: Determining minimum torque tolerance and Identifying suitable joint options

Websites of structural system suppliers and mechanical component suppliers such as [91]–[96] were investigated to find a suitable lockable joint for this application. These websites were found by mainly using the keywords *"lockable joint", "2 DoF joint"*, and *"heavy duty joint"*.

The consideration of torque tolerance for the lockable joint was necessitated by the technical requirements of lockability and weight-bearing capacity.

Therefore, a conservative value for the torque tolerance was made using equations 3.9 and

3.3 which served as the minimum torque tolerance for the joints that were investigated for this application. The steps for acquiring the estimated value for the center of mass ($r_{CM,xe}$) and the load (F_{ge}) can be found in section 4.5.1.

The same steps were followed for this part except the origin was from the pivot of the lockable joint instead of the column and the pivot was assumed to be in the middle of the lockable joint.

A few promising options for the lockable joint were found using the estimated torque tolerance, seen in Table 4.4.

Table 4.4: Lockable joint options.

Option	Name	DoF	Torque	Total cost	Location	Source
1	Incremental angle hinge	1	135.58 Nm	1966 SEK	USA	[97]
2	Incremental angle hinge (square)	1	50 Nm	1005 SEK	USA	[98]
3	Heavy duty alloy steel locking hinges - 2 round armatures	1	135.58 Nm	2529 SEK	USA	[99]
4	Kupo EZ Grip Twins KCP-320	2	10 Nm	688 SEK	Sweden	[100]
5	Lockable Swivel Joint Bosch Rexroth	1	100 Nm	1317 SEK	UK	[101]

4.5.3 Table attachment: Exploring solutions

The Test Rig was required to be portable and adaptable to tables of varying dimensions. As such, the table attachment needed to be lightweight and compact. Various solutions were explored, including the use of a bottom plate along with suction cups and clamps by investigating the websites of manufacturers of industrial equipment and supplies such as [91], [93], [95]. Keywords for this investigation were mainly *"suction cups", "heavy duty suction cups", "clamps", "heavy duty clamps", "industrial clamps", "bottom plate"*, and *"support plate"*. Custom designs for retractable legs were also explored.

The table attachment was required to support the Test Rig when utilizing an artificial arm, therefore an estimated value for the load it needed to sustain was calculated.

A simple force diagram can be seen in Figure 4.2. In this diagram, F_A is the force created by the weight of the horizontal components of the Test Rig (the cantilever beam), located at their common center of mass at $r_{cm,x}$. The center of mass was calculated with equation 3.3. F_C indicates the force that the table attachment causes on the system, and l_C its location on the x-axis. F_h is the force created by the mass of the vertical column of the Test Rig and F_p by the mass of the plate the Test Rig is mounted on. M is the moment around the pivot point of the whole Test Rig.

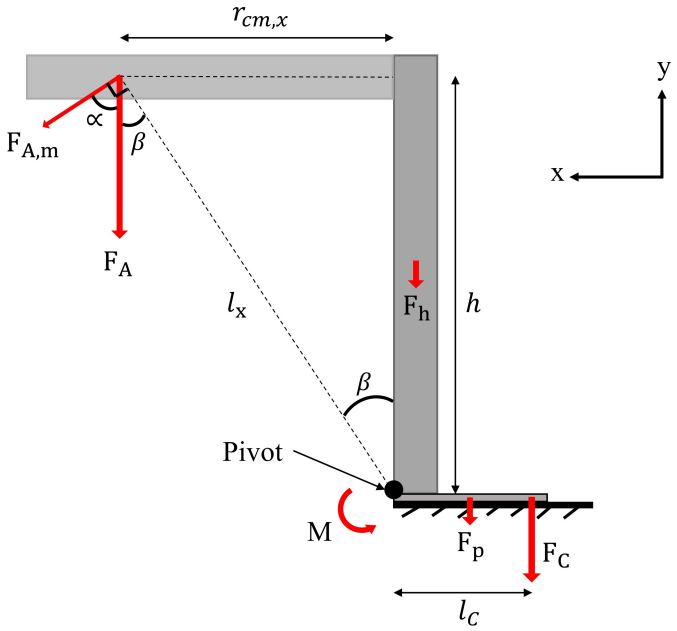

Figure 4.2: The force diagram used to calculate the table attachment force F_C.

To calculate the force the table attachment needs to create for the system to be stable, Newton's laws of motion, Pythagorean theorem, and sine laws were used. Essentially, for the system to be stable, the moment M needs to be zero.

Since the Test Rig is supposed to be lightweight, the forces F_h and F_p were considered negligible. In addition, as they create a moment in the same direction along the pivot point as the force F_C, disregarding them leads to the most conservative estimate of F_C.

With the values of F_A, $r_{cm,x}$, and h known, either the length l_C or the force F_C could be chosen, and the other one of them calculated. The equation for the moment M becomes

$$M = F_A cos(\alpha) \cdot l_x - F_C \cdot l_C = 0.$$

If the length l_C is known, the force F_C can be derived as

$$F_C = \frac{F_A cos(\alpha) \cdot l_x}{l_C} \tag{4.1}$$

where, according to Pythagorean theorem,

$$l_x = \sqrt{(r_{cm,x})^2 + h^2},$$

and according to sine rules,

$$\beta = arctan\left(\frac{r_{cm,x}}{h}\right)$$

and

$$\alpha = 90^\circ - \beta.$$

4.5.4 Abutment attachment

The abutment attachment piece was designed by mechanical engineers at the company where the thesis is conducted, and manufactured by a third party contractor.

The design inputs, including technical requirements, were given to the mechanical engineers through verbal and written communication.

4.5.5 Simulation test for the final Test Rig design

Static stress simulations were done in Fusion 360 on the final Test Rig design by applying a load at the conservative center of mass calculated in section 5.2.1.1 to evaluate the structural strength of the assembled Test Rig design. The screws and bottom plate were hidden in the Figure to allow for a better view of the stresses of the main components.

4.6 Test Software

Once the Test Device was designed and built, a software was needed to run the Test System from a computer. The Test Software in this project was written within the .NET Framework platform using the programming language C#. .NET is a developer platform from Microsoft, and it includes different libraries and tools to help with software development [102]. C# is a programming language that is supported on the .NET platform [102].

4.6.1 Setting up the Test Software

The work on the Test Software began with setting up a platform with a .NET framework on Windows. This was done in Visual Studio 2022 [103] by creating .NET framework solutions, first separate ones for different aspects of the Test Software and later a common one for the whole final version.

The first problem to solve was to find out how it is possible to read .mat-files into a C#-software. Third-party packages were investigated and one of them tested to import the EMG data file to the Test Software. To test this package, the .mat-file containing an EMG recording was read and printed as an output to the console.

4.6.2 DAC communications

After switching the USB2ANY to the Tiva as the interface adapter, the SPI communication was set up with firmware within the Tiva. This firmware was outsourced from Integrum. Afterward, a similar testing procedure took place as earlier when using the USB2ANY.

As both reading in the EMG data from the .mat-file and communicating with the DAC functioned properly, these two aspects were then combined and the EMG data streamed out through a DAC analog output channel. This was first done via one channel only, and afterward via all 16 channels simultaneously - each with data from the corresponding EMG recording channel.

4.6.3 Graphical user interface

A simple GUI was programmed for the Test Software to simplify its usage. This was done by creating a Windows forms app with the .NET framework in Visual Studio 2022 [103]. Windows Forms is a simple open-source UI framework that can be used to create simple GUIs [104]. The parts of the GUI were chosen and afterward, a function for each of them

was written.

4.6.4 The final steps

The final steps of creating the Test Software included making the code efficient with functions and different code files, as well as adding necessary comments to every part. In addition, a separate code file was created to store functions, and the main parts of the code were converted to clear functions in this file.

4.7 Testing the final Test System

Once all parts of the Test System were designed and built, the system was tested both separately and together with the ALC and an AL. This was done in a laboratory setting, both by simulating a sine wave as well as an EMG data recording through the whole Test System. Testing was made using the equipment seen in Table 4.5.

Table 4.5: The equipment used for testing

Part	Type	Equipment reference
Oscilloscope	MDO3014	[105]
Multimeter	Fluke 115	[106]
Digital hanging scale	Digital Hook Scale	[107]
Laboratory power supply	Keithley 2231A-30-3	[108]

4.7.1 Test Rig

The Test Rig was assembled as in Figure 5.15 and physical testing was done by applying a conservative load to it using a Digital Hook Scale from Biltema [107]. The conservative load (m), which should be applied at the end of the horizontal part of the Test Rig (r) (without anything attached to it), was calculated by utilizing the estimated conservative torque value (T_e) found in section 4.5.2, the torque equation 3.9 and Newton's second law.

After this initial testing, the ALC and its connectors, and an artificial arm were connected to the Test Rig. The TRs stability was observed, both when stationary as well as in movement created by the Test Software, Test Device, and ALC.

4.7.2 Evaluating the prototype boards

For evaluating the prototype boards some initial testing was made. The electronic components for the power unit and attenuators were assembled on a breadboard and connected to the DAC. A laboratory power supply was used to power the circuit, and the USB2ANY interface adapter was used to send a constant voltage of +2.5 V and -2.5 V with the DACs GUI into the DAC. Measurements were made and observed with a multimeter.

Once the power unit and attenuator circuits had been confirmed to work the prototype boards for the power unit and attenuators were then assembled on the DAC and the same steps as above were followed except the circuit was powered by an AC/DC adapter instead of a laboratory power supply.

4.7.3 Integration test for evaluating the Test Device and Test Software

The Test System was set up along with the abutment and ALC for evaluating the Test System. Both sine waves and two different recordings of EMG data were used in testing. Observations were made by comparing the original data of the two recordings plotted with MATLAB [109], and the output data of the Test System (recorded by the ALC).

4.7.4 Demonstration of the Test System with an artificial arm

After the integration testing, an artificial arm consisting of the DynamicArm Plus [88], the Electric Wrist Rotator [87] and the SensorHand Speed [86], all from Ottobock SE & Co. KGaA, was connected to the Test System. These components were selected based on their availability to the company. The whole assembly was left on a table overnight to further verify the structural strength of the Test Rig.

Afterward, to demonstrate that the Test System functions in combination with an artificial arm and the ALC, a simple simulation file was sent through the Test System, with the purpose of the ALC controlling each motor of the artificial arm to simulate the six possible movements of the artificial arm - elbow flexion and extension, hand opening and closing, and wrist pronation and supination. This simulation file contained six different channels, one programmed to control each of these six movements.

5

Results

This chapter describes the ALC Test System designed and built in this project in detail.

The Test system includes the Test Rig, the Test Device, and the Test Software as seen in Figure 5.1. The block diagram for an overview of the Test Software and Test Device can be seen in Figure 5.2 and the total cost of them can be seen in Table 5.1 along with applicable weights and sizes.

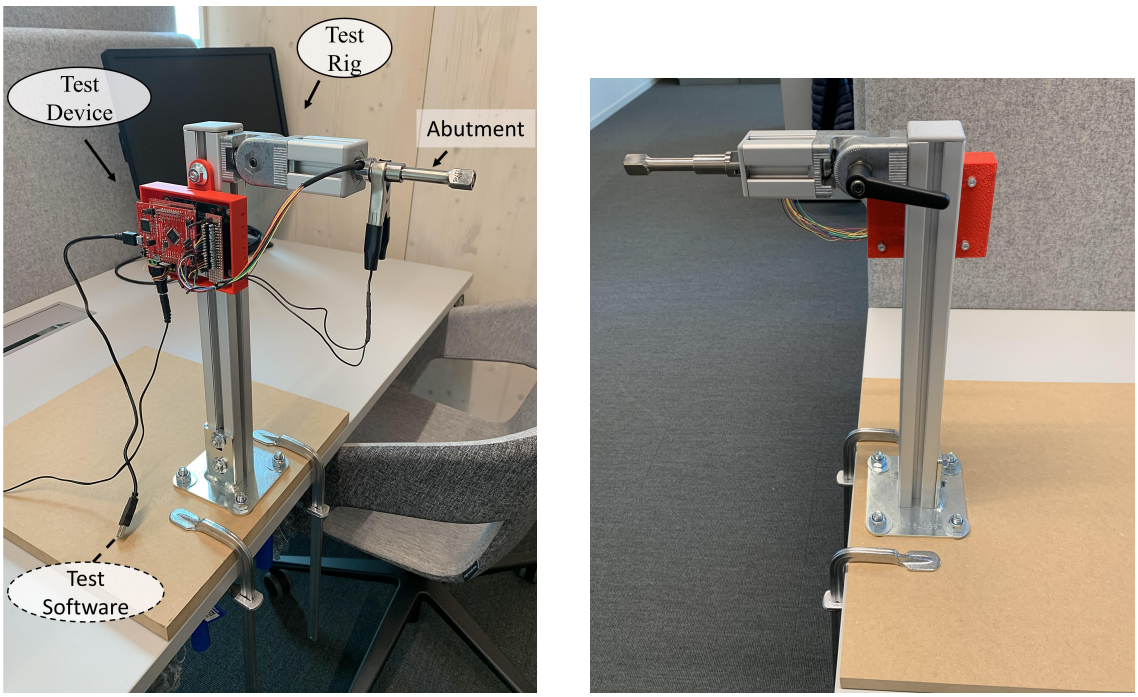

(a) **(b)**

Figure 5.1: The assembled Test System with the abutment attached. (a) Front view. (b) Back view, showing the clamping lever for the lockable joint.

Table 5.1: Parts of the Test System with their sizes, weights, when applicable, and functions.

Part	**LxWxH [mm]**	**Weight [kg]**	**Cost [SEK]**	**Function**
Test Rig	427x400x400	4.66	6497	For mounting an assembled artificial arm along with the ALC and allows testing of it in different positions
Test Device (incl. Test Device casing)	102x84x55	<0.2	1540	Electronics that provide EMG signals to the ALC without the use of a human subject to test the artificial control and allows for future installments for testing the neurostimulation
Test Software	—-	—-	0	Controls the communication between the computer and the Test Device
Total		< 4.86	8037	

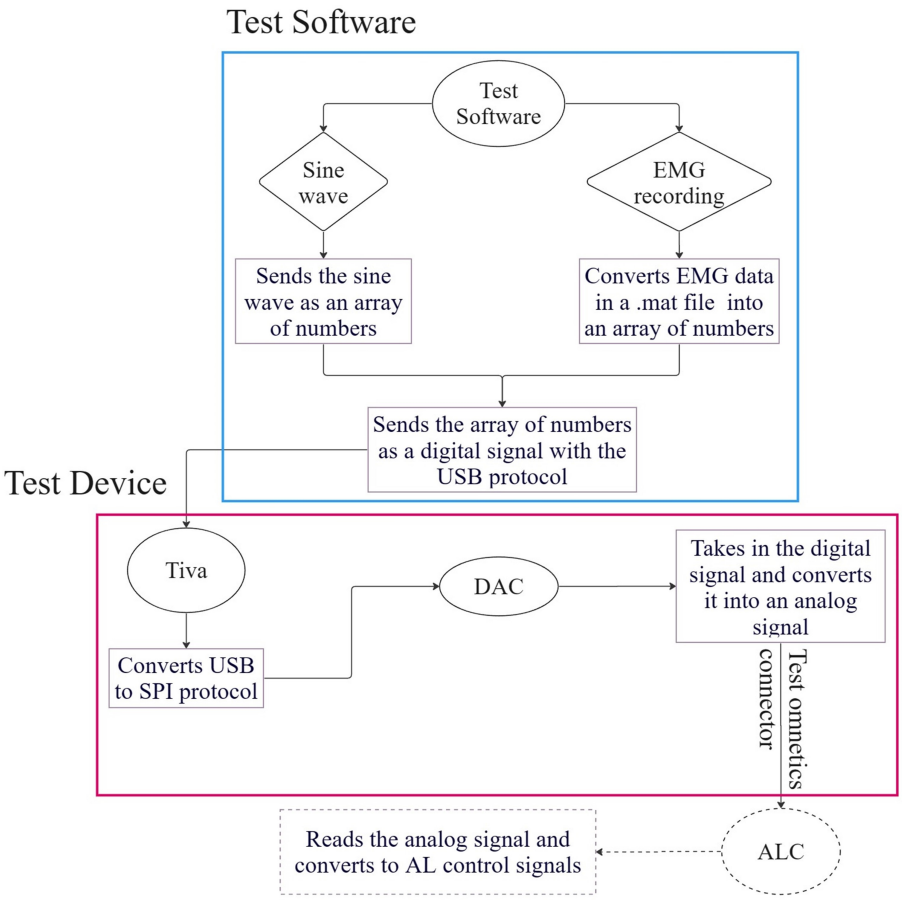

Figure 5.2: The data transmission through the to the ALC.

5.1 Test Device

The Test Device (seen in Figure 5.3) is an assembly of multiple electronic devices; a power unit consisting of an AC/DC power adapter and two voltage regulators (one linear voltage regulator and one DC/DC converter functioning as a switching voltage regulator), the Tiva board EK-TM4C123GXL (Tiva) [75] from Texas Instruments used as the interface adapter, the DAC81416 [74] from Texas Instruments, and attenuators consisting of two-resistor voltage dividers for each DAC analog output channel. Table 5.2 summarizes all components in the Test Device, their function, and cost.

The block diagram shown in Figure 5.4 gives a comprehensive view of the power and data transmission of the Test Device. The circuit schematic for the Test Device can be seen in Figure 5.5 and the design used for the prototype boards in Figure 5.6.

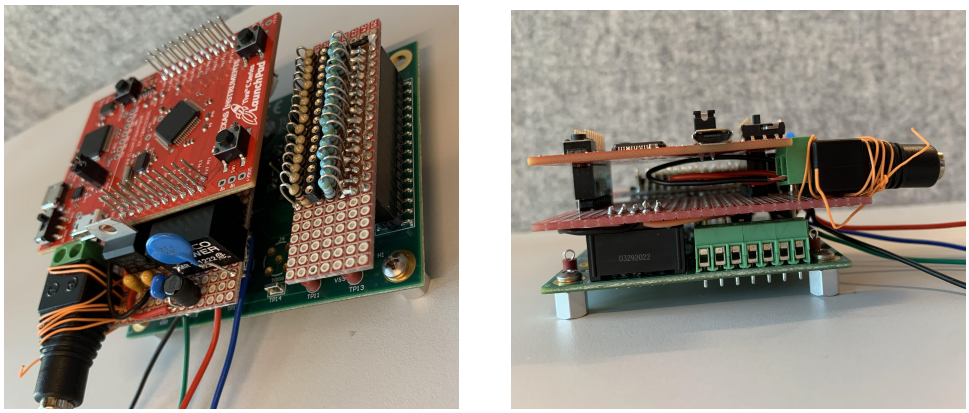

(a) **(b)**

Figure 5.3: The assembled Test Device. (a) Isometric view. (b) Side view.

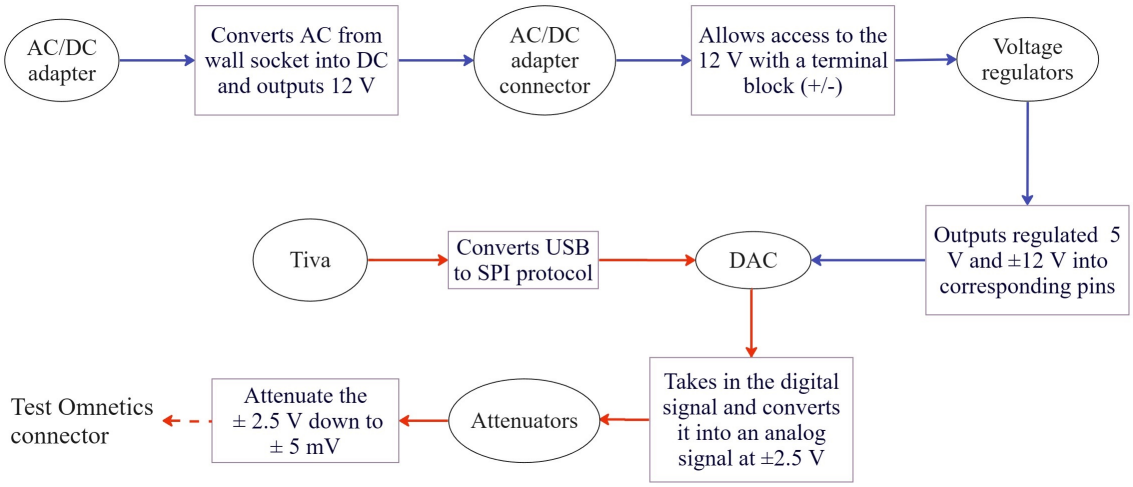

Figure 5.4: A more detailed block diagram for the Test Device, where the blue arrows show the power transmission and red the data transmission.

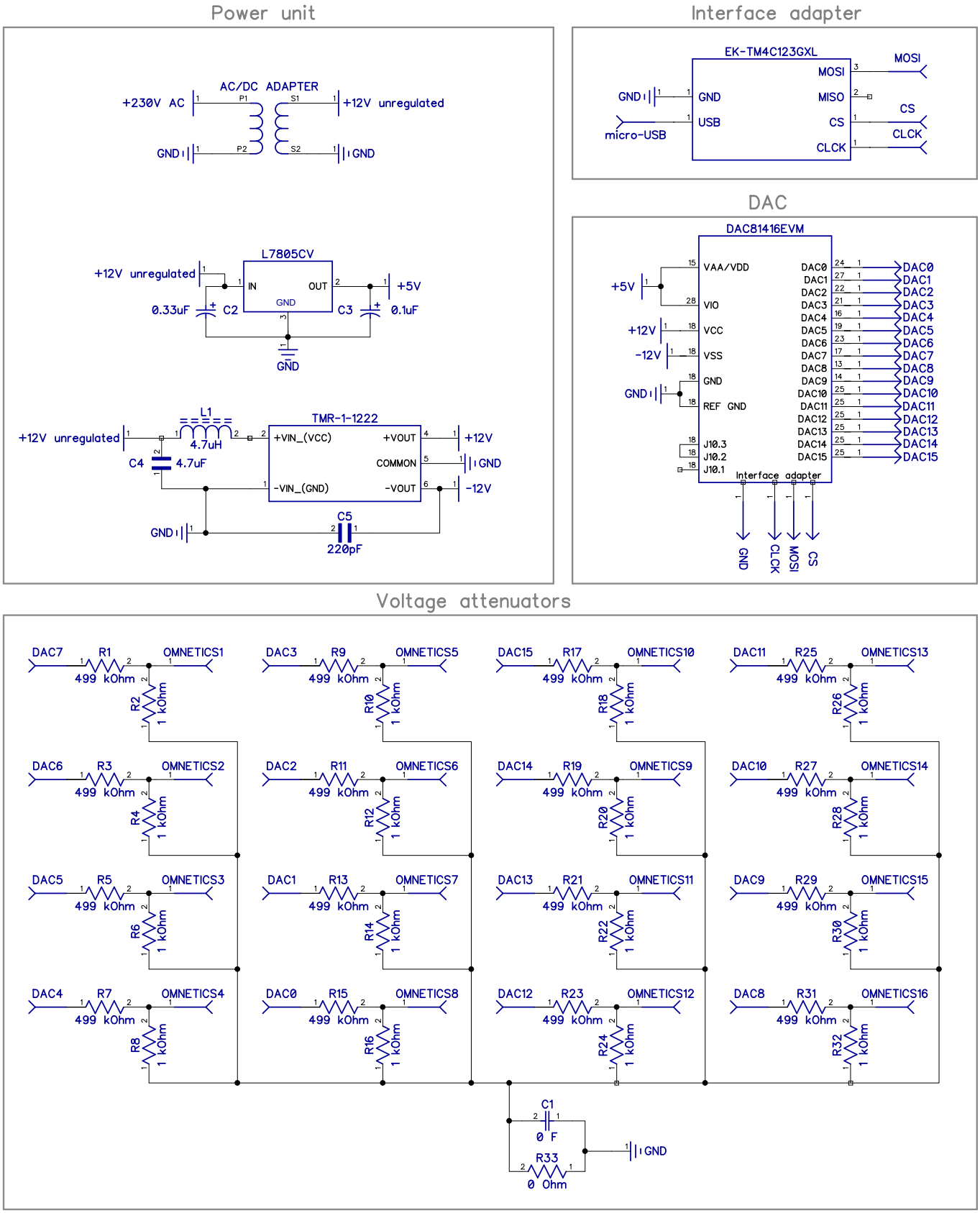

Figure 5.5: A schematic for the whole Test Device.

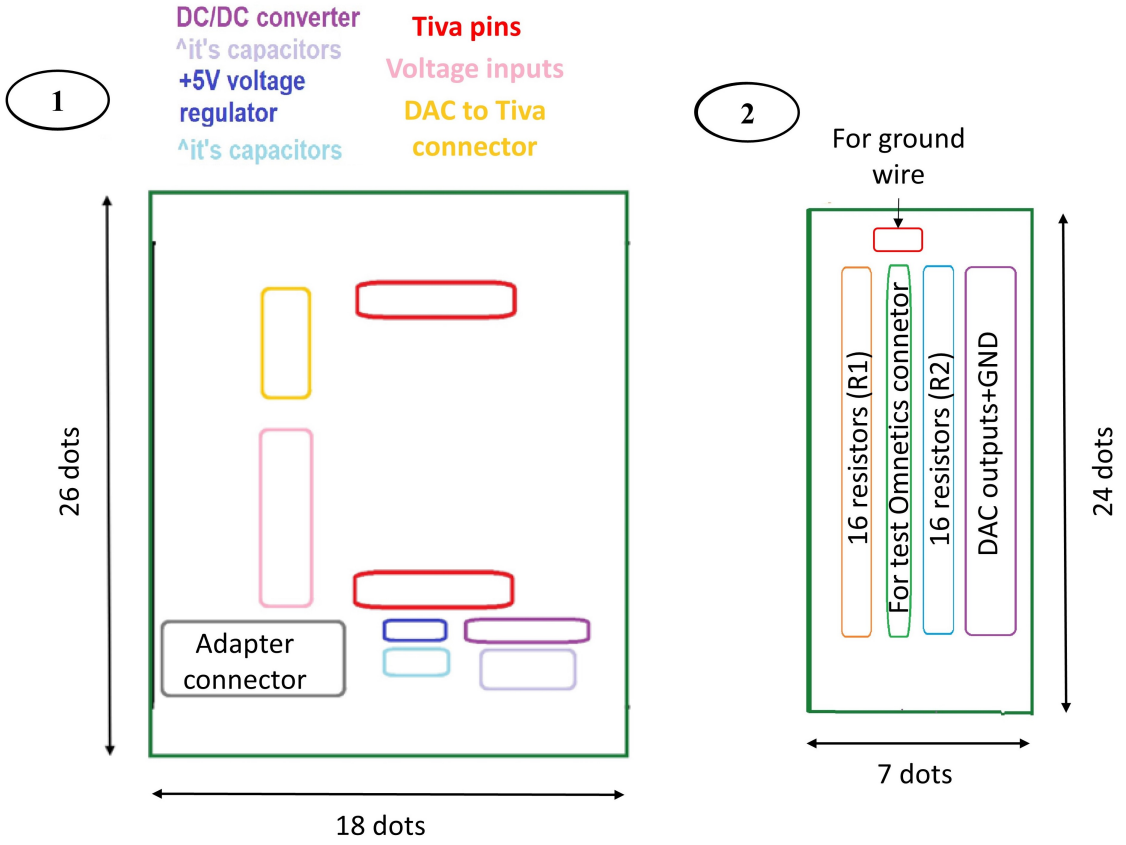

Figure 5.6: The prototype board design for the attenuators (1), power unit, and Tiva connections (2).

Table 5.2: Parts of the Test Device, their cost, and functions.

Part	**Component**	**Function**	**Nr.**	**Total cost [SEK]**	**Ref.***
Main component	DAC81416	Main component	1	1045.76	[110]
Interface adapter	Tiva EK-TM4C123GXL	Interface adapter	1	179.36	[111]
Power unit	TMR 1-1222	A DC/DC converter that has fully regulated dual outputs +-12V	1	114.74	[112]
Power unit	L7805CV	Linear voltage regulator that outputs +5V	1	7.11	[113]
Power unit	AC/DC adapter connector	For connecting the AC/DC adapter to the prototype board of the Test Device	1	20.6	[114]
Attenuators	Resistors, 499 kΩ	For the voltage dividers (R_2)	16	8.1408	[115]
Attenuators	Resistors, 1 kΩ	For the voltage dividers (R_1)	16	5.0752	[116]
Power unit, attenuators	Prototype board	To solder electronic components on, pad per hole	1	92.19	[117]
Power unit	Capacitor, 0.1 uF	For +5V voltage regulator circuit	1	4.635	[118]
Power unit	Capacitor, 0.33 uF	For +5V voltage regulator circuit	1	5.047	[119]
Power unit	Capacitor, 4.7 uF	For $\pm$12 V voltage divider circuit	1	6.335	[120]
Power unit	Capacitor, 200 pF	For $\pm$12 V voltage divider circuit	1	2.853	[121]
Power unit	Inductor, 4.7 uH	For $\pm$12 V voltage divider circuit	1	9.79	[122]
e-OPRA connection	Test Omnetics connector	Transfer data from Test Device to ALC	1	**	***
Connectors	Female connector 2x16	For DAC outputs	1	19.57	[123]
Connectors	Female connector 2x5	For DAC USB2ANY/TIVA connection	1	7.11	[124]
Connectors	Male connector 2x10	For Tiva	2	5.048	[125]
Connectors	Female connector 1x16	For the test Omnetics connector	1	6.4437	[126]
Ground wire	Female connector 1x1, two jump wires and conductive clamp	For grounding the abutment attachment piece and ALC	1	—-	****
Total				1539.8077	

**The references for the components*
***Cost included in the abutment attachment piece manufacturing (see Table 5.3)*
****Test Omnetics connector assembled by a third party and an engineer at the company the thesis was conducted at*
*****Made out of components available at the lab*

5.1.1 Digital-to-analog converter

DAC81416EVM [74] from Texas Instruments was chosen as the main component of the Test Device. It fulfills all the technical requirements needed for part one of the final test system. The DAC has 16 analog output channels and 16-bit resolution, and it can communicate via the SPI or I^2C interface [74].

5.1.2 Interface adapter selection and evaluation

To begin with, the USB2ANY interface adapter from Texas Instruments was used to communicate between the USB interface of the computer and the SPI interface of the DAC. However, this adapter had a maximum sampling time of 0.25 s in the communication when sending data through all 16 analog output channels of the DAC simultaneously. As can be seen in Figure 5.7, this caused a significant delay in the signal acquisition. According to the technical requirements, the sampling frequency of the Test System should be 1 kHz which corresponds to a sampling time of 0.001 s, calculated by using the Nyquist–Shannon sampling theorem

$$t_s = \frac{1}{f_s} \tag{5.1}$$

where t_s is the sampling time and f_s the sampling frequency.

Figure 5.7: The USB2ANY when sending the EMG data to all DAC channels simultaneously. The horizontal axis represents time, where each vertical dotted line marks 1.00 s. The purple plot is the data sent to the ALC through one DAC output channel. Each data point sent to the ALC can be visualized as a level change on the plot, happening approximately every 0.25 s.

Using the Tiva as the interface adapter, the communication was much faster with a sampling time of 0.001 s when simulating with EMG data with a sampling frequency of 1 000 Hz, which is correct according to equation 5.1. The acquired signal through an oscilloscope and its sampling time can be seen in Figure 5.8.

As the sampling time achieved with the USB2ANY was significantly higher than with the Tiva, a decision was made to use the Tiva as an interface adapter.

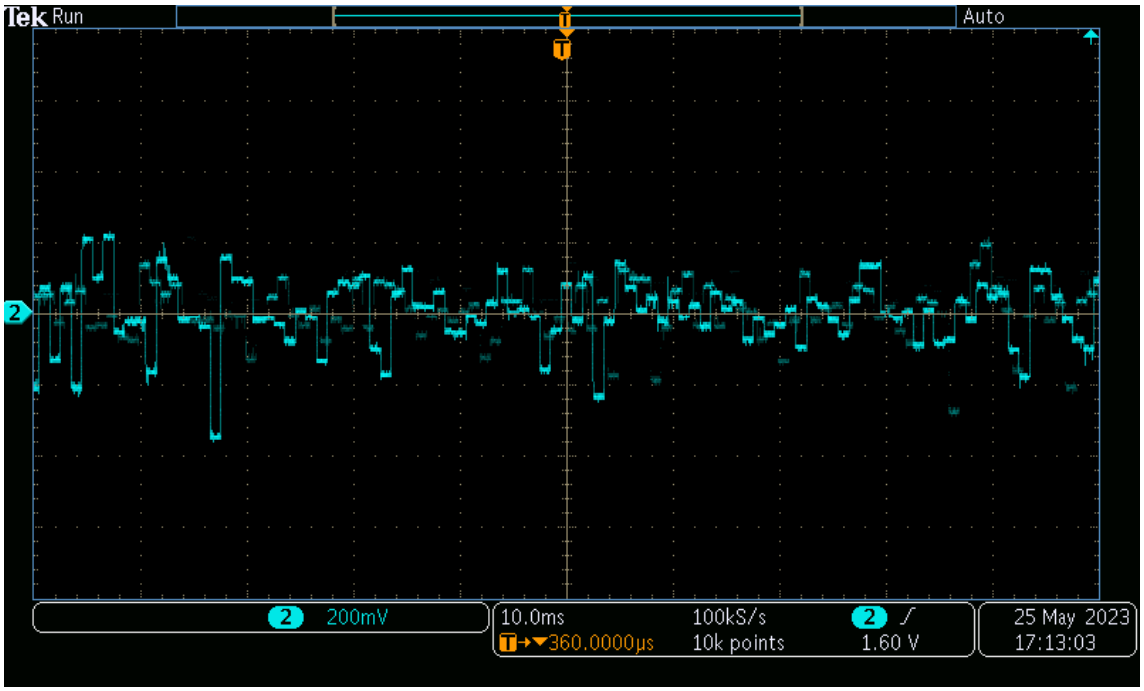

Figure 5.8: The Tiva when sending the EMG data to all DAC channels simultaneously. The horizontal axis represents time, where each vertical dotted line marks 0.01 s. The blue plot represents the EMG data sent to the ALC through one DAC output channel.

5.1.3 Power Unit and Tiva connection

The design of the prototype board for the power unit and Tiva connection can be seen in Figure 5.6 and the assembled prototype board in Figure 5.9.

The power unit of the Test Device consists of a 12 V AC/DC adapter, the voltage regulator L7805 [79] from STMicroelectronics, and the DC/DC converter TMR 1-1222 from Traco power [81]. The components needed for the power unit can be seen in Table 5.2. The circuit schematic of the power unit can be seen in Figure 5.5. The power unit circuitry is soldered on a prototype board which can be seen at the bottom of Figure 5.9.

The AC/DC adapter used in the power unit is a simple 12 V adapter from Hon-Kwang [127]. It connects to a wall socket and converts the AC voltage into a DC voltage of 12 V with a maximum current of 0.5A.

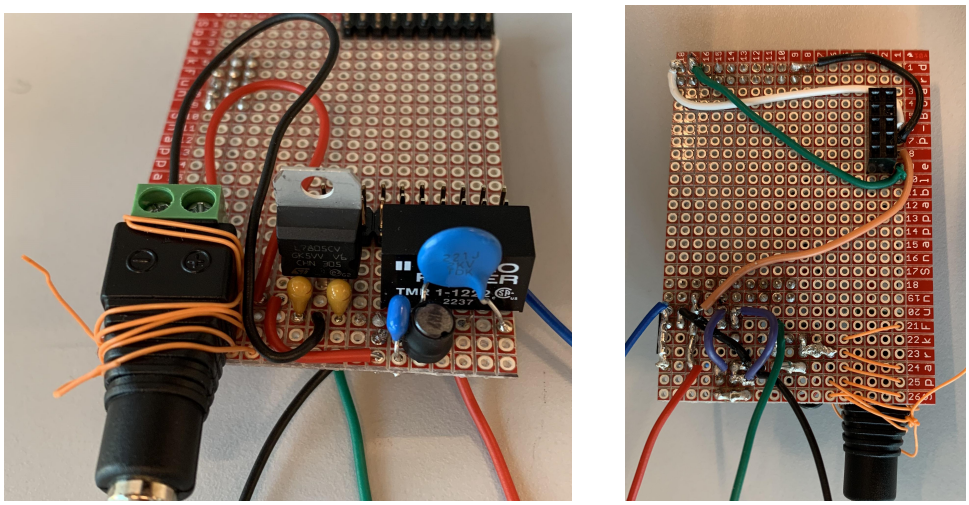

(a) **(b)**

Figure 5.9: The power unit and Tiva connection soldered on a prototype board. (a) The Power unit and Tiva pins behind it. (b) The back of the prototype board shows wire connections.

The voltage regulator L7805 and DC/DC converter TMR 1-1222 provide the DAC with regulated power inputs of 5 V and $\pm$12 V, respectively. The 5 V output is connected to the V_{IO} and V_{AA}/V_{DD} input pins of the DAC, the +12 V output to the V_{CC} and -12 V to V_{SS}. These amplitudes are all within the input voltage limitations of the DAC [74].

Testing of the power unit in a laboratory setting showed that the power unit functions as intended, more details can be seen in section 5.4.3.

The Tiva needed to connect to the DACs interface pins (J8 connector) [128] to enable sending continuous commands to the DAC during the streaming mode. Therefore pins PA5 (MOSI), PA2 (CS or chip select), PA3 (CLK or clock), and GND in the J2 connector according to the Tiva's datasheet [129] were connected to the corresponding pins on the J8 connector of the DAC [128] with wires soldered on the prototype board from the Tiva pins to the DAC to Tiva connector. This can be seen at the top of Figure 5.9b.

5.1.4 Voltage dividers as attenuators

Between each analog output channel of the DAC and the input connector wires to the ALC, the Test Device has voltage divider circuits functioning as attenuators. These circuits can be seen in Figure 5.5. The ALC has a maximum input of $\pm$5 mV and the lowest output the DAC can give is $\pm$2.5 V, therefore an attenuation with a gain of

$$G = \frac{0.005\ \text{V}}{2.5\ \text{V}} = \frac{1}{500}$$

is needed.

The resistances to use in the voltage dividers were calculated with equation 3.1. A value of 1 $k\Omega$ was chosen as R_2, and R_1 then calculated to be

$$R_1 = \left(\frac{V_1}{V_2} - 1\right) R_2 = \left(\frac{0.005\ \text{V}}{2.5\ \text{V}} - 1\right) \cdot 1\ 000\ \Omega = 499\ 000\ \Omega = 499\ \text{k}\Omega$$

After testing these resistors on a breadboard with a multimeter and a function generator, as well as later with the DAC, it was determined that the attenuators were stable with the correct gain.

The prototype design for the attenuators can be seen in Figure 5.6. The attenuators were soldered onto a prototype board (seen in Figure 5.3) and in the middle of the resistors, there is the 1x16 female connector [126] for the attenuated DAC channel outputs. The resistors were bridged together to a common ground as seen in Figure 5.10b. This common ground also creates a common reference point to allow for future implementations, and the extra pads on the prototype board make the design more modular.

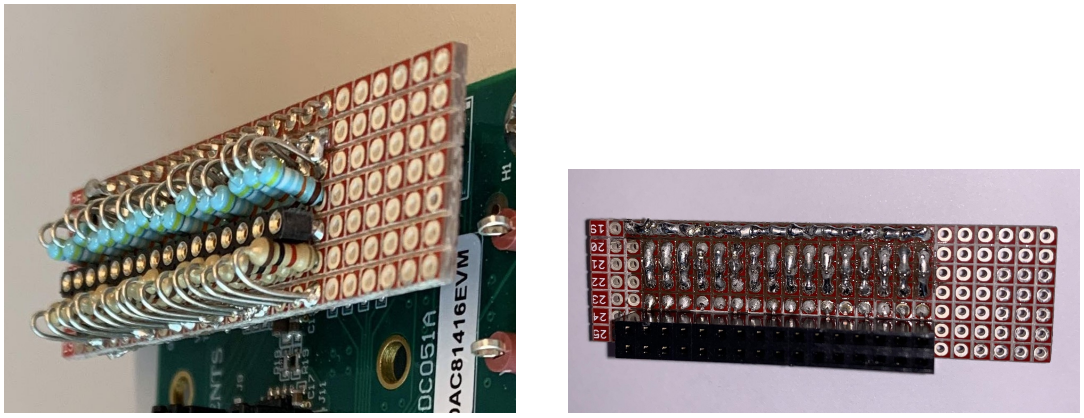

(a) **(b)**

Figure 5.10: The prototype board of the attenuators. (a) The front of the prototype board and access to the DAC output channels in the middle of the resistors. (b) The back of the prototype board.

5.1.5 Connecting the Test Device to the ALC

Two parts were needed to connect the Test Device to the ALC; the test Omnetics connector to transfer data from the Test System to the ALC, and the ground wire to reduce noise picked up by the ALC. These two components can be seen in Figure 5.11.

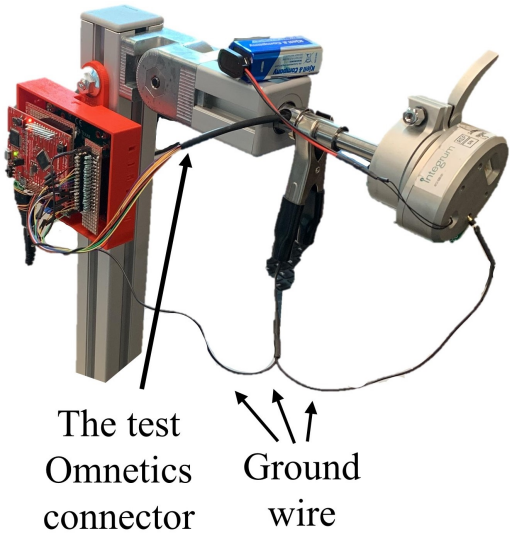

Figure 5.11: The test Omnetics connector and ground wire set up.

The test Omnetics connector (seen in Figure 5.12) has two connection parts; a circular female part and a 1x16 pin male part. The female part mates with the Omnetics connector on the ALC and the male part connects to the 1x16 female connector [126] (seen in the middle of Figure 5.10a). The test Omnetics connector reads the outputs of the 16 channels from the DAC and transfers them to the ALC. This connection can be seen in Figure 5.1.

(a) **(b)**

Figure 5.12: (a) The test Omnetics connector. The left end mates with the Omnetics connector on the ALC and the right end connects to the DAC outputs. (b) The end that mates with the Omnetics connector on the ALC.

The ground wire was assembled out of two jump wires and a conductive clamp. One wire extends to the Test Device and another to the ALC while the clamp is clamped around the abutment attachment piece (as can be seen in Figure 5.11) to ground the abutment in the same way as the bone of an amputee.

5.1.6 Test Device casing

As mentioned in section 4.4.5, the Test Device casing needed to fulfill two key requirements: first, it had to allow for easy disconnection and connection of the test Omnetics connector, and second, it had to enable signal readings with an oscilloscope without requiring the Test Device casing to be opened. To meet these requirements ventilation gaps were strategically incorporated into the casing design (as seen in Figure 5.13), providing both convenient wire access and air circulation. The two gaps for connection to the Tiva pins were added to allow access to the input channels of the Tiva for future implementations. The gap for the Test Device output channels was made larger than needed to allow for easy access with an oscilloscope and walls were added to it to help with the alignment of the test Omnetics connector (seen in Figure 5.14b).

To prevent any collision between the Test Device casing and the arm of the Test Rig, a small platform is integrated at the back of the casing. This platform ensures sufficient clearance and serves as a protective measure. A squeeze-release mechanism was incorporated into the design to enable an effortless opening of the Test Device casing. Alignment pieces were included on the opposing sides of the squeeze-release mechanism to facilitate seamless assembly.

The outer measurements of the Test Device casing can be seen in Figure 5.13 and the walls of it are 2 mm thick.

The 3D printed Test Device casing (seen in Figure 5.14) was made out of Polylactic acid (PLA) material. PLA is one of the most common materials used in 3D printing [130]. The casing was printed with Ø1,75 mm filament using a Leapfrog Xeed printer.

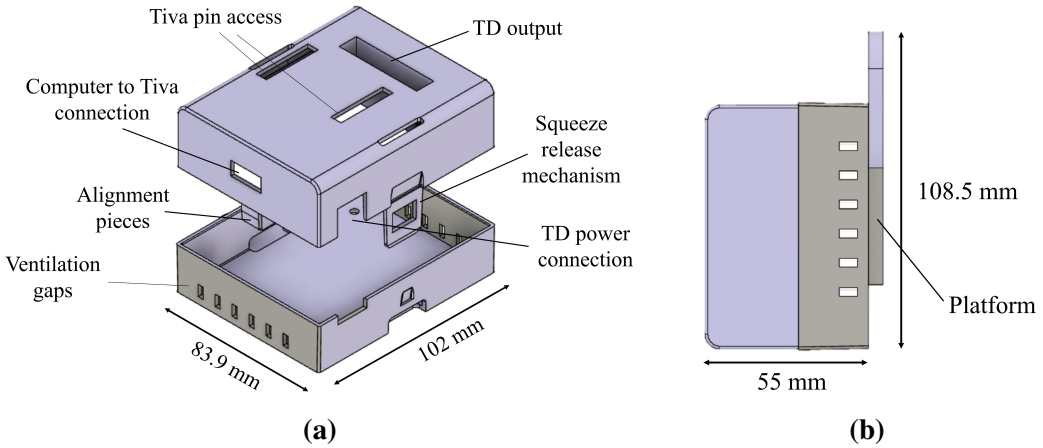

Figure 5.13: The Test Device casing design with dimensions and access points for the Test Device components labeled. (a) Exploded view. (b) Side view.

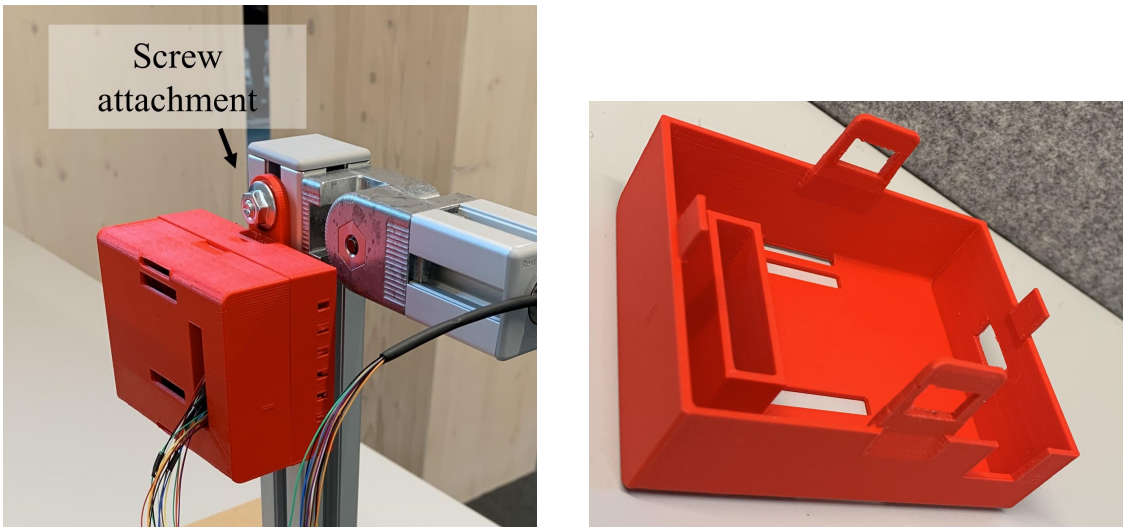

(a) (b)

Figure 5.14: The assembled Test Device casing. (a) The casing attached on the Test Rig. (b) Inside of the top half of the casing.

5.2 The design and selected components for the Test Rig

The Test Rig was designed to fulfill the technical requirements in Table 4.2 and ensure proper office ergonomics and adaptability to various heights of standard lab desks. The aim was to create a comfortable user experience when utilizing the Test System, irrespective of the specific desk height in a typical laboratory setting. The Test Rig has to be positioned at the edge of a desk to allow an artificial arm to move freely.

The Test Rig is made out of 4 parts (or seven components), a skeleton (a column and a short beam), a lockable joint, a table attachment (bottom plate, column attachment, and clamps), and an abutment attachment piece, as seen in Figure 5.15. All components were ordered from a distributor in Sweden to minimize shipping time, and the assembled Test Rig can be seen in Figure 5.1. The sizes, weights, and functions of each part of the Test Rig have been listed in Table 5.3. The Test Rig weighs in total 4.78 kg with its main components weighing 4.66 kg and other components 0.12 kg.

The following sections will go into more detail about each part.

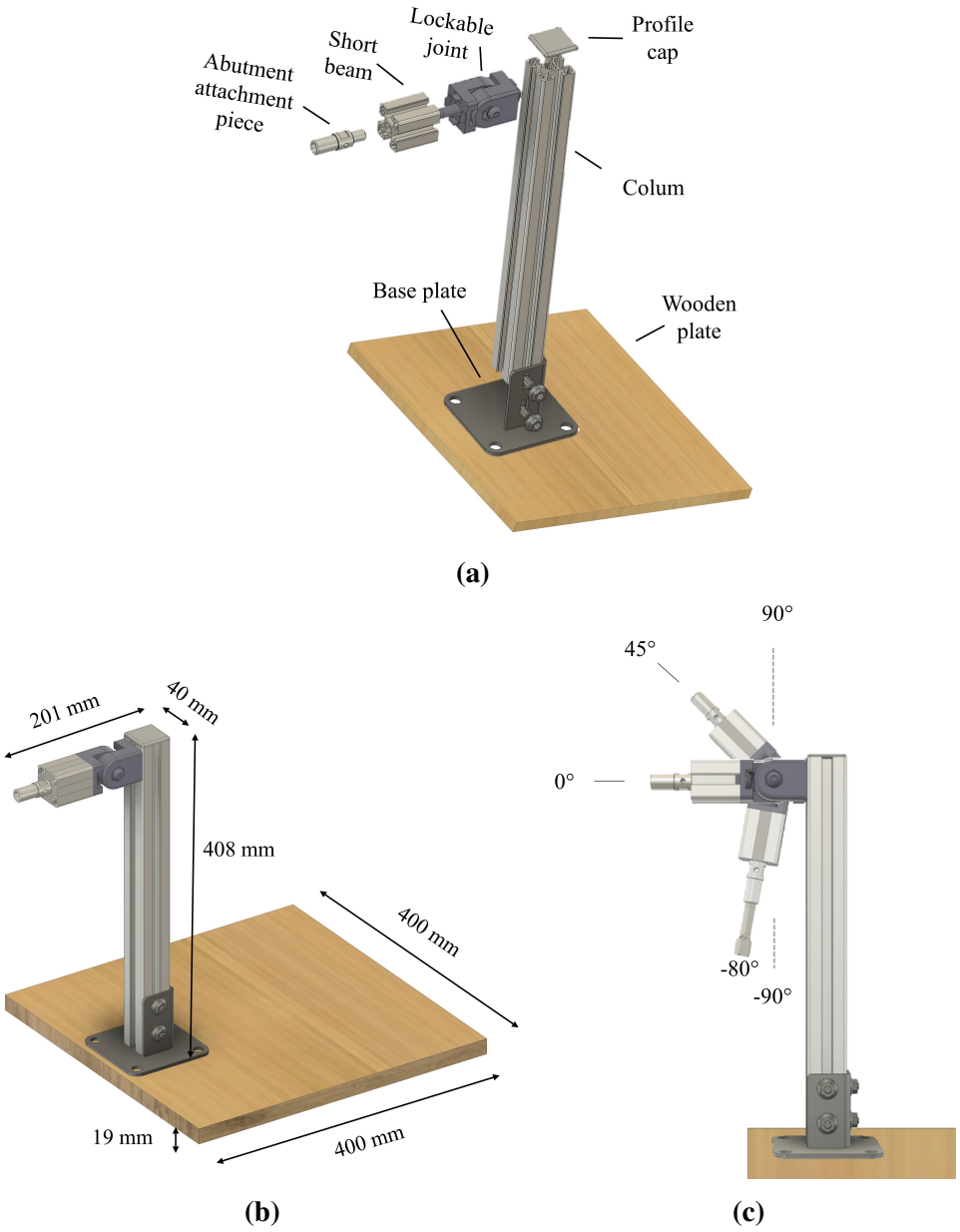

Figure 5.15: The final Test Rig design. (a) Exploded isometric view with components labeled. (b) Isometric view with dimensions. (c) The movement ranges of the Test Rig.

Table 5.3: Parts of the Test Rig, their sizes, weights, and functions

Part	**Component**	**LxWxH [mm]**	**Weight [kg]**	**Cost [SEK]**	**Function**	**Ref***
Skeleton (column)	Aluminum strut profile	400x40x40	0.60	80	Vertical structural support for the ALC and connected components	[131]
Skeleton (short beam)	Aluminum strut profile	50x40x40	0.060	20	Acts as a residual limb and for connecting the lockable joint to the abutment attachment	[131]
Lockable joint	Lockable swivel joint	68x40x40	0.53	660	Allows testing of the ALC in different positions. It has a 180° range of motion and a 100 Nm torque tolerance.	[101]
Abutment attachment piece	Custom aluminum piece	65x18x18	0.024	5000	For attaching the e-abutment to the short beam	**
Table attachment (column attachment)	Base plate	79x110x110	0.55	270	Enables securing the column to a bottom plate	[132]
Table attachment (clamps)	Two clamps	300x80x25	0.60	298	Secures the Test Rig to tables of all sizes	[133]
Table attachment (bottom plate)	Wooden plate	400x400x19	2.30	90	Enables securing the Test Rig to a table of all sizes	[134]
Total			4.66	6418		

**The references for the components*

***Designed by mechanical engineers of the company the thesis is conducted at*

Table 5.4: Other components of the Test Rig; fastening material and covering parts.

Part	Component	LxWxH [mm]	Weight [kg]	Cost [SEK]	Function	Ref*
Skeleton (short beam)	Cover cap (with a hole) profile	40x40x2	0.00465	12	A protective cover with a hole for the abutment attachment piece	[135]
Skeleton (column)	Cover cap profile	40x40x2	0.00465	12	A protective cover	[135]
Skeleton (column)	T-head bolt HS10-M8X20	20x8x8	0.013	8	One bolt for attaching the Test Device casing to the column	[136]
Skeleton (column)	Collar nut M8	68x40x40	0.0089	3	One nut for securing the Test Device casing to the column	[137]
Base plate	T-head bolt HS10-M8X20	20x8x8	0.052	32	Four bolts for attaching the column to the base plate	[136]
Base Plate	Collar nut M8	68x40x40	0.0356	12	Four nuts for securing the column to the base plate	[137]
Total			0.1188	79		

**The references for the components*

5.2.1 Skeleton: Structural design and Evaluation

This section will first go over the results for the estimated conservative value for the maximum bending stress of both the short beam and column. This estimate was used to decide on the selected components. The section will then go over the end design of the skeleton and its structural strength.

5.2.1.1 Evaluation of maximum bending stress for component selection

The initial assumptions made to acquire a conservative value for the maximum bending stress of both the short beam and column included assuming the whole cantilever beam and column had square cross-sections. Estimated values were made for each of the variables of the bending stress equations, 3.5 (for the short beam) and 3.8 (for the column),

and this also involved estimating the variables of the bending moment equations, 3.4 (for the short beam) and 3.6 (for the column).

For estimating the center of mass, using equation 3.3, the total length of the cantilever beam was estimated to be

$$0.44 \text{ m} \cdot 2 \text{ m} = 0.88 \text{ m}$$

using [85].

The cantilever beam under consideration in this project is composed of nine components. A 3 kg object, an artificial hand, wrist, arm, and elbow, the ALC and its connectors, the e-OPRA System, the short beam, and the lockable joint as demonstrated in Figure 5.16. The artificial hand, wrist, and arm used for testing in this project were components available to the company the thesis is conducted at. These components had their lengths and weights available in their respective data sheets as seen in Table 5.5, while the others needed to be determined through further design.

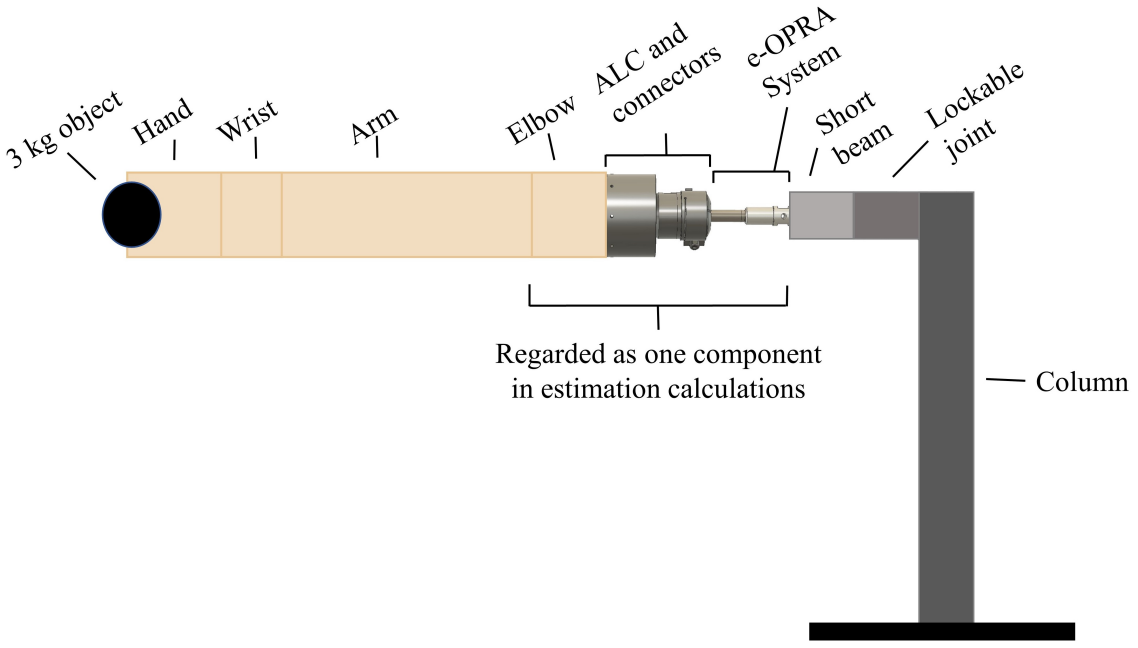

Figure 5.16: The Test Rig design before selection of components.

Table 5.5: The lengths and weight of the known components from Ottobock along with their corresponding datasheets.

Component	Length	Mass	Reference
SensorHand Speed	0.2035 m	0.462 kg	[86]
Electric Wrist Rotator	0.03 m	0.096 kg	[87]
DynamicArm Plus	0.305 m	1 kg	[88]
Total	0.5385 m	1.558 kg	

The short beam and the lockable joint were estimated to be 0.1 m long each. For simplification, the elbow, the ALC and connectors, and the e-OPRA were regarded as one component and were then estimated to be in total

$$0.88 \text{ m} - (538.5 \text{ m} + 0.1 \text{ m} + 0.1 \text{ m}) = 141.5 \text{ m}$$

Then the estimated weight of the unknown components was found with the minimum weight-bearing capacity requirement of 5 kg, including a 3 kg weight at the end of an artificial arm. All components of the cantilever beam after the lockable joint and the short beam (the e-OPRA, ALC and connectors, artificial elbow, wrist, arm, and hand) should therefore weigh 2 kg, and the unknown components

$$2 \text{ kg} - 1.558 \text{ kg} = 0.442 \text{ kg}.$$

Then an estimate was made that the lockable joint and the short beam should weigh 0.5 kg each and the height of the cross-section of the column was estimated as 0.05 m. This resulted in the estimated sum of all masses being M_e = 6 kg while the rest of the variables for calculating the estimated center of mass can be seen in the Table 5.6.

Table 5.6: Variables needed to calculate the estimated center of mass.

Component	i	x_{ie} [m]	m_{ie} [kg]
Lockable joint	1	0.1	0.5
Short beam	2	0.2	0.5
Elbow, ALC, connectors, and the e-OPRA	3	0.3415	0.442
DynamicArm Plus	6	646,5	1
Electric Wrist Rotator	4	676,5	0.096
SensorHand Speed	5	0.88	0.462
Object	6	0.88	3

The estimated center of mass $r_{CM,xe}$ ended up being 0.676 m from the column.

F_{ge} was then calculated as

$$F_{ge} = (3\ \text{kg} + 2\ \text{kg} + 0.5\ \text{kg} + 0.5\ \text{kg}) \cdot 9.81\ \text{m/s}^2 = 58.56\ \text{N}$$

resulting in the estimated bending moment of the short beam being

$$M_{be} = F_{ge} \cdot (x - (r_{CM,xe}) = 58.56\ \text{N} \cdot (0.1\ \text{m} - 0.676\ \text{m}) = -30.27\ \text{Nm}$$

where the negative sign is only indicating that the cantilever beam bends downwards, towards the ground [54]. Then the estimated bending moment for the column is

$$M_{be} = F_{ge} \cdot (r_{CM,xe} + d_e/2) = 58.56\ \text{N} \cdot (0.676\ \text{m} + 0.025\ \text{m}) = 41.05\ \text{Nm}.$$

With the cross-section estimated as a square, for both the short beam and column, and with a height of 0.05 m the estimated area and moment of inertia of the cross-section were

$$A_e = b \cdot h = 0.05\ \text{m} \cdot 0.05\ \text{m} = 0.0025\ \text{m}^2$$

and

$$I_e = \frac{bh^3}{12} = \frac{0.05\ \text{m} \cdot 0.05\ \text{m}^3}{12} = 0.00000052\ \text{m}^4$$

as shown by [57], [59], [60].

All the variables needed to calculate the estimated maximum bending stresses can be seen in Table 5.7.

Table 5.7: Variables needed to calculate the estimated maximum bending stress of the short beam and column.

Variable	Estimated value
F_{ge}	58.56 N
A_e	0.0025 m^2
I_e	0.00000052 m^4
M_{be} (column)	41.05 Nm
M_{be} (short beam)	30.27 Nm
c_e	0.025 m

The estimated conservative maximum bending stress (σ_{maxe}) for the short beam was determined to be 1455288.46 N/m^2 (or 1.455 MPa) and for the column 1995215.72 N/m^2 (or 1.995 MPa).

The component selected to investigate for this application was an aluminum strut profile from Bosch Rexroth [131]. Bosch Rexroth is a prominent supplier of automation solutions catering to a wide range of industrial and mobile applications [138]. Taking into account a safety factor of 2, the allowable bending stress (σ_{allow}) for the aluminum strut profile was determined to be 97.5 MPa, as per the Bosch Rexroth catalog [89]. As the estimated maximum bending stress of both the short beam and column are significantly lower than the allowable bending stress of the selected aluminum strut profile, it was concluded that it was appropriate for use in the final design [89].

5.2.1.2 Skeleton design and structural strength evaluation

The skeleton of the Test Rig is a combination of a vertical column for allowing testing of the ALC on tables of various heights and a short beam representing the residual limb of an amputee. Both parts are made out of the aluminum strut profile from Bosch Rexroth, at the cost of 100 SEK in total [131].

The aluminum strut profile chosen has a rectangular shape with a width and height of 40 mm as well as a 10 mm profile slot as seen in Figure 5.17.

The aluminum strut profile, as indicated by [131], has a weight of 1.5 kg/m. The chosen length of the column is 0.40 m, and the length of the short beam is 0.05 m. Consequently, the total weight of the skeleton amounts to 0.66 kg.

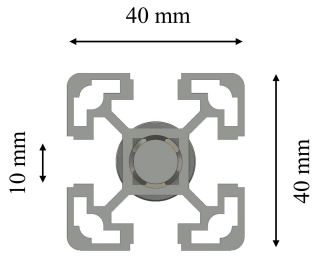

Figure 5.17: Cross-section view of the aluminum profile [131].

An M12 threading was added to the aluminum strut profile to match the fastening screw to the lockable joint [101].

The actual maximum bending stress the short beam had to withstand in the final design was observed as 72.05 MPa and the column as -40.39 MPa in a simulation in Fusion 360 [84]. This result is still within the limits of the allowable bending stress (σ_{allow} = 97.5 MPa) of the aluminum strut profile selected. The simulation results for the column and the short beam can be seen in figures 5.18 and 5.19.

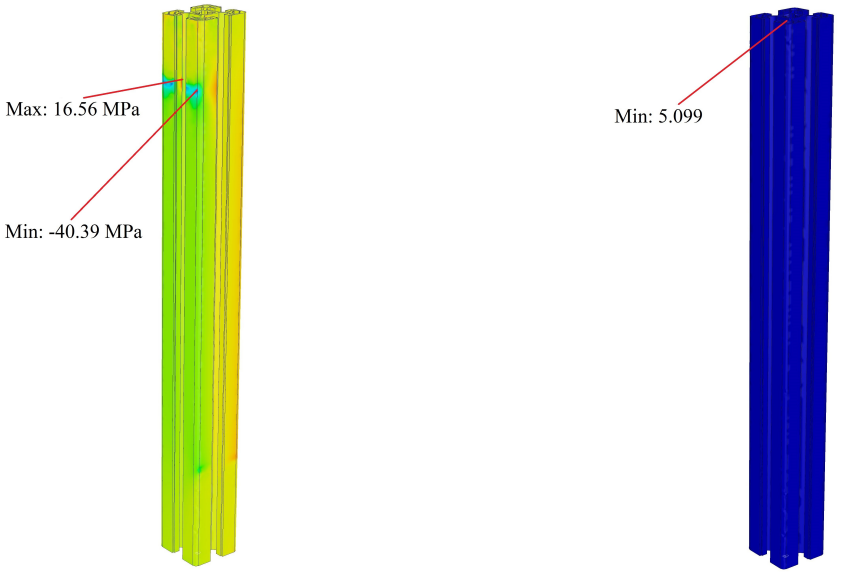

(a) **(b)**

Figure 5.18: Simulation results for the column. (a) Stress along the neutral axis. (b) Minimum safety factor.

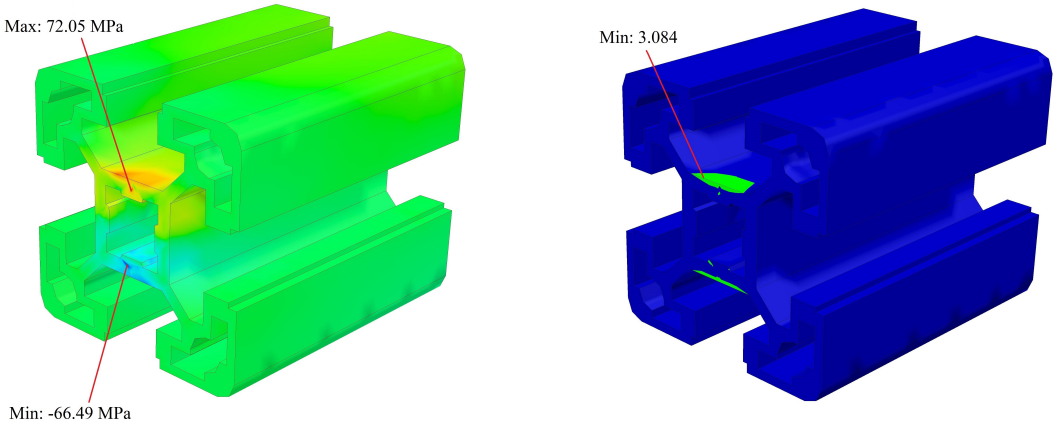

(a) **(b)**

Figure 5.19: Simulation results for the short beam. (a) Stress along the neutral axis. (b) Minimum safety factor.

5.2.2 Lockable joint: Overview and Description

The conservative torque tolerance used to investigate the lockable joint options was 36.658 Nm. This value was obtained by using equation 3.9 and estimating the length from the

pivot of the joint to be 0.05 m, the center of mass at 0.626 m, and load F_{ge} = 58.56 N.

The chosen lockable joint was the Lockable Swivel Joint at the cost of 1317 SEK, including its fastening materials, from Bosch Rexroth [101]. In order to utilize the lockability feature of the lockable joint, a clamping lever had to be procured at the cost of 80 SEK [139]. The clamping lever weighs only 0.088 kg [139].

Assembly instructions [140] were followed for ensuring the correct assembly of the lockable joint.

In Figure 5.20 the upper image is showing the front of the lockable joint and the middle screw there is where the clamping lever is used to lock the lockable joint.

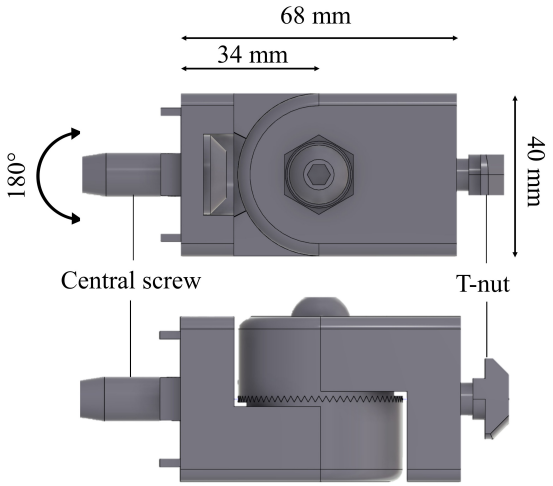

Figure 5.20: The dimensions and range of motion of the lockable joint from Bosch Rexroth [101]. The upper image is the front of the joint and the lower is the side view.

The lockable joint is made out of diecast zinc and has a torque tolerance of 100 Nm [101], well above the estimated conservative torque tolerance needed. It weighs 0.53 kg and is of length 0.068 m when fully extended and 0.040 m in height and width [101]. The lockable joint has 1 DoF and a 180° range of motion [101], as demonstrated in Figure 5.15c, so it fulfilled the technical requirements in Table 4.2 when orienting the joint to the side of the column.

An additional benefit of this lockable joint is its lockability at 5° intervals, coupled with clearly visible markings [101] that facilitate precise degree measurements. This feature enhances usability by providing a reliable and convenient means to ascertain the exact positioning within the lockable joint.

The lockable joint has two fastening materials, a T-nut for attachment to the side of the column and a center screw for attaching the short beam. The T-nut has an M8 threading and is 16mm in length while the center screw has an M12 threading and is 30mm in length [101].

5.2.3 Table attachment

The table attachment is a combination of a wooden plate from Bauhaus [134], a steel base plate from Bosch Rexroth [132], and clamps from Biltema [133].

The base plate only weighs 0.549 kg [132] and its dimensions can be seen in Figure 5.21. This base plate is designed to work as a support for the same aluminum strut profile chosen for the skeleton of the Test Rig [132]. The additional fastening materials needed to attach the aluminum strut profile to the base plate are a T-bolt with M8 threading of length 20 mm [136] and a corresponding collar nut [137]. The head of the T-bolt fits into the 10 mm profile slot of the aluminum strut profile.

The base plate is then attached to the square wooden plate [134] that has a length and width of 40 cm and is 19 mm thick. This wooden plate was chosen to offer more stability to the rig and to ease table attachment.

The minimum force the clamps need to create to keep the system stable was calculated with equation 4.1 as described in section 4.5.3. With the length l_C estimated to be 0.10 m, the force F_C became

$$F_C = \frac{50.4\ \text{N} \cdot cos\left(90° - arctan\left(\frac{0.676\ \text{m}}{0.42\ \text{m}}\right)\right) \cdot \sqrt{(0.676\ \text{m})^2 + (0.42\ \text{m})^2}}{0.10\ \text{m}} = 340.7\ \text{N}.$$

The clamps chosen (seen in Figure 5.22) have a clamping force of 2 500 N and a clamp length of 80 mm [133] each. With l_C as 0.08 m, the force F_C becomes

$$F_C = \frac{50.4\ \text{N} \cdot cos\left(90° - arctan\left(\frac{0.676\ \text{m}}{0.42\ \text{m}}\right)\right) \cdot \sqrt{(0.676\ \text{m})^2 + (0.42\ \text{m})^2}}{0.08\ \text{m}} = 425.9\ \text{N},$$

and as two clamps of 2 500 N are used, the system is stable with a large safety factor.

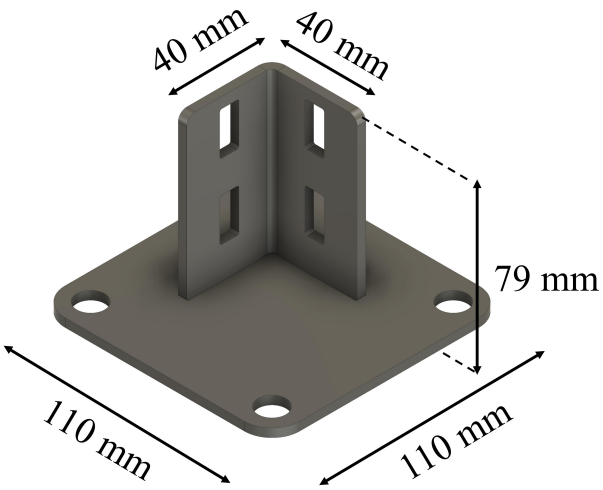

Figure 5.21: The base plate and its dimensions.

Figure 5.22: The clamps used.

5.2.4 Abutment attachment

The design inputs for this piece included that the test Omnetics connector should be accessible through the abutment attachment piece and it should fit into an aluminum strut profile of 50 mm in length and 40 mm in height and width (the short beam).

The cylindrical abutment attachment piece (seen in Figure 5.23) was made out of titanium and the screw part of it has an M12 threading to be inserted into the short beam. Incorporated into the attachment piece is a purposeful side gap that enables the extension of the test Omnetics connector, a key element of the e-OPRA. This gap facilitates the secure attachment of the connector to the Test Device by allowing it to extend out of the abutment attachment piece.

The abutment attachment piece weighs only 24 g and is 65.3 mm long with the largest diameter of 18 mm.

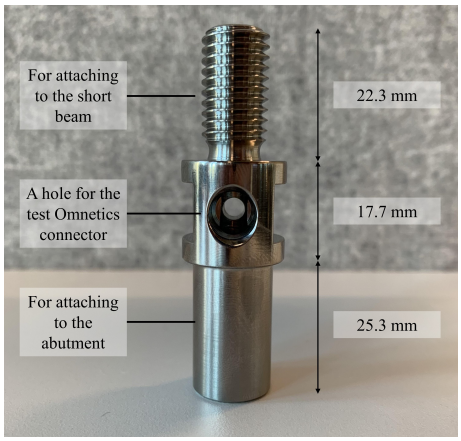

Figure 5.23: The abutment attachment piece and its dimensions.

5.2.5 Simulations of the assembled Test Rig design

Stress simulations for structural strength were done on the final design for the Test Rig as seen in Figure 5.24. A load of 50.4 N was placed at the conservative center of mass calculated in section 5.2.1.1. The results show that the maximum stress the Test Rig will experience in a test scenario is 89.19 MPa and the safety factor of the rig is 3.084 at minimum.

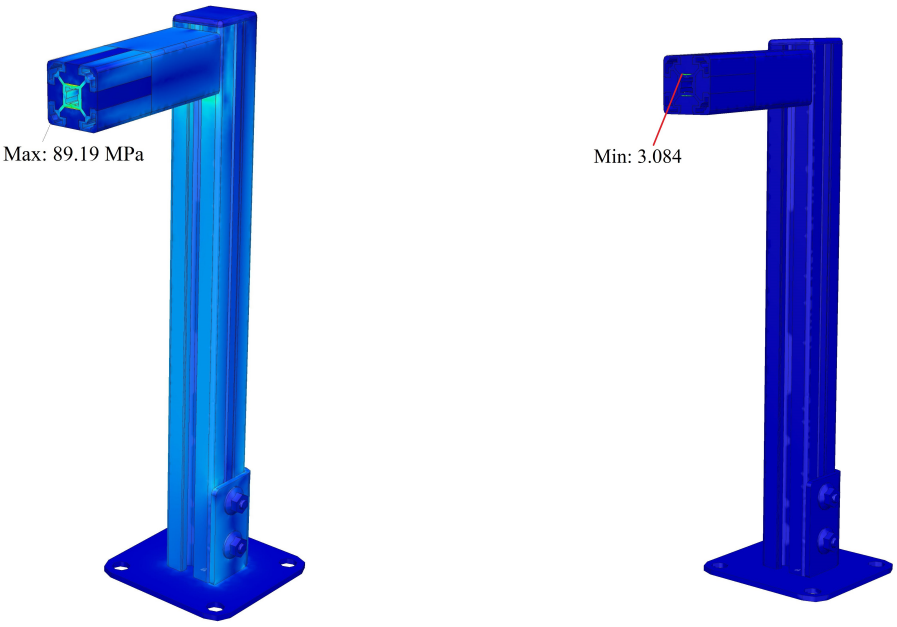

(a) **(b)**

Figure 5.24: The simulation results for the whole Test Rig design. (a) Von Mises stress results. (b) Minimum safety factor results.

5.3 Test Software

The overall structure of the Test Software can be seen in the block diagram in Figure 5.25. The Test Software consists of three code files that communicate together, as well as a GUI. The user interacts with the GUI which then communicates the user's commands to the other parts of the Test Software. All these parts will be discussed in more detail in the following sections.

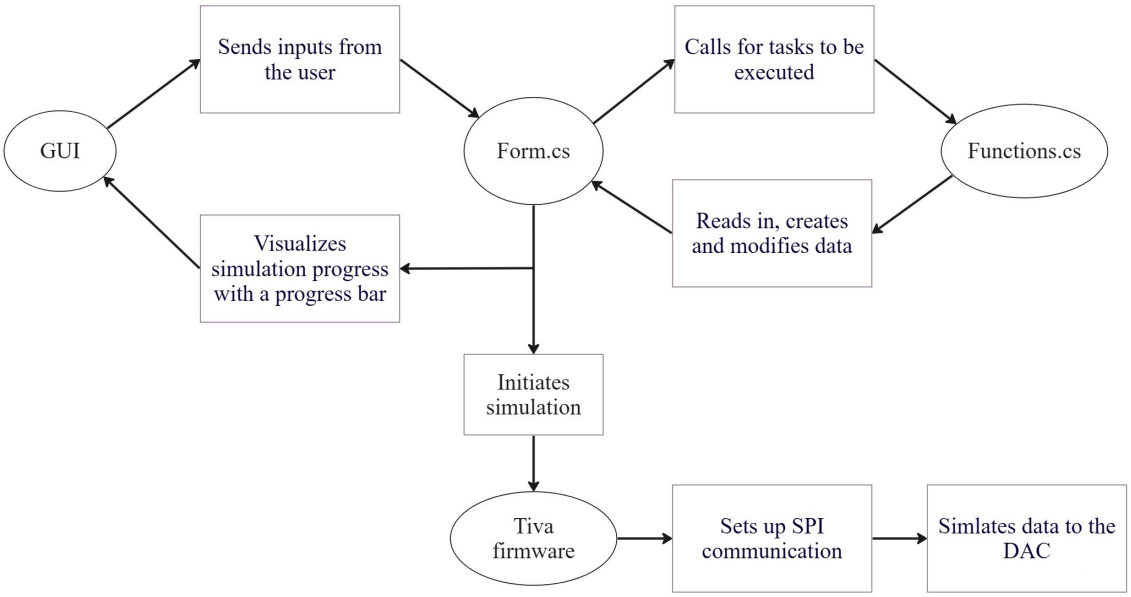

Figure 5.25: A block diagram of the Test Software.

5.3.1 Graphical user interface

The GUI of the Test Software, which can be seen in Figure 5.26, is simple and has an emphasis on functionality. It provides the user with the necessary options to be able to operate the Test System - the choice of the sampling frequency, the choice between an EMG recording and a sine wave, and the choice of adding noise to the signal. Adding noise to the signal could be useful to accommodate for background noise often acquired during EMG signal acquisition. The GUI also has the option to start and stop the simulation and visualize the simulation progress with a progress bar."

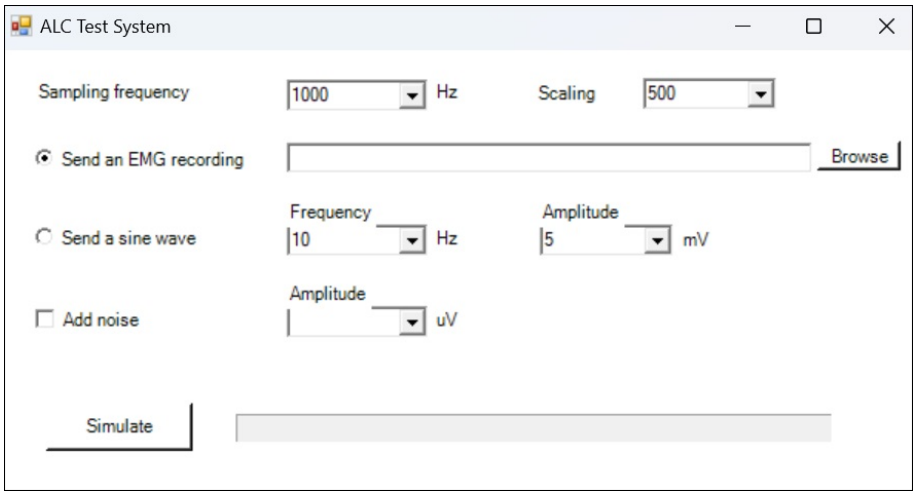

Figure 5.26: The GUI of the Test Software.

To begin with, the user needs to choose the sampling frequency and the scaling the signal will be sent with to the DAC. The options for scaling are 1, 10, 50, 100, 500, 1 000, and 5 000, with 500 as the preselected option. The options for the sampling frequency are 2 Hz, 20 Hz, 200 Hz, 500 Hz, 1 000 Hz, and 2 000 Hz with a preselected option of 1 000 Hz. These options include the Nyquist frequencies [141] of all sine wave frequency options that the user can choose from later in the GUI, as well as the option of 500 Hz that can be used to simulate the EMG data instead of 1 000 Hz if necessary.

After this, the user needs to make a decision on whether to simulate the ALC with an EMG recording or a sine wave. The choice is made with simple radio buttons that only allow the user to choose one of the two options [142]. This is done in order to avoid errors with the user selecting both the options or none, and to make the interface clear for the user. The simulation with the EMG recording is the default option that is selected automatically when the GUI starts up.

Next to the radio button of the EMG recording, there is an address bar as well as a browse button that the user can click in order to browse for a file on their computer. Clicking this button opens the Windows file explorer in the folder the user is currently in. The file type required by the GUI is .mat, and therefore this file type is the only one the user is able to choose in the file explorer. Once a file is chosen, its address in the local computer will be visible in the address bar next to the browse button.

In regards to the sine wave, the user needs to choose a frequency and an amplitude of the wave from preset options of 1 Hz, 10 Hz, 100 Hz, 500 Hz, and 1 000 Hz (with 10 Hz as the preselected option) and 2 mV, 5 mV or 10 mV (with 5 mV being the preselected option). This is done via two separate drop-down menus. The amplitude of 5 mV and the frequencies of 500 Hz and 1 000 Hz were added as options to create a signal as similar as possible to the recorded EMG data, and the other options were added to allow for easy testing and debugging in case of errors.

Below the simulation choice, there is a simple checkbox for the user to add noise to the signal. This option has not been implemented yet but is set in the GUI as a future possibility.

The final part the user needs to do is to click the *'Simulate'* -button. Clicking this button will start a function that checks if the user had chosen to simulate an EMG recording or a sine wave, then creates the data buffer corresponding to that choice, and finally sends it to the DAC to output through all of its 16 analog output channels. Next to the button on the GUI, there is a progress bar that displays the progress of the simulation, so it is easier for the user to anticipate when the simulation is over.

Regardless of what the user chooses in terms of simulation type, they are not able to browse for and select an EMG recording or select the options for a sine wave or noise while a simulation is ongoing. This is to make sure the user does not affect the simulation in any way, and that a possibly connected artificial arm will be able to finish the movement sequence the ALC is sending to it as an input. After the simulation is finished, the user is

able to change the settings and start a new simulation at any moment.

5.3.2 Functions.cs file

All the functions of the Test Software are stored in a separate code file called functions.cs. This file is imported into the other files of the Test Software, such as the form.cs which controls the GUI, and thus the code in those files can call and use the functions.

The functions include the main aspects that the Test Software needs to do:

- **readMAT:** This function takes a user-chosen file address as an input, loads the .mat-file on the address, and converts it into a simple array of double values. A third party package called MatFileHandler was installed into Visual Studio 2022 in order to be able to import the EMG data stored in the .mat-files [143]. This package allows the Test Software to read .mat-files and extract the data they contain, for example, into an array [143].

- **outputEMGToDAC:** This function reads in the EMG data array from the function readMAT, divides the data on the 16 EMG electrodes, and outputs it to 16 DAC channels respectively. In addition, the function initializes and runs a progress bar to show the user the simulation progress.

- **playSine:** This function creates a sine wave of specific frequency and amplitude that are chosen by the user in the GUI. It then sends it to all DAC outputs simultaneously through the Tiva board. In addition, similarly to when sending the MAT-file to the DAC, this function uses a progress bar to show the user the simulation progress.

5.3.3 Interface adapter communication

When using the USB2ANY-board as the interface adapter, it was possible to use a DLL file provided with the DAC as a means of communication between it and the USB2ANY. The DLL provided for the DAC, called usb2any.dll, included ready-made functions for initiating the SPI communication between the two boards as well as reading and writing data to and from the DAC.

Because of the limited speed of the USB2ANY interface adapter, it was changed to the Tiva board. Since a DLL allowing interface conversion was not readily provided by the manufacturer of the components, firmware with similar functionality for the Tiva was outsourced from a firmware engineer within the company. This firmware, similar to the one provided for the USB2ANY, allows for the SPI communication to be set up and data read and written to and from the DAC.

5.3.4 Form.cs file

The code file form.cs controls the GUI. It imports all the functions in the functions.cs file as well as the serial communication functions of the interface adapter, and begins with setting up and opening the SPI interface to the DAC.

5.4 Testing of the Test System

Following the assembly of all components, a usability assessment was conducted on the Test System. This chapter examines the test results of the Test System, further evaluating its compliance with the technical requirements.

5.4.1 Evaluating the physical Test Rig

The Test Rig was assembled and loaded with a conservative load as seen in Figure 5.27. The conservative torque value of 36.658 Nm was used to find the conservative load to test with. First, calculations were made to find the gravitational force F_g

$$T_e = F_g \cdot r \Rightarrow F_g = \frac{36.658 \text{ Nm}}{0.126} = 290.93 \text{ N}$$

and then the conservative load was found by

$$F_g = m \cdot g \Rightarrow m = \frac{F_g}{g} = 29.477 \text{ kg}.$$

When applying a 29.48 kg load positioned at the end of the abutment attachment piece, which was 0.126 m away from the pivot point, the Test Rig did not budge. The Test Rig still confirmed its mechanical strength when applying 30.27 kg at the same position.

After verifying that the mechanical strength of the Test Rig could hold the conservative load estimated (and therefore the real load), an additional test was made with a load 20% higher than the conservative load, or 35.37 kg, at the end of the abutment attachment piece. This resulted in the central screw of the lockable joint sliding out of its threading at a load of roughly 35 kg. After re-screwing the central screw in place the Test Rig still functioned as intended.

(a) **(b)**

Figure 5.27: Testing the Test Rig with the Digital Hook Scale [107]. (a) The testing in process. (b) Showing the load applied.

5.4.2 Prototype boards evaluation

The test results from the power unit and attenuator electronics on a breadboard, connected to the DAC and the USB2ANY interface adapter showed that the circuits work. The test points TP1-5, TP11, and TP13 for the voltage inputs of the DAC [128] showed that it was powered correctly and the attenuated output channels of the DAC showed that the attenuators lowered the output voltage 500 times, as expected. The results were observed on a multimeter as seen in Figure 5.28. After confirming that the circuits worked, the prototype boards were tested in the same way. This was done to confirm that the soldered electronics worked as intended. The same results were acquired with the prototype boards as with the breadboard.

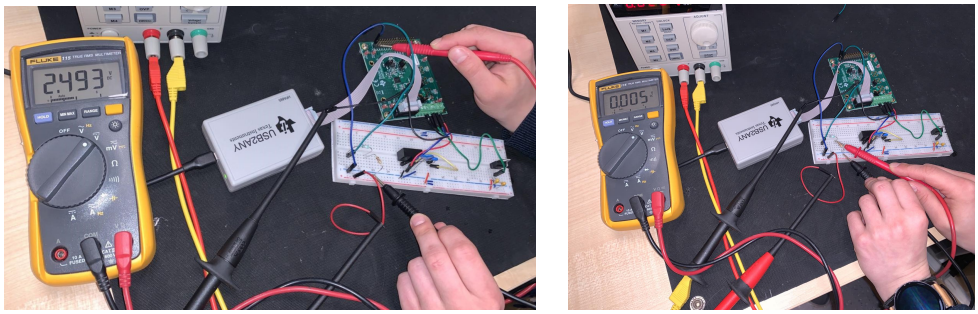

(a) **(b)**

Figure 5.28: Testing of the power unit and attenuators on a breadboard using a laboratory power supply. (a) The ±2.5 V DAC output while being powered by the power unit. (b) The ±5 mV attenuator output.

5.4.3 Integration testing the Test Software and Test Device

The Test Device was mounted on the Test Rig with a T-nut and connected to the Test Software via a USB to micro-USB cable. The abutment and ALC were then mounted on the Test Rig with the abutment attachment piece. The abutment attachment piece, and therefore the abutment, and ALC were then grounded with a common ground on the Test Device with the ground wire. The ALC was then powered with a 9 V battery and connected to via Bluetooth by an engineer at the company the thesis is conducted at. This setup can be seen in Figure 5.29. By observing the signals (sine wave and EMG data) being sent from the Test Software and the outputted signals of the ALC a confirmation was made that the Test Software and Test Device work as intended. These results can be seen in Figures 5.31 and 5.33, for the first and second recordings, respectively.

The EMG data recorded by the ALC in the integration testing phase is very similar to the original EMG data (seen in Figures 5.30 and 5.32) for both of the two recordings used for simulation. The timing of the data is correct, and the data is clear and visible for all channels. There is some noise present in the output data of the Test System, but it is not prominent enough to confuse with the EMG data peaks. The test setup also showed that the Test Rig works for mounting the abutment and ALC.

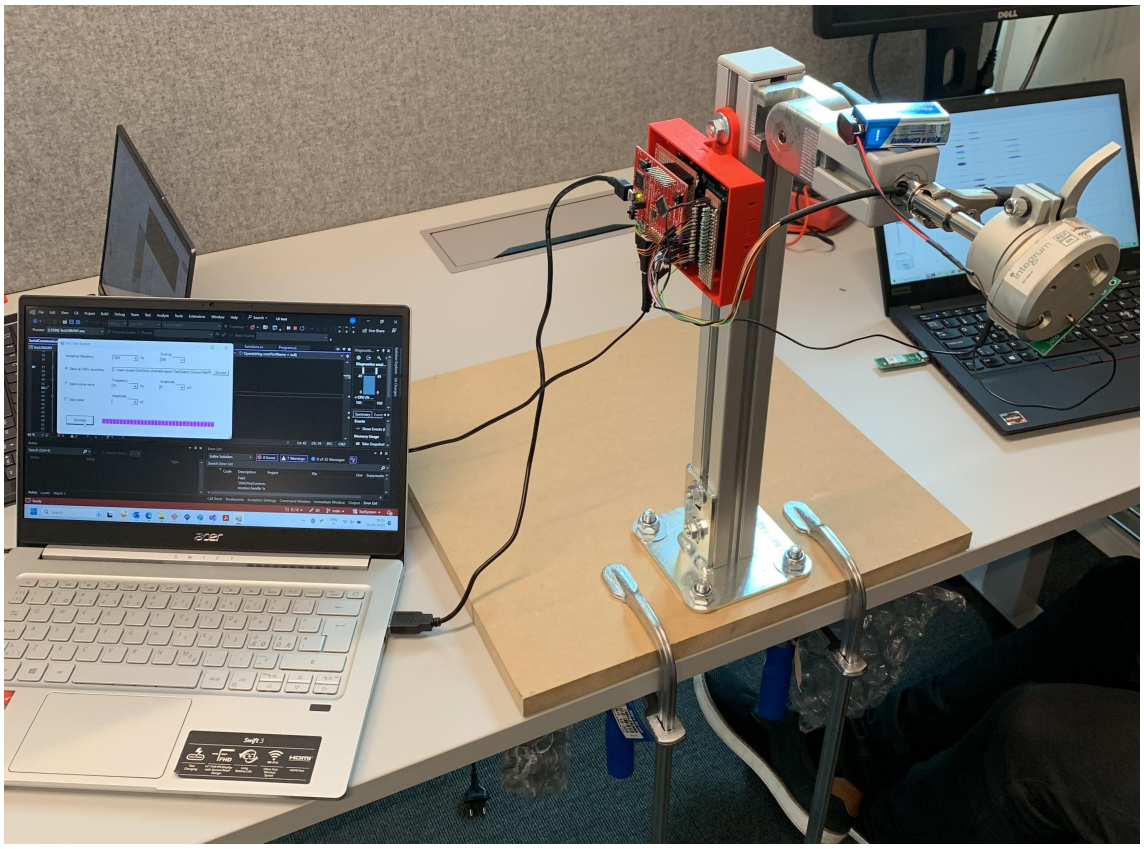

Figure 5.29: The Test System set up.

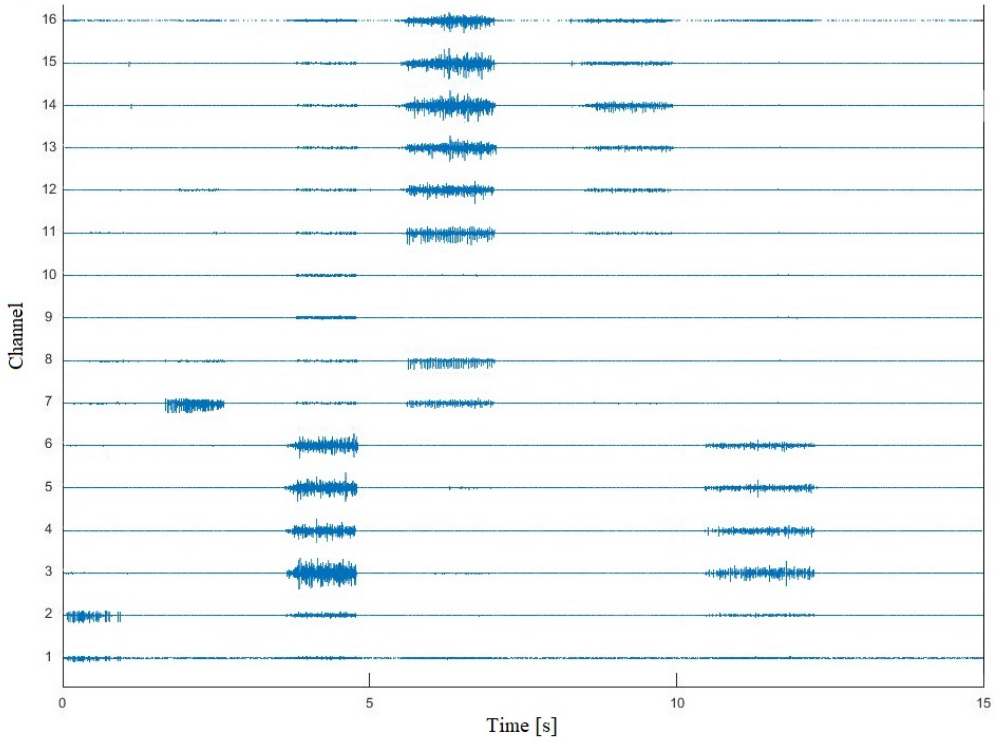

Figure 5.30: The original data of the first recording.

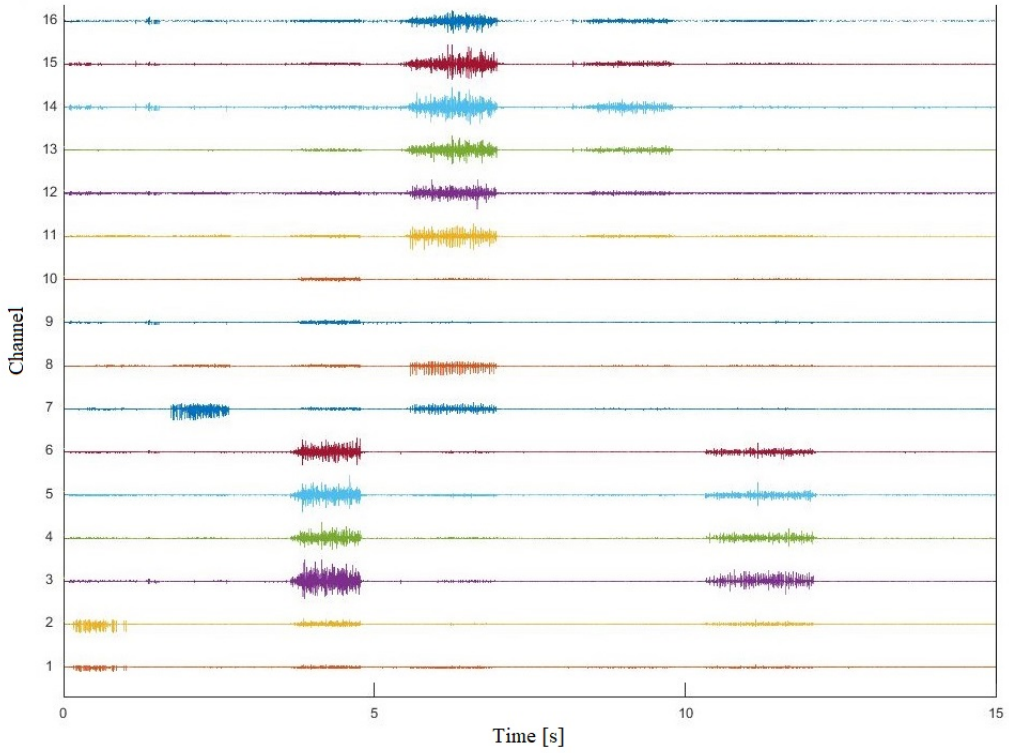

Figure 5.31: The simulation output of the first recording.

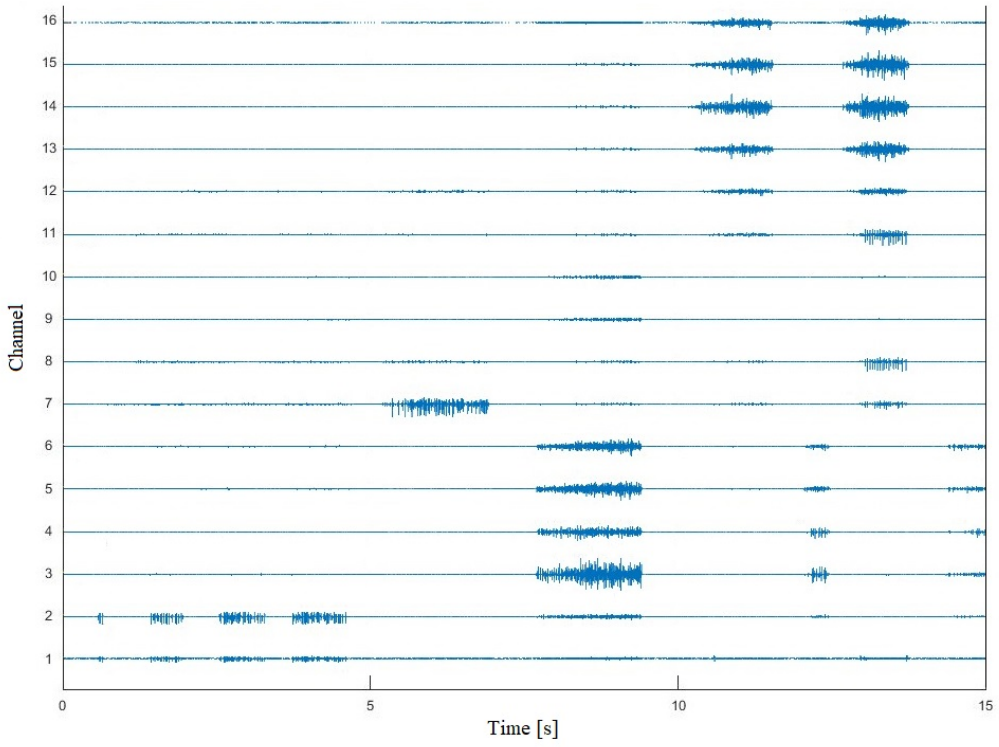

Figure 5.32: The original data of the second recording.

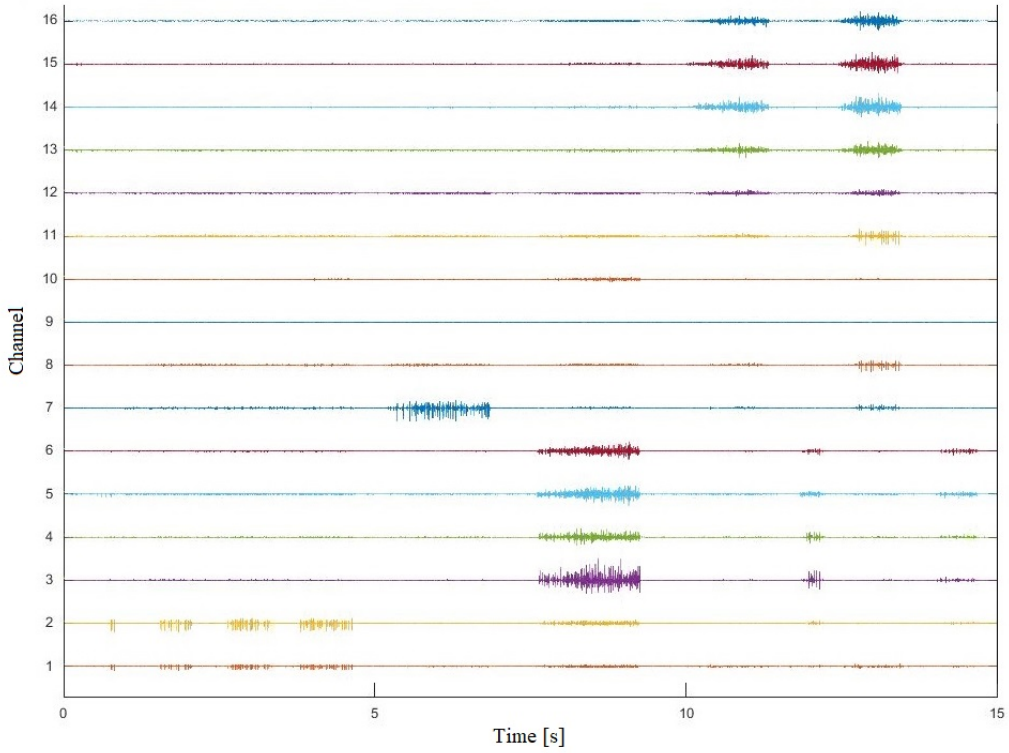

Figure 5.33: The simulation output of the second recording.

5.4.4 Demonstration of the Test System

The assembled Test Rig with the ALC and artificial arm attached can be seen in Figure 5.34. The demonstration of the Test system together with an artificial arm and the ALC was successful, and the artificial arm moved as intended by the simulation data. The structural strength of the Test Rig was also further verified, as leaving the artificial arm and ALC assembled and attached to the Test Rig overnight did not affect the Test Rig in any way.

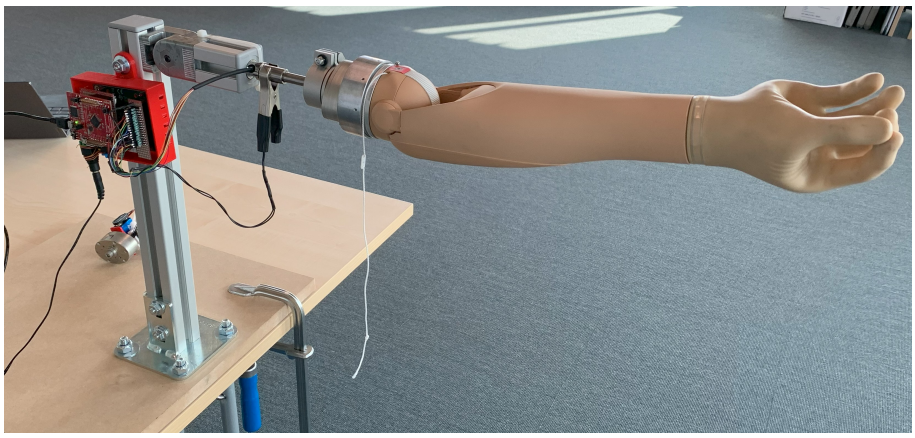

Figure 5.34: The Test Rig with the ALC and artificial arm attached to it.

6

Discussion

In this thesis project, a modular and well-functioning Test System was created for the ALC being developed by Integrum AB. The Test System contains an electronic Test Device, a mechanical Test Rig as well as a Test Software. The Test System is capable of simulating real, recorded EMG data to the ALC with 16 channels simultaneously, as well as simulating a sine wave of frequency and amplitude chosen by the user. The Test System can also mount the ALC and an artificial arm.

This chapter discusses the main components of the Test System, all results of its testing as well as possible future implementations.

6.1 Test Device

6.1.1 Main component decision

Of the three options described in section 4.4.1, an off-the-shelf DAC was chosen since they are relatively cheap and easy to implement whilst a complete input/output device, including both 16 analog input channels and 6 analog output channels as well as multiple communication protocols, can be expensive [1]. As a trade-off for the lower price of a DAC, it needed other external components by its side to fulfill all the technical requirements of the Test System.

There are several reasons why creating a Test Device using a microcontroller or -processor, like an Arduino or Raspberry Pi would have taken too much time compared to using an off-the-shelf input/output device for this application.

Firstly, developing a Test Device using a microcontroller or -processor would require a significant amount of programming and integration work to ensure that the system functions correctly and meets the necessary specifications for this application. A large amount of time would be needed to create a software or firmware to function with the microcontroller or -processor, design all necessary electrical circuits, and test and debug all of these

parts. Additionally, the digital-to-analog conversion could only be done via pulse-width modulation, as components such as Arduino or Raspberry Pi are not capable of creating true analog signals, as they are completely digital devices [144], [145]. Pulse-width modulation allows for creating a waveform that resembles an analog signal by controlling the timing and pulse width of a digital output [146], [147]. Using pulse-width modulation instead of creating a true analog signal could cause problems since the ALC requires an analog signal as an input.

In contrast, using an off-the-shelf input/output device designed for this application could have significantly reduced development time and effort. These devices are typically designed with specific use cases in mind and often come with pre-built libraries and software tools that can streamline the development process. This could have enabled more focus on the higher-level aspects of this project, such as designing and testing algorithms and protocols, rather than worrying about the underlying hardware and software infrastructure. However, even complex off-the-shelf input/output devices require some time and effort to customize them for the purpose they are needed for [148].

Using an off-the-shelf device can provide more reliability and stability compared to a custom-built solution. The devices are typically tested and validated to work with a wide range of input and output signals and have built-in safety features to protect against hardware failures. Thus, they could potentially save resources and speed up the design and testing phase of the development of the Test System.

6.1.2 Prototype board design

The electronic components of the Test Device were soldered on a prototype board. This approach, while commonly used for initial prototyping, is not optimal for long-term use. The prototype board is rather large and the electrical connections are created with wires instead of small, conductive traces as on a Printed Circuit Board (PCB) [149]. The wires might cause noise in the simulated signal, and also easily break or wear with time [150].

Soldering can also be a time-consuming process as one must exercise great care when affixing components, ensuring there are no gaps between the solder and the board, and avoiding unintended bridges or connections.

Careful considerations must be taken when building the circuits and soldering parts. It is important to measure the characteristics of each part prior to assembling them together. If not done correctly some components might break due to overload. The prototype board for the power unit had to be resoldered due to the +5V voltage regulator breaking, which was caused by it not being grounded correctly.

6.1.3 Attenuators

The attenuators could have been created with voltage dividers or inverting amplifiers. Both of these options were deemed functional in testing. The voltage dividers were chosen since they use fewer components and are thus simpler to implement and take less space on a prototype board.

As the Test System is modular, the attenuators could be changed into inverting amplifiers in the future if the voltage dividers would, for example, create too much noise in the signal outputted to the ALC.

6.1.4 Power Unit

The voltage regulators provide a constant output voltage irrespective of changes to the input voltage or load conditions. The circuits for the voltage regulators were added to further stabilize the output voltage of the regulators and reduce noise.

Using an AC/DC adapter as a power source instead of a battery is convenient when working in a laboratory environment where an adapter is standard equipment on hand. In addition, it helps avoid the need for frequent battery replacement.

6.1.5 The interface adapter

After testing the Test Device with the USB2ANY as an interface adapter, it was deemed too slow to communicate the EMG data to the DAC and therefore discarded. This is because the problem was likely in the electronics inside the USB2ANY, and there was no realistic way to improve the communication speed [83]. A conversation with Texas Instruments cleared that the USB2ANY would not have worked for its intended purpose in this project, as it had never been designed or tested for real-time input/output communication [151].

As the Tiva has a greater clock speed and faster electronics [152], and it was on hand in the company, it was a natural upgrade as the interface adapter. However, as it needed additional firmware to be able to convert data from USB to SPI, this needed to be outsourced from the company the thesis was conducted at.

Once the firmware of the Tiva was created, it could be tested in combination with a computer, the DAC, and the ALC. Measuring the outputs of the DAC with an oscilloscope showed that the communication through the Tiva was significantly faster than through the USB2ANY, which allowed for simulating an EMG recording or a sine wave with a sampling frequency of 1 000 Hz as required.

6.1.6 Test Device casing design

The design of the Test Device casing was made so that it would be possible to access the Tiva pins for inputting data into the Tiva for future implementations but the gaps were misaligned by a 1.2 mm and the gap for the USB to micro-USB cable was also misaligned by a few millimeters. This was most likely a human error due to the measurements of the assembled Tiva being made by a ruler and then moved to the design in Fusion 360. To prevent this from happening the gaps could be made larger to allow for a larger error in alignments. The gap for the Test Device output channels was made larger than needed to allow for easier access but due to the test Omnetics connector being fairly small and the female connector being low in the casing, the gap could be made larger in the future. This can be easily changed in the CAD design for the Test Device casing. The lid of the Test Device casing is a bit far from the female connector since the Tiva is assembled higher than the female connector inside the casing. This could also be improved by adding a longer female connector or assembling a couple of female connectors to bring the connection higher up in the casing or by lowering the Test Device casing where the Test Device output channels are located. This was something that was looked into during the design of the Test Device casing but the alignment for the indent had to be very precise due to how close the prototype boards are to each other. This would therefore most likely require 3D printing a couple of designs to find the correct one and that can take up to 5 hours with the 3D printer at hand. Due to lack of time, this was not implemented in this design.

6.2 Test Rig

6.2.1 Aluminum profiles as structural members

Aluminum profiles are known for their high strength-to-weight ratio and properties that make them versatile and durable structural materials [153]. This fact highly influenced the choice of a component to use for the skeleton of the Test Rig and also the compatibility with the lockable joint that was chosen.

The 10 mm profile slot of the aluminum strut profile [131] makes it easy to attach things to the Test Rig by utilizing T-head bolts that fit into that profile like the one used for attaching the Test Device to the Test Rig [136]. This proved useful for the attachment of the Test Device to the Test Rig.

6.2.2 Compatibility with standard lab desks and stability of the Test Rig

The Test Rig had to be usable on any standard lab desk of any dimension, therefore the Test Rig needed to have some height so that an artificial arm would not be hanging too low from a desk causing discomfort to the test user but also not too high up as well to ensure the Test Rig would be easily portable, for example, in standard plastic boxes.

The height of the vertical column ended up being 40 cm, this was around half the length of the whole arm so the arm was only hanging about halfway from the table.

The short beam is essentially acting as the residual limb of an amputee and the length of it ended up being 5 cm. This was to ensure proper proportions to the human body to make the testing more realistic as well as ensure enough space to attach the lockable joint and the abutment to it.

The chosen clamps [133] allow attaching to any lab desk of any thickness and they were selected so the position of the tightening screws was not too far from the edge of the table to ease the use of the table attachment.

The bottom wooden plate [134] was chosen to offer more stability to the Test Rig since the welding on the base plate deformed the flat bottom surface of the base plate a bit but the base plate would have sufficed by itself with the clamps that were chosen.

6.2.3 Reasoning of choice for the lockable joint and considerations regarding its assembling

The lockable joint is important for doing realistic testing of the ALC because it might send different motor signals depending on the ALC's orientation [83]. The choice of components for the lockable joint and the skeleton highly influenced each other. The fact that this joint fulfilled the technical requirements and was compatible with the aluminum strut profile chosen was very convenient and one of the main reasons it was chosen. It was also relatively cheap compared to its torque tolerance and the other joint options explored. The next best option would have been to use the square incremental angle hinge [98] that had 50 Nm torque tolerance but there was only a 312 SEK cost difference between him and the chosen lockable joint so therefore that one was not chosen.

When attaching the lockable joint to the column of the Test Rig two of the extended pieces on the back of the lockable joint had to be removed as instructed in its assembly instructions [140]. Then when attaching it to the column the sides of the extended pieces had to be filed down with around ten strokes with a metal file to ensure a proper fit into the slot of the aluminum strut profile. It should have fitted without any alterations according to the assembly instructions but there must have been a manufacturing error.

6.2.4 The abutment attachment

During manufacturing of the abutment attachment piece, the hole through it needed to be enlarged. The abutment attachment piece was designed to fit the Omnetics connector through it which is smaller in diameter than the test Omnetics connector therefore it was impossible to pull the test Omnetics connector through the hole. This was easily fixed and did not affect its structural strength due to it being made out of titanium but it added R&D cost that was disregarded in the cost of the Test System.

6.2.5 The mechanical strength considerations

The Test Rig should be able to hold the ALC and an artificial arm. Artificial arms can differ in weight and weight distribution so the tolerance requirement made by Integrum was that it should tolerate a load of 5 kg. This involved assuming the artificial arm weighed 2 kg at most and then a 3 kg test object in the hand of the arm. This assumption was made to ensure that the Test Rig could hold most artificial arms irrespective of their weight and weight distribution. To further ensure this the center of mass of each part of the artificial arm was assumed to be at its furthest end from the pivot point.

The artificial arm consisted of the DynamicArm Plus [88], the Electric Wrist Rotator [87] and the SensorHand Speed [86], all from Ottobock SE & Co. KGaA. They were chosen due to their availability to the company. The design of the Test Rig was therefore based on the weight and lengths of these parts but by assuming the center of mass of all parts being at its furthest end from the pivot a conservative load assumption was made.

Even though testing was only done with this artificial arm, the Test Rig should be able to hold most artificial arms due to its conservative load tolerance, as the average weight of an artificial arm is 1.2 kg [69].

6.3 Test Software

The Test Software functioned well when testing it, both with an EMG data recording and a sine wave as a simulation option. All options the user could select in the GUI worked and affected the signal as intended.

However, as the firmware outsourced from the company was created with an older version of the .NET framework than the GUI and the functions of the Test Software, compatibility issues were present, and the GUI code and the functions needed to be copied and converted into the same .NET framework version as the firmware. This took time and effort, but the Test Software functioned well with all of its components afterward.

Besides the .NET framework incompatibility, the firmware, the functions, and the GUI also needed to be matched to communicate together efficiently. The matching included scaling the data correctly and using the correct input and output variables when communicating between the GUI and the firmware. After this work was done, all aspects of the Test Software functioned perfectly.

6.4 Issues during testing of the Test System

6.4.1 Mechanical strength of the Test Rig

The threading of the central screw that came as fastening material for the lockable joint is not of a standard pitch this led to a manufacturing error. The error happened due to not so well documented specifications in this early phase and an M12 threading was added into the entire short stump, therefore the screw did not fit perfectly into it. Luckily, the central screw is self-tapping, so when using the correct torque tool the screw was easily attached. The difference between the central screws threading and the short beam threading could affect the tolerance of the screw since it can move between the threading it made and the already-made threading in the short beam if too much load is applied, as happened in the testing situation described in section 5.4.1.

6.5 Integration testing of the Test Device and the Test Software

The interface adapter connection on the DAC is very sensitive. When not properly connected it can break the DAC by providing voltage output to the wrong pins. This happened when trying to assemble the power unit prototype board to the DAC, when the female and male connectors for the interface adapter connection were misaligned by one pin, so too high voltage might have been applied to some of the pins on the DAC. During testing with an oscilloscope, there was no sine wave transmitted and after confirming the DAC still got the proper input voltages a problem was found regarding the SPI clock in the interface adapter connection, it was non-functioning. After confirming that the Tiva was still giving proper outputs, a new DAC was tested and that fixed the issue with the clock connection.

There were still problems arising regarding getting the EMG data through to the DAC. The communication of the Tiva and the DAC seemed to depend on the correct timing of powering them, as otherwise, they would be out of sync and not able to communicate with each other. This was fixed by pressing and holding the reset button on the Tiva and disconnecting and reconnecting the AC/DC adapter before letting go of the button. Afterwards, the Tiva and the DAC were back in sync and able to transmit data.

As the DAC used in the Test Device has its analog outputs arranged not in sequence, the data channels recorded by the ALC in the integration testing were not in the correct order compared to the original EMG data. This is something that was fixed later when analyzing the data. Additionally, after the integration testing the Test Software was modified so that the correct EMG channel data is sent as an output through each DAC channel, allowing the ALC to pick them up in the correct sequence automatically.

As can be seen in section 5.4.3, the Test System managed to transmit the EMG data very well and clearly with only minor noise present. This noise is likely caused by the long wires of the test Omnetics connector as well as some rather long connections on the electronics soldered on the prototype board.

Later in the integration testing, one of the Test Device output channels stopped transmitting data, likely due to a minor error in the electronics. This was fixed by resoldering the connections on the attenuator prototype board, but to prevent further future problems designing and ordering a professionally made PCB to use instead of the prototype board would be an improvement.

6.6 Demonstration of the functionality of the Test System

The demonstration of the Test System along with the ALC and an artificial arm was done with a simple, six-channel dataset, with each channel corresponding to one possible movement of the artificial arm. A dataset like this was used rather than a real EMG recording in order to simplify the programming of the ALC and the artificial arm.

The control of an AL that the ALC implements is very complex and individualized specifically for each user. To program the ALC to recognize movements based on the EMG recordings existent at the company would have been very time consuming, and was redeemed irrelevant for the purpose of demonstrating the functionality of the Test System. In addition, verifying that the Test System functions correctly is simpler when using a dataset with one EMG channel per movement, as the signal sent to the ALC by the Test System can clearly be visualized for each channel separately by observing the movements of the artificial arm.

6.7 The modularity of the Test System and future improvements

As this thesis was part of a large project of creating a complete test system for the ALC, there are many things that could and will be improved in the future by the company the thesis was conducted at. This was kept in mind during the design of the Test System allowing for a modular design. This section will describe these possible implementation-

s/improvements in more detail.

6.7.1 The assembly of the Test Device

The Test Device has two prototype boards; one for the attenuators and one for the power unit and Tiva connections. The prototype boards can easily be cut into smaller boards, meaning that if needed the Tiva connections could also be detached as a single prototype board resulting in the Test Device having three prototype boards. Therefore, if any problems arise or new implementations were to be added for one part of the Test Device, it can be replaced without having to replace all of the electrical components.

6.7.2 Printed circuit board design

In future iterations of the Test Device, a PCB with surface-mounted components could be designed and ordered from a specialized manufacturer. This would be a big improvement for the Test Device since surface-mounted components and professionally assembled PCBs are often much smaller in size, more reliable with function, and less prone to broken connections [150]. During the investigation of voltage regulators, there were many switching voltage regulators that could have been replaced by the DC/DC converter with a lower cost but they were only available as surface-mounted components which is often the case for these types of voltage regulators [154].

A PCB design was not created in the thesis, since ordering one from a manufacturer could take weeks or months, as they are custom-made [152].

6.7.3 A faster interface adapter

The Tiva board currently allows the Test System to simulate EMG recordings with a sampling rate of 1 000 Hz. Even though this is sufficient for the technical requirements of this thesis, an even higher sampling rate would provide a more reliable signal transfer and thus possibly more realistic simulation of the EMG data.

To improve this and allow for a higher sampling rate, a newer version of the Tiva board or a completely new component could be used as the interface adapter. Since the Test Device is modular, switching the component should not be difficult and only require minimal work on the Test Device and the Test Software.

6.7.4 Emulating signal crossover in soft tissue

The 16 electrodes of the e-OPRA are located rather close to each other, creating a small electrical crosstalk signal between them [155]. To emulate this effect, a small resistor and a capacitor could be added in series between the common node of the attenuators and the ground, as can be seen in Figure 5.5 with components $R33$ and $C1$. To accommodate for this future improvement, the 1 kΩ resistors of each voltage divider were connected into a common node, and this node connected to the ground with a wire to allow space for mounting this emulator in the future.

6.7.5 Emulating soft tissue impedance

To make the Test Device even more realistic, small resistors of 1 kΩ to 20 kΩ could be added between each of the attenuator outputs and their corresponding Omnetics connector input. This would emulate a small impedance that occurs naturally in the tissue of the residual limb of the amputee when the EMG signal travels from the muscle tissue to the implanted electrode [148]. In addition, for the neurostimulation validation part of the final test system, an oscilloscope could be connected between this resistor and the corresponding attenuator to measure the neurostimulation pulses.

6.7.6 Artificial limb control validation

The next main aspect of the final test system after the EMG simulation would be to validate the AL control data from the ALC. Therefore, when choosing the interface adapter the Tiva was a solid option since this validation could be done using its analog inputs. Additionally, the AL control data is communicated via a UART interface which the Tiva supports. A comparison of the AL control data and the EMG data sent into the ALC would need to be made to validate that the ALC functions correctly. To do this an analog-to-digital conversion has to be made for a computer to be able to read a signal sent by the ALC. The Tiva has an analog-to-digital conversion functionality but to utilize it some electronic as well as software aspects need to be added.

6.7.7 Sensory feedback

After the validation of the AL control, the next step in the complete test system would be to simulate pressure sensor data recorded from an AL and validate the neurostimulation the ALC sends to the RL of the amputee based on it. Similarly to the AL control validation, this part would include work in the electronics as well as the software.

6.7.8 Test Rig design flexibility

Due to the detachable nature of the components of the Test Rig, replacing a malfunctioning part or implementing future possibilities becomes straightforward. For example, it is possible to replace the abutment attachment piece for the ALC-TH with another abutment attachment piece designed for the ALC-TR once that has been manufactured. It is also easy to shorten the column if wanted since it is made out of aluminum and the table attachment does not depend on the size of it. Removing the lockable joint from the column can be accomplished relatively effortlessly, enabling more compact storage.

The original table attachment design was only utilizing the base plate as a bottom plate but due to its instability as mentioned in section 6.2.2 the wooden plate was added last minute so little time was available for carefully choosing the dimension of the wooden plate. The dimensions of the wooden plate could be smaller, it could for example be reduced to a 200x200 mm square plate instead of a 400x400 mm square plate without having any effect on the mechanical strength of the Test Rig. This could be done by cutting the wooden plate into desired dimensions, and it would lower the weight of the Test System significantly as the wooden plate currently weighs 2.30 kg.

6.7.9 Two Degrees of Freedom design

An analysis was conducted to identify potential approaches for transforming certain 1 DoF joints into 2 DoF joints. Options one and three in Table 4.4 were identified as potential candidates for this purpose, primarily due to their possession of rounded arms, which provided opportunities for adaptability.

A simple design of a customized tube with a tightening screw was made that could have fitted both options with slight fixes on its dimensions.

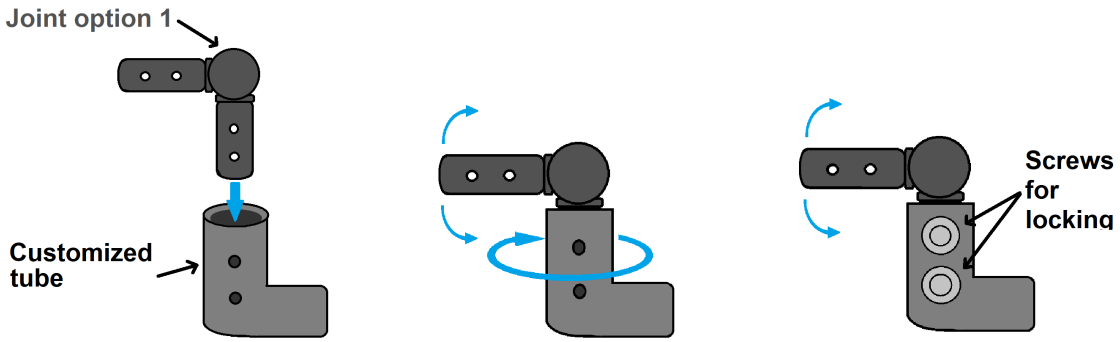

Figure 6.1: Demonstration of how the customized tube would have allowed for 2 DoF.

However, upon closer examination, it was observed that option one possessed a limited in-

cline angle of 220°, resulting in a restricted range of motion from 0° to 70°. Consequently, option one was deemed unsuitable for the intended application. Conversely, option three showed potential due to its offset feature enabling a complete 360° rotation within the existing design. However the joint itself was found to be prohibitively expensive, and the additional cost and time required for manufacturing a customized tube rendered it impractical for this version of the Test System. This could be implemented in future iterations if the budget is higher, to allow for 2 DoF for the lockable joint.

6.7.10 Test Rig covering

For aesthetic purposes, a covering could be created for the whole Test Rig. This could be made for example out of plastic or silicone, and should ideally resemble a human torso and RL. The covering could surround at least the column, the short beam, and the abutment attachment piece, and likely a part of the abutment as well.

7

Conclusion

In this thesis project, a Test System for an ALC was created. An extensive investigative effort went into finding suitable components for the Test System. The design of the Test System is complex, as it is composed of electronics, mechanical components, and hardware which all communicate and function together, allowing for realistic and efficient testing of the ALC without a human test subject.

The Test System mounts the ALC along with an AL and simulates data to the ALC with real EMG data recordings from amputees with the e-OPRA, as well as a sine wave. Both mechanical and integration testing was done on the Test System, and successful test results verify its structural strength and functionality. The Test System fulfills all of the design and technical requirements set for it.

From a broader point of view, the Test System is only a part of a larger project of creating a finalized test system to verify and validate all functionalities of the ALC. Therefore, a lot of future work will be built and based on the Test System created in this thesis.

Bibliography

[1] B. Davidsson, private communication, Feb. 23, 2023.

[2] S. Micera, "Staying in touch: Toward the restoration of sensory feedback in hand prostheses using peripheral neural stimulation," *IEEE Pulse*, vol. 7, no. 3, pp. 16–19, 2016. DOI: 10.1109/MPUL.2016.2539760. [Online]. Available: https://ieeexplore.ieee.org/document/7469462.

[3] R. Brånemark, P. Brånemark, B. Rydevik, and R. Myers, "Osseointegration in skeletal reconstruction and rehabilitation: A review," *Journal of rehabilitation research and development*, vol. 38, pp. 175–81, Mar. 2001.

[4] Integrum. "PATIENT LABELING - OPRA^{TM} Implant System." (2020), [Online]. Available: https://www.accessdata.fda.gov/cdrh_docs/pdf19/P190009D.pdf (visited on 11/15/2022).

[5] Medical Center Orthotics and Prosthetics. "Osseointegration prosthetics - the complete guide to osseointegrated prosthetics for amputees." (2012), [Online]. Available: https://mcopro.com/blog/resources/osseointegration-prosthetics-for-amputees/ (visited on 12/29/2022).

[6] Ontario Health, "Osseointegrated prosthetic implants for people with lower-limb amputation: A health technology assessment," *Ont Health Technol Assess Ser*, vol. 19, no. 7, pp. 1–126, 2019. [Online]. Available: https://www.ncbi.nlm.nih.gov/pmc/articles/PMC6939984/.

[7] J. Tillander, K. Hagberg, L. Hagberg, and R. Brånemark, "Osseointegrated titanium implants for limb prostheses attachments: Infectious complications," *Clinical Orthopaedics and Related Research®*, vol. 468, no. 10, pp. 2781–2788, Oct. 2010. DOI: 10.1007/s11999-010-1370-0. [Online]. Available: https://doi.org/10.1007/s11999-010-1370-0.

[8] K. Hagberg and R. Brånemark, "Consequences of non-vascular trans-femoral amputation: A survey of quality of life, prosthetic use and problems," *Prosthetics and Orthotics International*, vol. 25, no. 3, 2001. [Online]. Available: https://journals.lww.com/poijournal/Fulltext/2001/25030/Consequences_of_non_vascular_trans_femoral.7.aspx.

[9] K. Hagberg and R. Brånemark, "One hundred patients treated with osseointegrated transfemoral amputation prostheses–rehabilitation perspective," *Journal of rehabilitation research and development*, vol. 46, no. 3, pp. 331–344, 2009. [Online]. Available: https://pubmed.ncbi.nlm.nih.gov/19675986/.

[10] OTN Innovations. "LUCI - Where simplicity meets elegance." (), [Online]. Available: https://otninnovations.com/en/product/luci/ (visited on 02/20/2023).

[11] E. Mastinu *et al.*, "Grip control and motor coordination with implanted and surface electrodes while grasping with an osseointegrated prosthetic hand," *Journal of NeuroEngineering and Rehabilitation*, vol. 16, no. 1, p. 49, Apr. 2019. DOI: 10.1186/s12984-019-0511-2. [Online]. Available: https://doi.org/10.1186/s12984-019-0511-2.

[12] S. H. Roy, G. De Luca, M. S. Cheng, A. Johansson, L. D. Gilmore, and C. J. De Luca, "Electro-mechanical stability of surface EMG sensors," *Medical & Biological Engineering & Computing*, vol. 45, no. 5, pp. 447–457, May 2007. DOI: 10.1007/s11517-007-0168-z. [Online]. Available: https://doi.org/10.1007/s11517-007-0168-z.

[13] T. R. Farrell and R. F. f. Weir, "A comparison of the effects of electrode implantation and targeting on pattern classification accuracy for prosthesis control," *IEEE Transactions on Biomedical Engineering*, vol. 55, no. 9, pp. 2198–2211, 2008. DOI: 10.1109/TBME.2008.923917.

[14] A. Masteller, S. Sankar, H. B. Kim, K. Ding, X. Liu, and A. H. All, "Recent developments in prosthesis sensors, texture recognition, and sensory stimulation for upper limb prostheses," *Annals of Biomedical Engineering*, vol. 49, no. 1, pp. 57–74, Jan. 2021. DOI: 10.1007/s10439-020-02678-8. [Online]. Available: https://doi.org/10.1007/s10439-020-02678-8.

[15] Integrum AB. "e-OPRA^{TM} IMPLANT SYSTEM Mind-controlled prosthesis." (), [Online]. Available: https://integrum.se/what-we-do/our-products-future-solutions/e-opra/ (visited on 02/20/2023).

[16] M. B. I. Reaz, M. S. Hussain, and F. Mohd-Yasin, "Techniques of EMG signal analysis: detection, processing, classification and applications," *Biological Procedures Online*, vol. 8, no. 1, pp. 11–35, Dec. 2006. DOI: 10.1251/bpo115. [Online]. Available: https://doi.org/10.1251/bpo115.

[17] B. Davidsson, "System Architecture e-OPRA/ALC," unpublished.

[18] B. Abrahamsson, "e-OPRA Device Description," J. Millenaar, Ed., unpublished.

[19] M. Ortiz-Catalan, R. Brånemark, B. Håkansson, and J. Delbeke, "On the viability of implantable electrodes for the natural control of artificial limbs: Review and discussion," *BioMedical Engineering OnLine*, vol. 11, no. 1, p. 33, Jun. 2012. DOI: 10.1186/1475-925X-11-33. [Online]. Available: https://doi.org/10.1186/1475-925X-11-33.

[20] EM, "Design Description ALC System," BD, Ed., unpublished.

[21] M. Schiefer, D. Tan, S. M. Sidek, and D. J. Tyler, "Sensory feedback by peripheral nerve stimulation improves task performance in individuals with upper limb loss using a myoelectric prosthesis," en, *J Neural Eng*, vol. 13, no. 1, p. 016 001, Dec. 2015. [Online]. Available: https://www.ncbi.nlm.nih.gov/pmc/articles/PMC5517302/.

[22] E. Mastinu, "Firmware Description ALC," unpublished.

[23] K. L. Collins *et al.*, "A review of current theories and treatments for phantom limb pain," *The Journal of Clinical Investigation*, vol. 128, no. 6, pp. 2168–2176, Jun.

2018. DOI: 10.1172/JCI94003. [Online]. Available: https://doi.org/10.1172/JCI94003.

[24] D. M. Page *et al.*, "Motor control and sensory feedback enhance prosthesis embodiment and reduce phantom pain after long-term hand amputation," *Frontiers in Human Neuroscience*, vol. 12, 2018. DOI: 10.3389/fnhum.2018.00352. [Online]. Available: https://www.frontiersin.org/articles/10.3389/fnhum.2018.00352.

[25] H. Flor, "Phantom-limb pain: Characteristics, causes, and treatment," *The Lancet Neurology*, vol. 1, no. 3, pp. 182–189, 2002. DOI: https://doi.org/10.1016/S1474-4422(02)00074-1. [Online]. Available: https://www.sciencedirect.com/science/article/pii/S1474442202000741.

[26] L. Nikolajsen and K. F. Christensen, "Chapter 2 - phantom limb pain," in *Nerves and Nerve Injuries*, R. S. Tubbs, E. Rizk, M. M. Shoja, M. Loukas, N. Barbaro, and R. J. Spinner, Eds., San Diego: Academic Press, 2015, pp. 23–34. DOI: https://doi.org/10.1016/B978-0-12-802653-3.00051-8. [Online]. Available: https://www.sciencedirect.com/science/article/pii/B9780128026533000518.

[27] O. W. Samuel *et al.*, "Intelligent emg pattern recognition control method for upper-limb multifunctional prostheses: Advances, current challenges, and future prospects," *IEEE Access*, vol. 7, pp. 10 150–10 165, 2019. DOI: 10.1109/ACCESS.2019.2891350. [Online]. Available: https://ieeexplore.ieee.org/document/8612917.

[28] B. Viher, D. Korosec, and D. Zazula, "Computer simulator of electromyographic signal," in *Proceedings Ninth IEEE Symposium on Computer-Based Medical Systems*, 1996, pp. 47–52. DOI: 10.1109/CBMS.1996.507124. [Online]. Available: https://ieeexplore.ieee.org/stamp/stamp.jsp?tp=&arnumber=507124.

[29] D. Farina, A. Crosetti, and R. Merletti, "A model for the generation of synthetic intramuscular EMG signals to test decomposition algorithms," *IEEE Transactions on Biomedical Engineering*, vol. 48, no. 1, pp. 66–77, 2001. DOI: 10.1109/10.900250. [Online]. Available: https://ieeexplore.ieee.org/document/900250.

[30] M. Al-Faiz and Y. Al Mashhadany, "Human Arm Movements Recognition Based on EMG Signal.," *MASAUM Journal of Basic and Applied Sciences*, vol. 1, Oct. 2009. [Online]. Available: https://citeseerx.ist.psu.edu/doc/10.1.1.212.6582.

[31] S. Patrick, J. Meklenburg, S. Jung, Y. Mendelson, and E. A. Clancy, "An electromyogram simulator for myoelectric prosthesis testing," in *Proceedings of the 2010 IEEE 36th Annual Northeast Bioengineering Conference (NEBEC)*, 2010, pp. 1–2. DOI: 10.1109/NEBC.2010.5458134. [Online]. Available: https://ieeexplore.ieee.org/document/5458134.

[32] X. Li and W. Li, "A novel electromyography simulator based on experiment data," in *2014 Fourth International Conference on Instrumentation and Measurement, Computer, Communication and Control*, 2014, pp. 87–92. DOI: 10.1109/

IMCCC.2014.26. [Online]. Available: https://ieeexplore.ieee.org/document/6994996.

[33] H. Shirzadfar and S. Arab, "A simple surface electromyogram signal simulator for testing of measurement equipment," vol. 2, pp. 39–42, Nov. 2018. [Online]. Available: https://www.researchgate.net/publication/330343160_A_Simple_Surface_Electromyogram_Signal_%5C%5CSimulator_for_Testing_of_Measurement_Equipment.

[34] J. Lenin Ramón Valencia and R. Alonso Espinosa Medina, "Development of a surface electromyography simulator to evaluate neuromusculoarticular rehabilitation," in *2021 IEEE 2nd International Congress of Biomedical Engineering and Bioengineering (CI-IBBI)*, 2021, pp. 1–4. DOI: 10.1109/CI-IBBI54220.2021.9626128. [Online]. Available: https://ieeexplore.ieee.org/document/9626128.

[35] L. Hao, X. Xu, and J. Cheng, "A test-bed for above-knee intelligent prosthesis," in *2006 IEEE International Conference on Robotics and Biomimetics*, 2006, pp. 1311–1315. DOI: 10.1109/ROBIO.2006.340118. [Online]. Available: https://ieeexplore.ieee.org/document/4142055.

[36] B. J. Borbély, Z. Kincses, Z. Vöröshazi, Z. Nagy, and P. Szolgay, "A modular test platform for real-time measurement and analysis of EMG signals for improved prosthesis control," in *2014 14th International Workshop on Cellular Nanoscale Networks and their Applications (CNNA)*, 2014, pp. 1–2. DOI: 10.1109/CNNA.2014.6888643. [Online]. Available: https://ieeexplore.ieee.org/document/6888643.

[37] A. Poliakov *et al.*, "System synthesis of a testbench for testing modules and control systems of lower-limb prostheses," in *2015 International Conference on Biomedical Engineering and Computational Technologies (SIBIRCON)*, 2015, pp. 150–155. DOI: 10.1109/SIBIRCON.2015.7361872. [Online]. Available: https://ieeexplore.ieee.org/document/7361872.

[38] A. C. Etoundi, A. Dobner, S. Agrawal, C. L. Semasinghe, I. Georgilas, and A. Jafari, "A robotic test rig for performance assessment of prosthetic joints," en, *Front Robot AI*, vol. 8, p. 613 579, Mar. 2022. [Online]. Available: https://www.frontiersin.org/articles/10.3389/frobt.2021.613579/full.

[39] Q. Tian, M. Liu, L. Min, J. An, X. Lu, and H. Duan, "An automated data verification approach for improving data quality in a clinical registry," *Comput Methods Programs Biomed*, vol. 181, p. 104 840, Jan. 2019. [Online]. Available: https://pubmed.ncbi.nlm.nih.gov/30777618/.

[40] H. I. Aly, S. Youssef, and C. Fathy, "Hybrid brain computer interface for movement control of upper limb prostheses," in *2018 International Conference on Biomedical Engineering and Applications (ICBEA)*, 2018, pp. 1–6. DOI: 10.1109/ICBEA.2018.8471729.

[41] Y. Gu, D. Yang, Q. Huang, W. Yang, and H. Liu, "Robust EMG pattern recognition in the presence of confounding factors: features, classifiers and adaptive learning," *Expert Systems with Applications*, vol. 96, pp. 208–217, 2018. DOI: https://doi.org/10.1016/j.eswa.2017.11.049. [Online]. Avail-

able: https://www.sciencedirect.com/science/article/pii/S0957417417308060.

[42] S. Pancholi and A. Joshi, "INTELLIGENT UPPER-LIMB PROSTHETIC CONTROL (iULP) WITH NOVEL FEATURE EXTRACTION METHOD FOR PATTERN RECOGNITION USING EMG," *Journal of Mechanics in Medicine and Biology*, vol. 21, p. 2 150 043, Jun. 2021. DOI: 10.1142/S0219519421500433.

[43] J. J. Carr, "Resolution," in *Practical Radio Frequency Test and Measurement - A Technician's Handbook*, Burlington, MA, USA: Elsevier, 2002, pp. 10–11. [Online]. Available: https://app.knovel.com/hotlink/khtml/id:kt006PJ1G6/practical-radio-frequency/resolution (visited on 05/27/2023).

[44] R. SUNDARARAJN, E. PETERSON, and R. NOWLIN, "Attenuators," in *Encyclopedia of RF and Microwave Engineering, Volumes 1 - 6*, K. Chang, Ed., Hoboken, NJ, USA: John Wiley Sons, 2005, pp. 452–480. [Online]. Available: https://app.knovel.com/hotlink/khtml/id:kt003XY3D1/encyclopedia-rf-microwave/attenuators (visited on 05/19/2023).

[45] P. Kosky, R. Balmer, W. Keat, and G. Wise, "Voltage Dividers," in *Exploring Engineering - An Introduction to Engineering and Design*, 5th ed., London, United Kingdom: Elsevier, 2021, pp. 217–218. [Online]. Available: https://app.knovel.com/hotlink/khtml/id:kt012RMJC1/%20exploring-engineering/voltage-dividers (visited on 05/17/2023).

[46] N. Ida, "The Inverting Amplifier," in *Sensors, Actuators, and Their Interfaces - A Multidisciplinary Introduction*, 2nd ed., London, United Kingdom: Institution of Engineering and Technology (The IET), 2020, pp. 673–674. [Online]. Available: https://app.knovel.com/hotlink/khtml/id:kt012HI2F2/sensors-actuators-their/inverting-amplifier (visited on 05/17/2023).

[47] D. Lacamera, "Interfaces and peripherals," in *Embedded Systems Architecture*, R. Singh, P. Sahu, and S. Editing, Eds., 2nd ed., Birmingham, United Kingdom: Packt Publishing, 2023, pp. 12–14. [Online]. Available: https://app.knovel.com/hotlink/khtml/id:kt0134O8C6/embedded-systems-architecture/interfaces-peripherals (visited on 05/19/2023).

[48] P. Barry and P. Crowley, "Part ii. embedded systems architecture and opedatasheetn," in *Modern Embedded Computing - Designing Connected, Pervasive, Media-Rich Systems*, T. Green and R. Day, Eds., Waltham, MA, USA: Elsevier, 2012, pp. 80–95. [Online]. Available: https://app.knovel.com/hotlink/khtml/id:kt00BPZA6D/modern-embedded-computing/part-ii-embedded-systems (visited on 05/19/2023).

[49] "Encyclopedia Britannica - USB." (), [Online]. Available: https://www.britannica.com/technology/USB (visited on 05/11/2023).

[50] R. Hibbeler, "6.3 bending deformation of a straight member," in *Mechanics of Materials*, ser. Always learning, Pearson, 2017, pp. 307–310. [Online]. Available: https://books.google.se/books?id=oMP5sgEACAAJ.

[51] R. Hibbeler, "6.4 the flexure formula," in *Mechanics of Materials*, ser. Always learning, Pearson, 2017, pp. 311–327. [Online]. Available: https://books.google.se/books?id=oMP5sgEACAAJ.

[52] R. Hibbeler, "Appendix a geometric properties of an area," in *Mechanics of Materials*, ser. Always learning, Pearson, 2017, pp. 810–823. [Online]. Available: https://books.google.se/books?id=oMP5sgEACAAJ.

[53] S. Ling, J. Sanny, and W. Moebs, *University Physics Volume 1* (University Physics). Samurai Media Limited, 2017. [Online]. Available: https://books.google.se/books?id=x8VqswEACAAJ.

[54] R. Hibbeler, "Bending," in *Mechanics of Materials*, ser. Always learning, United Kingdom: Pearson, 2017, pp. 281–385. [Online]. Available: https://books.google.se/books?id=oMP5sgEACAAJ.

[55] R. Budynas and K. Nisbett, "Appendix a," in *Shigley's Mechanical Engineering Design*, NYC, United States: McGraw-Hill Education, 2010, pp. 1011–1066. [Online]. Available: https://books.google.se/books?id=eT1DPgAACAAJ.

[56] W. C. Young, "Beams; flexure of straight bars," in *Roark's formulas for stress and strain*, McGraw-Hill, Sep. 2001, pp. 125–266. DOI: 10.1036/007072542X.

[57] R. Hibbeler, *Buckling of Columns* (Always learning). United Kingdom: Pearson, 2017, pp. 385–431. [Online]. Available: https://books.google.se/books?id=oMP5sgEACAAJ.

[58] W. C. Young, "Tension, compression, shear, and combined stress," in *Roark's formulas for stress and strain*, McGraw-Hill, Sep. 2001, pp. 109–124. DOI: 10.1036/007072542X.

[59] W. C. Young, "Appendix a: Properties of a plane area," in *Roark's formulas for stress and strain*, McGraw-Hill, Sep. 2001, pp. 799–812. DOI: 10.1036/007072542X.

[60] M. W. Reimer, "13 - stress and strain," in *Rules of Thumb for Mechanical Engineers*, J. E. Pope, Ed., Burlington: Gulf Professional Publishing, 1996, pp. 294–328. DOI: https://doi.org/10.1016/B978-088415790-8/50013-8. [Online]. Available: https://www.sciencedirect.com/science/article/pii/B9780884157908500138.

[61] T. Megson, "Shear force and bending moment," in *Structural and Stress Analysis (2nd Edition)*. Oxford, U.K: Elsevier, 2005, pp. 42–80. [Online]. Available: https://app.knovel.com/hotlink/khtml/id:kt00512HS3/structural-stress-analysis/shear-force-bending-moment.

[62] *IEEExplore*, 2023. [Online]. Available: https://ieeexplore.ieee.org/Xplore/home.jsp.

[63] *PubMed*, 2023. [Online]. Available: https://pubmed.ncbi.nlm.nih.gov/.

[64] *Web of Science*, 2023. [Online]. Available: https://www.webofscience.com/wos/woscc/basic-search.

[65] *Chalmers library*, 2023. [Online]. Available: https://www.lib.chalmers.se/en/search/.

[66] *Google scholar*, 2023. [Online]. Available: https://scholar.google.com/.

[67] P. Dhaker. "Introduction to SPI Interface." (), [Online]. Available: https://www.analog.com/en/analog-dialogue/articles/introduction-to-spi-interface.html (visited on 05/15/2023).

[68] J. Valdez and J. Becker, "Understanding the I2C Bus," Texas Instruments Inc., Dallas, TX, USA, Tech. Rep. SLVA704, May 2015. [Online]. Available: https://www.ti.com/lit/an/slva704/slva704.pdf.

[69] A. S. Arockia Doss, B. Mishra, S. Mohammed, P. K. Lingampally, and M. Short, "Robotic arm for biomedical applications," in *Handbook of Smart Materials, Technologies, and Devices: Applications of Industry 4.0*, C. M. Hussain and P. Di Sia, Eds. Cham, Switzerland: Springer International Publishing, 2020, pp. 1–24. DOI: 10.1007/978-3-030-58675-1_38-1. [Online]. Available: https://doi.org/10.1007/978-3-030-58675-1_38-1.

[70] H. T. Lancashire, Y. Al Ajam, R. P. Dowling, C. J. Pendegrass, and G. W. Blunn, "Hard-wired epimysial recordings from normal and reinnervated muscle using a bone-anchored device," en, *Plast Reconstr Surg Glob Open*, vol. 7, no. 9, e2391, Sep. 2019. [Online]. Available: https://pubmed.ncbi.nlm.nih.gov/31741811/.

[71] "An ADC and DAC Least Significant Bit (LSB)." (), [Online]. Available: https://masteringelectronicsdesign.com/an-adc-and-dac-least-significant-bit-lsb/ (visited on 03/10/2023).

[72] A. S. Morris and R. Langari, "5.1 introduction," in *Measurement and Instrumentation - Theory and Application*, Elsevier, 2012, pp. 115–133. [Online]. Available: https://app.knovel.com/hotlink/khtml/id:kt009BGQB8/measurement-instrumentation/data-acquisition-introduction.

[73] TI Inc., *AMC7836*, SLAS986D, REVISED FEBRUARY 2018, Texas Instruments Inc., Nov. 2014.

[74] TI Inc., *DACx1416*, SLASEO0B, REVISED JUNE 2021, Texas Instruments Inc., Jul. 2018.

[75] TI Inc., *Tiva™ TM4C123GH6PM Microcontroller*, SPMS376E, REVISED JUNE 2014, Texas Instruments Inc., 2007.

[76] Texas Instruments Inc., "USB2ANY interface adapter." [Online]. Available: https://www.ti.com/tool/USB2ANY?keyMatch=&tisearch=search-everything&usecase=hardware (visited on 05/18/2023).

[77] B. Adryan, D. Obermaier, and P. Fremantle, "Conventional ac/dc adapters," in *Technical Foundations of IoT*, Norwood, MA, USA: Artech House, 2017, pp. 160–162. [Online]. Available: https://app.knovel.com/hotlink/khtml/id:kt012GLMSB/technical-foundations/conventional-ac-dc-adapters (visited on 05/17/2023).

[78] "AC DC Desktop, Wall Adapters," digikey.se, Accessed: 2023-05-28. [Online]. Available: https://www.digikey.se/en/products/filter/ac-dc-skrivbords-v%5C%C3%5C%A4ggadaptrar/130.

[79] STMicroelectronics, *L78 Datasheet*, DS0422, rev 36, STMicroelectronics, 2018.

[80] Y. M. Laid, "Integrated circuit voltage regulators," in *Power Electronics Handbook*, M. H. Rashid, Ed., 4th ed., Oxford, United Kingdom: Elsevier, 2018, pp. 665–668. [Online]. Available: https://app.knovel.com/hotlink/

khtml/id:kt00CXD4R1/power-electronics-handbook/linear-shunt-voltage (visited on 05/17/2023).

[81] Traco Electronic AG, *DC/DC Converter TMR 1 Series, 1 Watt*, rev 36, Traco Power, 2022.

[82] J. W. Matiko and S. P. Beeby, "Step-up dc-dc switching regulator," in *Applications of Energy Harvesting Technologies in Buildings*, Norwood, MA, USA: Artech House, 2017, pp. 73–77. [Online]. Available: https://app.knovel.com/hotlink/khtml/id:kt012ZZDS3/applications-energy-harvesting/step-up-dc-dc-switching (visited on 05/19/2023).

[83] B. Davidsson, private communication, Mar. 23, 2023.

[84] *Fusion 360*, version 2.0.16009, Autodesk, Inc., May 2, 2023. [Online]. Available: https://www.autodesk.com/.

[85] A. J. Gannon, W. F. Moroney, and D. W. Biers, "The validity of anthropometric predictions derived from proportional multipliers of stature," *Proceedings of the Human Factors and Ergonomics Society Annual Meeting*, vol. 42, pp. 1356–1360, 19 1998. DOI: 10.1177/154193129804201906. (visited on 05/15/2023).

[86] "SensorHand Speed," ottobock.us, Accessed: 2023-05-23. [Online]. Available: https://shop.ottobock.us/Prosthetics/Upper-Limb-Prosthetics/Myo-Hands-and-Components/Myo-Terminal-Devices/SensorHand-Speed/p/8E39~58.

[87] "Electric Wrist Rotator," ottobock.us, Accessed: 2023-05-23. [Online]. Available: https://shop.ottobock.us/Prosthetics/Upper-Limb-Prosthetics/Myo-Hands-and-Components/Myo-Wrist-Units-and-Rotation/Electric-Wrist-Rotator/p/10S17.

[88] "DynamicArm Plus," ottobock.us, Accessed: 2023-05-23. [Online]. Available: https://shop.ottobock.us/Prosthetics/Upper-Limb-Prosthetics/Myoelectric-Elbows/DynamicArm-Plus-Elbow/DynamicArm-Plus/p/12K110N~545.

[89] B. Rexroth, "Basic Mechanic Elements 14.0," (2019), Accessed: 2023-05-21. [Online]. Available: https://www.boschrexroth.com/media/e4b73828-3e16-46cf-b003-112c6d172303.

[90] *MTpro*, version 5.2.1.1, Bosch Rexroth AG, 2023. [Online]. Available: https://www.boschrexroth.com/en/gb/products/product-groups/assembly-technology/topics/engineering-software-mtpro/.

[91] "Structural Systems," se.rs-online.com, Accessed: 2023-05-17. [Online]. Available: https://se.rs-online.com/web/c/engineering-materials-industrial-hardware/structural-systems/.

[92] "Aluminum Profiles - Solutions Components," boschrexroth.com, Accessed: 2023-05-17. [Online]. Available: https://www.boschrexroth.com/en/us/products/product-groups/assembly-technology/topics/aluminum-profiles-solutions-components/.

[93] "Fastening Joining," mcmaster.com, Accessed: 2023-05-17. [Online]. Available: https://www.mcmaster.com/.

[94] "ROTARY HINGE TECHNOLOGY," adjustablelockingtech.com, Accessed: 2023-05-17. [Online]. Available: http://www.adjustablelockingtech.com/index.php.

[95] "Armar Fästen," focusnordic.se, Accessed: 2023-05-16. [Online]. Available: https://www.focusnordic.se/produkter/foto/belysningsstativ-och-fasten/armar-fasten/.

[96] "Joints," part-on.co.uk, Accessed: 2023-05-16. [Online]. Available: https://www.part-on.co.uk/category/joints/.

[97] "Incremental-Angle Hinge Round Arms," mcmaster.com, Accessed: 2023-05-16. [Online]. Available: https://www.mcmaster.com/1258A12/.

[98] "Incremental-Angle Hinge Square Arms," mcmaster.com, Accessed: 2023-05-16. [Online]. Available: https://www.mcmaster.com/1258A1/.

[99] "HEAVY DUTY ALLOY STEEL LOCKING HINGES 2 ROUND ARMATURES 360° Offset Model," adjustablelockingtech.com, Accessed: 2023-05-16. [Online]. Available: http://www.adjustablelockingtech.com/products_variloc_steel_dimensions2.php.

[100] "KUPO KCP-320 Ez Grip Twins," focusnordic.se, Accessed: 2023-05-16. [Online]. Available: https://www.focusnordic.se/produkter/foto/belysningsstativ-och-fasten/armar-fasten/kupo-kcp-320-ez-grip-twins/.

[101] "40 x 40mm Lockable Swivel Joint Bosch Rexroth 3842562087 | 3842516847," part-on.co.uk, Accessed: 2023-05-16. [Online]. Available: https://www.part-on.co.uk/product/bosch-rexroth-10mm-slot-40x40-joint-3842562087-3842516847/.

[102] "What is .NET?" (), [Online]. Available: https://dotnet.microsoft.com/en-us/learn/dotnet/what-is-dotnet (visited on 05/04/2023).

[103] *Visual Studio 2022*, version 17.5.3, Microsoft Corporation, Mar. 21, 2023. [Online]. Available: https://visualstudio.microsoft.com/vs/.

[104] "Desktop Guide (Windows Forms .NET)." (), [Online]. Available: https://learn.microsoft.com/en-us/dotnet/desktop/winforms/overview/?view=netdesktop-7.0 (visited on 05/11/2023).

[105] "MDO3000 Mixed Domain Oscilloscope," tek.com, Accessed: 2023-05-20. [Online]. Available: https://www.tek.com/en/products/oscilloscopes/mdo3000.

[106] "Fluke 115 Field Technicians Digital Multimeter," fluke.com, Accessed: 2023-05-10. [Online]. Available: https://www.fluke.com/en-in/product/electrical-testing/digital-multimeters/fluke-115.

[107] "Digital Hook Scale, 40 kg," biltema.se. [Online]. Available: https://www.biltema.se/en-se/leisure/travel/travel-accessories/digital-hook-scale-40-kg-2000030993.

[108] "Keithley 2231A-30-3," tek.com, Accessed: 2023-05-23. [Online]. Available: https://www.tek.com/en/products/keithley/dc-power-supplies/2220-2230-2231-series.

[109] *MATLAB*, version 9.14.0.2254940 (R2023a) Update 2, Mathworks, Inc., Apr. 17, 2023. [Online]. Available: https://www.mathworks.com/.

[110] "DAC81416EVM," ti.com, Accessed: 2023-05-22. [Online]. Available: https://www.ti.com/tool/DAC81416EVM.
[111] "EK-TM4C123GXL," ti.com, Accessed: 2023-05-22. [Online]. Available: https://www.ti.com/tool/EK-TM4C123GXL.
[112] "TMR 1-1222," digikey.se, Accessed: 2023-05-22. [Online]. Available: https://www.digikey.com/en/products/detail/traco-power/TMR-1-1222/9345039.
[113] "L7805CV," digikey.se, Accessed: 2023-05-22. [Online]. Available: https://www.digikey.com/en/products/detail/stmicroelectronics/L7805CV/585964.
[114] "368," digikey.se, Accessed: 2023-05-22. [Online]. Available: https://www.digikey.se/en/products/detail/adafruit-industries-llc/368/5629434.
[115] "RNF14FTD499K," digikey.se, Accessed: 2023-05-22. [Online]. Available: https://www.digikey.se/en/products/detail/stackpole-electronics-inc/RNF14FTD499K/1682306.
[116] "CF14JT1K00," digikey.se, Accessed: 2023-05-22. [Online]. Available: https://www.digikey.se/en/products/detail/stackpole-electronics-inc/CF14JT1K00/1741314.
[117] "PRT-13268," digikey.se, Accessed: 2023-05-22. [Online]. Available: https://www.digikey.se/en/products/detail/sparkfun-electronics/PRT-13268/5623212.
[118] "TAP104K035SCS," digikey.se, Accessed: 2023-05-22. [Online]. Available: https://www.digikey.se/en/products/detail/kyocera-avx/TAP104K035SCS/563934.
[119] "TAP334K035SCS," digikey.se, Accessed: 2023-05-22. [Online]. Available: https://www.digikey.se/en/products/detail/kyocera-avx/TAP334K035SCS/563986.
[120] "FG26X7R1H475KRT06," digikey.se, Accessed: 2023-05-22. [Online]. Available: https://www.digikey.se/en/products/detail/tdk-corporation/FG26X7R1H475KRT06/5803056.
[121] "CC45SL3DD221JYVNA," digikey.se, Accessed: 2023-05-22. [Online]. Available: https://www.digikey.se/sv/products/detail/tdk-corporation/CC45SL3DD221JYVNA/10481126.
[122] "7447462047," digikey.se, Accessed: 2023-05-22. [Online]. Available: https://www.digikey.se/en/products/detail/w%5C%C3%5C%BCrth-elektronik/7447462047/2440386.
[123] "PPPC162LFBN-RC," digikey.se, Accessed: 2023-05-22. [Online]. Available: https://www.digikey.se/en/products/detail/sullins-connector-solutions/PPPC162LFBN-RC/810255.
[124] "PPTC052LFBN-RC," digikey.se, Accessed: 2023-05-22. [Online]. Available: https://www.digikey.se/en/products/detail/sullins-connector-solutions/PPTC052LFBN-RC/807243.
[125] "PH2-20-UA," digikey.se, Accessed: 2023-05-22. [Online]. Available: https://www.digikey.se/en/products/detail/adam-tech/PH2-20-UA/9830418.

[126] "310-41-116-41-001000," digikey.se, Accessed: 2023-05-22. [Online]. Available: https://www.digikey.se/sv/products/detail/mill-max-manufacturing-corp/310-41-116-41-001000/4455036.

[127] "Hon-Kwang Electric Co., Ltd." honkwang.com, Accessed: 2023-05-23. [Online]. Available: https://www.honkwang.com/.

[128] T. I. Inc., "DAC81416EVM User's Guide (Rev. A)," (2018), Accessed: 2023-05-22. [Online]. Available: https://www.ti.com/lit/ug/slau777a/slau777a.pdf?ts=1685034180159&ref_url.

[129] Texas Instruments Inc., "Tiva™ C Series TM4C123G LaunchPad Evaluation Board User's Guide," (2013), Accessed: 2023-05-21. [Online]. Available: https://www.ti.com/lit/ug/spmu296/spmu296.pdf?ts=1685255486638.

[130] F. M. Mwema and E. T. Akinlabi, "Basics of fused deposition modelling (fdm)," in *Fused Deposition Modeling: Strategies for Quality Enhancement*, Switzerland: Springer International Publishing, 2020, pp. 1–15. DOI: 10.1007/978-3-030-48259-6_1. [Online]. Available: https://doi.org/10.1007/978-3-030-48259-6_1.

[131] "STRUT PROFILE 40X40L," boschrexroth.com, Accessed: 2023-05-13. [Online]. Available: https://store.boschrexroth.com/Assembly-Technology/Basic-Mechanic-Elements/Profiles-and-accessories/Strut-profile/STRUT-PROFILE_3842993120?cartId=dfdd0b65-aff7-4b74-9b5f-45025768042d&cclcl=sv_SE.

[132] "BASE PLATE 40X40," boschrexroth.com, Accessed: 2023-05-12. [Online]. Available: https://store.boschrexroth.com/Assembly-Technology/Basic-Mechanic-Elements/Feet/Base-plate-steel-40x40/BASE-PLATE_3842542667?cartId=dfdd0b65-aff7-4b74-9b5f-45025768042d&cclcl=sv_SE.

[133] "Brick clamp," biltema.se, Accessed: 2023-05-23. [Online]. Available: https://www.biltema.se/en-se/tools/hand-tools/screw-clamps/brick-clamp-2000024014.

[134] "HYLLPLAN MDF 19X400X800MM," bauhaus.se. [Online]. Available: https://www.bauhaus.se/hyllplan-mdf-19x400x800mm.

[135] "Täcklock profil 40x40 svart ESD," logicsystemab.se, Accessed: 2023-05-15. [Online]. Available: https://shop.logicsystemab.se/sv/tacklock-profil-40x40.

[136] "T-HEAD BOLT HS10-M8X20," boschrexroth.com, Accessed: 2023-05-13. [Online]. Available: https://store.boschrexroth.com/Assembly-Technology/Basic-Mechanic-Elements/Connection-elements/Flange-nut-T-bolt/T-HEAD-BOLT_3842528715?cartId=dfdd0b65-aff7-4b74-9b5f-45025768042d&cclcl=sv_SE.

[137] "COLLAR NUT M8," boschrexroth.com, Accessed: 2023-05-13. [Online]. Available: https://store.boschrexroth.com/Assembly-Technology/Basic-Mechanic-Elements/Connection-elements/Flange-nut-T-bolt/COLLAR-NUT_3842345081?

cartId=dfdd0b65-aff7-4b74-9b5f-45025768042d&cclcl=sv_SE.

[138] "WE MOVE. YOU WIN." boschrexroth.com, Accessed: 2023-05-22. [Online]. Available: https://www.boschrexroth.com/en/dc/company/we-move-you-win/.

[139] "CLAMPING LEVER GN300-63-M8-40-SW," boschrexroth.com, Accessed: 2023-05-13. [Online]. Available: https://store.boschrexroth.com/Assembly-Technology/Basic-Mechanic-Elements/Joints/Joint/CLAMPING-LEVER_3842516847?cartId=dfdd0b65-aff7-4b74-9b5f-45025768042d&cclcl=sv_SE.

[140] B. Rexroth, "Assembly instructions," (2020), Accessed: 2023-05-21. [Online]. Available: https://www.boschrexroth.com/en/us/media-details/ae8275a7-7608-43bc-a71b-292443d89e3a.

[141] G. J. Miao, "Nyquist Sampling Theorem," in *Signal Processing in Digital Communications*, ser. Artech House Signal Processing Library, Boston, MA, USA: Artech House, 2006, pp. 94–96. [Online]. Available: https://ebookcentral.proquest.com/lib/chalmers/detail.action?docID=338745 (visited on 05/15/2023).

[142] K. Watson, C. Nagel, J. Pedersen, J. Reid, and M. Skinner, *Beginning Visual C# 2010*. Wiley, 2011. [Online]. Available: https://books.google.se/books?id=xFhZME%5C_NbxsC.

[143] "MatFileHandler." (), [Online]. Available: https://github.com/mahalex/MatFileHandler (visited on 03/22/2023).

[144] "Arduino - Analog Output," wiki.nus.edu.sg, Accessed: 2023-05-27. [Online]. Available: https://wiki.nus.edu.sg/display/Arduino/Analog+Output#:~:text=Arduino%5C%20does%5C%20not%5C%20generate%5C%20true,is%5C%20always%5C%200V%5C%20or%5C%205V..

[145] "Analog Inputs for Raspberry Pi Using the MCP3008," learn.adafruit.com, Accessed: 2023-05-27. [Online]. Available: https://learn.adafruit.com/reading-a-analog-in-and-controlling-audio-volume-with-the-raspberry-pi?view=all.

[146] T. Wilmshurst, "Pulse width modulation used for digital-to-analog conversion," in *Designing Embedded Systems with PIC® Microcontrollers - Principles and Applications*, 2nd ed., Oxford, United Kingdom: Elsevier, 2010, pp. 280–283. [Online]. Available: https://app.knovel.com/web/view/khtml/show.v/rcid:kpDESPICM7/cid:kt0092LQ35/viewerType:khtml//root_slug:designing-embedded-systems/url_slug:pulse-width-modulation?b-q=pulse-width%5C%20modulation%5C%20analog&include_synonyms=no&sort_on=default&view=collapsed&zoom=1&page=13&q=pulse-width%5C%20modulation%5C%20analog (visited on 05/27/2023).

[147] T. Wilmshurst, "Pulse width modulation used for digital-to-analog conversion," in *Designing Embedded Systems with PIC® Microcontrollers - Principles and Applications*, 2nd ed., Oxford, United Kingdom: Elsevier, 2010,

pp. 280–283. [Online]. Available: https://app.knovel.com/hotlink/khtml/id:kt0092LQ92/designing-embedded-systems/taking-timing-pulse-width (visited on 05/27/2023).

[148] B. Davidsson, private communication, May 27, 2023.

[149] C. Bowick, J. Blyler, and C. Ajluni, "Pcb design," in *RF Circuit Design (2nd Edition)*, Burlington, MA, USA: Elsevier, 2008, pp. 216–218. [Online]. Available: https://app.knovel.com/web/view/khtml/show.v/rcid:kpRFCDE00A/cid:kt0082UAM3/viewerType:khtml//root_slug:rf-circuit-design-2nd/url_slug:pcb-design?b-q=PCB%5C%20traces&include_synonyms=no&sort_on=default&view=collapsed&zoom=1&page=14&q=PCB%5C%20traces (visited on 05/24/2023).

[150] G. Roberts, F. Taenzler, and M. Burns, "Prototype DIBs versus PCB DIBs," in *Introduction to Mixed-Signal IC Test and Measurement*, 2nd ed., Oxford, NY, USA: Oxford University Press, 2012, pp. 684–685. [Online]. Available: https://app.knovel.com/hotlink/khtml/id:kt00A4QGC1/introduction-mixed-signal/prototype-dibs-versus (visited on 05/27/2023).

[151] T. I. customer service, private communication, Mar. 17, 2023.

[152] B. Davidsson, private communication, Apr. 20, 2023.

[153] E. Georgantzia, M. Gkantou, and G. S. Kamaris, "Aluminium alloys as structural material: A review of research," *Engineering Structures*, vol. 227, p. 111 372, 2021. DOI: https://doi.org/10.1016/j.engstruct.2020.111372. [Online]. Available: https://www.sciencedirect.com/science/article/pii/S0141029620339730.

[154] T. I. customer service, private communication, May 1, 2023.

[155] B. Davidsson, private communication, May 5, 2023.

DEPARTMENT OF ELECTRICAL ENGINEERING
CHALMERS UNIVERSITY OF TECHNOLOGY
Gothenburg, Sweden
www.chalmers.se

CHALMERS
UNIVERSITY OF TECHNOLOGY